On Model-Based Estimation and Control of Heterogeneous Multi-Battery Systems (Volvo Technology AB)

Master's thesis in Systems, Control and Mechatronics

Yusuf Alamaz and Jerry Knutsson

Department of Electrical Engineering

Chalmers University of Technology
Gothenburg, Sweden 2021
www.chalmers.se

Abstract

This thesis investigates the effect of pack-to-pack heterogeneity on the State-of-Power (SOP) in parallel-connected battery-packs. The analysis is performed in two different frameworks: MATLAB/Simulink and Simcenter Amesim. Five different state/parameter heterogeneities are examined: Differences in State-of-Health (SOH), coolant flow-rate, coolant temperature, initial pack temperature and initial State-of-Charge (SOC). The SOP is estimated through look-up tables. The analysis has found that differences in SOH, coolant temperature and initial SOC have the largest impact, while the remaining heterogeneities are less significant.

The thesis has also explored a way of utilizing the results from the sensitivity analysis in estimating SOP for a multi-pack battery system. We formulate an Economic Model Predictive Control (EMPC) scheme that utilizes a simple Equivalent Circuit Model (ECM). The ECM consists of an Open-Circuit-Voltage (OCV) source in series with an internal resistance, to model the individual packs. Two different formulations are presented. Both are based on current-split prediction, one of which also allows for SOC prediction, hence permits implementation of SOC constraints over the prediction horizon. As the proposed controller may violate terminal voltage constraints, an ad-hoc solution is presented to mitigate these effects.

Abstrakt

Arbetet undersöker effekttillståndet i parallellanslutna batterisystem, vid fall av heterogenitet mellan batteripack. Analysen är utförd i två olika ramverk: MATLAB/Simulink och Simcenter Amesim. Fem olika tillstånd/parameter-heterogeniteter har undersökts: Skillnad i åldring, kylvätskeflöde, kylvätsketemperatur, initial packtemperatur och initialt laddningstillstånd. Effekttillståndet estimeras genom uppslagstabeller. Studien har upptäckt att skillnad i åldring, kylvätsketemperatur och initialt laddningstillstånd har störst inflytanden på effekttillståndet. De resterande faktorerna visade sig vara av mindre betydelse.

Arbetet har även utforskat ett sätt att tillgodogöra resultaten från föregående analys vid estimering av effekttillståndet av ett batterisystem. Vi formulerar en ekonomisk modell-prediktiv regulator. Metoden använder en enkel ekvivalent kretsmodell där en OCV källa i serie med en resistor modellerar de individuella packen. Två olika system presenteras. Båda bygger på estimering av strömfördelning, medan en av metoderna även tillåter estimering av laddningstillståndets utveckling, och kan därmed bilägga begräsningar på tillåtet laddningsintervall. Eftersom den föreslagna regulatorn kan överskrida spänningsbegränsningar, presenteras en ad-hoc lösning för att mildra denna effekt.

Acknowledgements

We would like to thank our industrial supervisor Faisal Altaf for providing support and vision during our master thesis. He gave us the opportunity to work with one of the largest and well-known companies in Sweden, in exploring the fast trending field of electric vehicles.

We would also like to thank our Chalmers examiner Torsten Wik, a prominent researcher in the battery field. He contributed with both his valuable time and helpful feedback.

Finally, we would like to thank Gunnar Latz and Christopher Helbig from Siemens Digital Industries Software for training us and supporting our use of the Simcenter Amesim software.

Contents

List of Figures

List of Tables

Acronyms

BEV	Battery Electric-Vehicle
BMS	Battery Management System
BP	Battery-Pack
CC-CV	Constant Current Constant Voltage
CM	Characteristic Maps
DOD	Depth-of-Discharge
ECM	Equivalent Circuit Model
EIS	Electrochemical Impedance Spectroscopy
EKF	Extended Kalman Filter
EMPC	Economic Model Predictive Control
EOL	End-Of-Life
ESC	Enhanced Self-Correcting
ESS	Energy Storage System
EU	European Union
EV	Electric-Vehicle
HEV	Hybrid Electric-Vehicle
HPPC	Hybrid Pulse Power Characterization
LPV	Linear Parameter Varying
LTV	Linear Time Varying
MCC	Multiple Stage Constant Current
MPC	Model Predictive Control
OCV	Open Circuit Voltage
PCM	Parallel-Connected Module
PHEV	Plug-in Hybrid Electric Vehicle
RHC	Receding Horizon Control
SCM	Series-Connected Module
SOC	State-of-Charge
SOE	State-of-Energy
SOH	State-of-Health

SOP State-of-Power

SPKF Sigma Point Kalman Filter

SSM State Space Model

Glossary

Battery Energy Storage System (BESS)
The BESS refers to the complete system of possibly several sets of battery-packs and BMS, coupled with converter electronics and supervisory control [1].

Battery module
A *battery module* is a group of cells connected in series and/or parallel [2]. In the extreme cases, they are all in parallel (PCM) or all in series in (SCM).

Battery pack
A *battery-pack* consists of battery modules connected in series and/or parallel [2].

C-rate
The *C-rate* specifies the current-rate at which the cell can be charged or discharged in 1h [3]. For example, a fully charged cell, when discharged at a rate of 10C should be fully discharged within around six minutes.

Capacity (discharge/nominal/total)
The *discharge capacity* specifies charge quantity that can be utilized at a certain constant rate [2]. The *nominal capacity* is the rated capacity. The *total capacity* specifies the total charge in the cell.

Conduction
Conduction is the transfer of heat through molecular collision [4].

Constant Current - Constant Voltage (CC-CV)
This is a charging strategy in which a constant current is applied until a voltage limit is reached, and then a constant voltage is applied until the current is negligible [2].

Convection
Convection describes the transfer of heat between a solid and a fluid in motion [4].

Depth-of-Discharge (DOD)
This is the complement to the SOC, i.e. $\text{DOD} = 1 - \text{SOC}$ [3].

Diffusion
Ions in a cell can be transported due to a gradient in concentration [5].

Electrochemical Impedance Spectroscopy (EIS)
The internal impedance of a battery can be determined by applying a current at different frequencies and measuring the voltage with EIS equipment [6].

End-Of-Life (EOL)
A cell is commonly considered to be at its End-Of-Life (EOL), when its total capacity has decreased by 20% and its resistance has doubled [7].

Equivalent Circuit Model (ECM)
ECMs model battery behavior by using electric components [8]. The components can be linear or non-linear.

Hysteresis
Hysteresis is the phenomenon which describes the OCV discrepancy exhibited when cells are charged vs discharged [9].

Multiple Stage Constant Current (MCC)
This is a charging strategy in which there are several (decreasing) constant-current stages [10].

Open-Circuit-Voltage (OCV)
Open-Circuit-Voltage (OCV) is the cell teminal voltage at complete equilibrium in the absence of a load [3].

Radiation
Radiation is the transfer of energy through electromagnetic radiation, induced by temperature differences [4].

Simcenter Amesim
Simcenter Amesim is a simulation platform for mechatronic systems [11].

Specific power/energy
Specific power and energy describes the power and energy density in W/Kg and Wh/Kg, respectively [12].

State-of-Charge (SOC)
When fully charged the cell is at 100% SOC, and 0% SOC when fully discharged [3].

State-of-Energy (SOE)
When fully charged the cell is at 100% SOE, and 0% SOE when fully discharged [13]. This quantity is in terms of energy as opposed to charge.

State-of-Health (SOH)
State-of-Health (SOH) is related to the functionality of the battery [6]. It is often determined through capacity- and power-fade [7].

State-of-Power (SOP)
State-of-Power (SOP) estimation refers to the amount of available power (to accept or deliver) over a certain time horizon [14].

Terminal voltage
The *terminal voltage* is the voltage measured across the terminals [15].

Symbols

State-space-model

A	State-space matrix relating states to the state dynamics.
B	State-space matrix relating input to the state dynamics.
C	State-space matrix relating states to the output.
D	State-space matrix relating input to the output.
u	Input vector.
x	State vector.
y	Output vector.
$\dot{x}$	State dynamics vector.

Cell states and inputs

SOC_i	SOC in cell i.
I_{dem}	Total demanded current.
$T_{c,i}$	Temperature of cell i.
$V_{\mathrm{OCV},i}$	Open-Circuit-Voltage (OCV) in cell i.
$V_{RC1,i}$	Voltage over the first RC-network in cell i.
$V_{RC2,i}$	Voltage over the second RC-network in cell i.
W_i	Quantity related to thermodynamics in cell i.

Cell parameters

η_i	Coulombic efficiency of cell i.
$C_{1,i}$	Capacitance of first RC-network in cell i.
$C_{2,i}$	Capacitance of second RC-network in cell i.
Q_i	Capacity of cell i.
$R_{0,i}$	Ohmic resistance of cell i.
$R_{1,i}$	Resistance of first RC-network in cell i.
$R_{2,i}$	Resistance of second RC-network in cell i.

Cell thermal dynamics

C_c	Heat capacity of the cell.
q_c	Heat generation in the cell.
R_{ca}	Heat-transfer resistance of natural convection.
R_{cf}	Heat-transfer resistance of forced convection.
T_a	Temperature of the ambient.
T_f	Temperature of the coolant.

Sensitivity analysis

SOC_0	Initial SOC of battery-pack.
SOH	State-of-Health of battery-pack.
T_0	Initial temperature of battery-pack.
T_{coolant}	Temperature of battery-pack coolant.
V_{coolant}	Flow-rate of battery-pack coolant.

Model predictive estimation

Δt	Time-horizon for a constant power.
I_{lim}	Current-limit for ESS.
I_i	Current to battery-pack i.
J	Cost function.
P_i	Power from battery-pack i.
T_c	Control horizon.
T_p	Prediction horizon.
V_{T_i}	Terminal voltage of battery-pack i.
y_{lim}	Current-limit for battery-packs.

1 Introduction

In a 2019 text from the European Parliament [16], it is stated that nearly 30% of the total CO_2 emissions in the European Union (EU) comes from transport. Although passenger cars are presented as the major polluters, in 2016, heavy- and light-duty trucks stood for roughly a third of the total road transport-related CO_2 emissions. By 2030, the European Commission has the aim to, compared to the levels of 1990, cut 55% of the greenhouse gas emissions [17]. An aid in this mission could be electric cars, as a tool developed by *Transport and Environment* suggests that in Europe, electric cars (on average) emit less CO_2 than petrol and diesel ones [18].

During the year of 2020, worldwide sales of Battery Electric-Vehicles (BEVs) and Plug-in Hybrid Electric Vehicles (PHEVs) increased by 40% and 74%, respectively [19]. There may be a long-term trend to be observed, as BloombergNEF estimates that by the year 2030, BEVs will constitute 28% of the global passenger vehicle sales [20]. This trend may not be limited to passenger vehicles, as they also estimate that by the same year, 58% of municipal buses, and 40% of 2-wheelers will be electric. The International Energy Agency (IEA) expects that over the coming decade, the lithium-ion chemistry is likely to be the dominant one used in Electric-Vehicles [21].

State-of-Power (SOP) estimation refers to the amount of available power (to accept or deliver) from a battery over a certain time horizon [14]. Accurate SOP estimation can both optimize performance of a battery system and extend battery life-time. This can be of high importance especially from an environmental aspect, as the lithium-ion battery may constitute roughly a third of the total life-cycle emissions of an average European EV [22].

This thesis examines parallel-connected lithium-ion battery-packs. The investigation can be divided into two main topics:

I. The implications of pack-to-pack heterogeneity on the State-of-Power (SOP) for a multi-pack battery system.

II. An investigation of computationally efficient State-of-Power (SOP) estimation, using a model predictive framework.

1.1 Pack-to-pack Heterogeneity

Heterogeneities can occur between battery cells due to several factors [23]. For parallel-connected cells, this can lead to accelerated ageing [24], while in battery-packs, this can result in inefficiencies and affect the performance of the system [23].

Hence, there is motivation for investigating the underlying principles and gain intuition around the cause and effects of battery-pack heterogeneity. In this work, the analysis is conducted with the purpose of determining some influential state/parameter variations w.r.t. the power capability.

The investigation is conducted through an experimental model-based sensitivity analysis. Evidently, this can be done in several different ways using different models. Here we use two different frameworks to obtain the relevant data; one based on MATLAB/Simulink and one based on Simcenter Amesim.

- The MATLAB/Simulink framework uses a second order RC model to describe cells, and then scales the cells to pack level. The thermal-model assumes convective heat exchange, both through a coolant and by ambient air.
- The Simcenter Amesim framework is intended to have a similar setup as the MATLAB/Simulink one. This software allows for easier design of the desired system, as the user does not need to be concerned about the underlying equations. Also, models in this framework can more easily be extended to capture other complex behavior. However, simulations may be slower compared to the previous framework.

The results gathered in this analysis, can then be utilized when formulating a power estimation algorithm.

1.2 Model Predictive Power Estimation

In a Battery Management System (BMS), one of the most challenging tasks is to estimate the State-of-Power (SOP) [25]. This task is also one of high importance, as it can affect the performance of the battery. The SOP estimation algorithms can be divided into Characteristic Maps and algorithms utilizing Equivalent Circuit Models [25]. The former method is used in the sensitivity analysis, while a formulation using the latter is proposed for question/topic II.

The Hybrid Pulse Power Characterization (HPPC) is a method that can be used to determine the static power-capability [26]. This method uses a simple model and voltage-limits to calculate instantaneous peak charge- and discharge-power. However, it has three key drawbacks as it utilizes a simple model, does not explicitly consider a prediction horizon and neglects constraints on key quantities [27].

The work presented here aims to estimate current-split and maximum allowable current in a multi-pack battery system, using a model-predictive framework. Examples of previous work that utilizes model based current-split prediction in aid of estimating power-capability includes work by Zou et al. in [28] and Altaf and Klintberg in [29, 30].

Current-split prediction may not only be used in power estimation, as Altaf et al. [31] instead utilize this for controlling the electrical connection of parallel-connected battery-packs. In this setup, the control for connecting or disconnecting battery-packs is based on the maximum magnitude of the predicted individual pack currents.

1.3 Thesis Structure and Contributions

The thesis structure and main contributions are given below.

Chapter 2
In this chapter, the reader is provided with a background theory related to batteries, power estimation, and Model Predictive Control (MPC). Readers that are unfamiliar

with these fields, may want to carefully read this chapter. As one might realize, batteries can exhibit some very complex behavior.

Chapter 3
Equipped with the background theory, the third chapter introduces the two different frameworks used in the sensitivity analysis (MATLAB/Simulink and Simcenter Amesim). Both models consist of second order RC-networks, with a key difference in their thermal modelling. The Simcenter Amesim model also includes reversible heat generation (entropic heat). At the end of this chapter, the two frameworks are compared using a Plug-in Hybrid Electric Vehicle (PHEV) current load-profile, which shows an observable difference between the models.

Chapter 4
This chapter addresses the first (I) question/topic in the thesis, specifically, the effect of battery state-/parameter heterogeneity on the SOP. The two models are investigated using a dynamic current-profile. The setups consists of six parallel-connected battery-packs, where one of the packs is altered in order to capture the effect of the investigated heterogeneity. Five different states/parameters are analyzed:

- Ageing through capacity fade and resistance increase (State-of-Health (SOH)).
- Coolant flow-rate.
- Coolant temperature.
- Initial temperature.
- Initial State-of-Charge (SOC).

The analysis concludes that, the most significant state/parameter variations seem to be SOH, coolant temperature and SOC. The remaining two factors proved to be less significant over the duration of the experiment.

Chapter 5
This chapter addresses the second (II) question/topic in the thesis. It presents two different model-predictive power estimation formulations that utilize the result from the sensitivity analysis. Both formulations use a simple Equivalent Circuit Model (ECM) where an Open-Circuit-Voltage (OCV)-source in series with a resistance models the individual packs. Constraints can be placed on the current and pack terminal voltage. One of the formulations also estimates the SOC evolution, and allows us to specify a charging window.

Two different kinds of tests are conducted: Open-loop estimation and charging through feedback. The feedback control test showed that terminal voltage-constraints may be violated. Hence we propose an ad-hoc solution to mitigate these effects.

Chapter 6
This is the final chapter of the thesis. It presents conclusions and suggestions for future work pertaining to both the sensitivity analysis and the model-predictive power estimation. Following this chapter, the reader can find appendices that may aid in gaining a better understanding of the thesis.

Short Summary of Thesis Contributions
The main contributions of this thesis are:

- Development of a Simcenter Amesim model for a multi-pack battery-system, using both free and forced convection in the thermal model.
- Investigation to find some significant state/parameter heterogeneities affecting the SOP of a multi-pack battery system.
- Two novel model-predictive power estimation formulations.
- An ad-hoc solution to respect terminal voltage constraints for a charging window during feedback control using Model Predictive Control.

2 Background Theory

In the following chapter, the reader is provided with a background theory beneficial for grasping the concepts and results presented in subsequent chapters. For unfamiliar terms and abbreviations, the reader is referred to the glossary and acronyms sections, respectively. Please note that some terms are hyperlinked to their description in the glossary. For additional material the reader is referred to the bibliography.

2.1 Battery Cells

In comparison to other commonly used batteries, the lithium-ion chemistry provides high energy-density and power, while maintaining a long life [32]. The lithium-ion cell can have more than three times the specific energy and more than twice the specific power capability of the still widely used lead-acid chemistry [33, 34]. Some of the popular lithium-ion chemistries are $LiFePO_4$, $LiCoO_2$, and LiNMC [35].

Below, is a list of some properties and phenomena that can occur in a cell.

- *Open-Circuit-Voltage (OCV)* is the cell terminal voltage at complete equilibrium in the absence of a load [3].
- A so-called *diffusion* voltage can be recovered in a lithium-ion cell when it is allowed to rest [3].
- *Hysteresis* is the phenomenon which describes the OCV discrepancy exhibited when cells are charged vs discharged [9]. See Figure 1.
- There are several sources of *resistance* in a cell, such as from the electrolyte, current collector and the active mass [5].

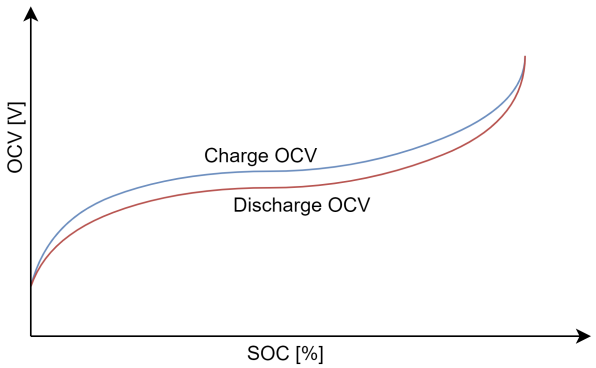

Figure 1: A rough sketch of how hysteresis may affect the OCV-SOC curve of a battery. A corresponding plot for the $LiFePO_4$ chemistry can be found in [32].

2.1.1 Battery Modelling

There are different ways to group battery models in order to distinguish between theories and techniques in use. Suresh et al. [36], proposes a scheme where the models are divided into four groups:

I. *First principle models:*
These models consider mass- and energy-balance equations as well as electrochemistry present in a battery-cell. Depending on assumptions made regarding battery-characteristics these can be made to have varying levels of accuracy and complexity.

II. *Surrogate first principle models:*
Here the battery-cell is modeled using a surrogate. An example is the ECM which describes characteristic dynamics using electrical components.

III. *Data based models:*
Data based models are divided into stochastic and empirical models. The former tries to explain specific effects in the battery with stochastic approaches. The latter tries to fit experimental data to parameters of intuitively or empirically derived equations.

IV. *Hybrid models:*
Hybrid models result from integrating features of the above mentioned models, with the aim of achieving high accuracy with low computational complexity.

Equivalent Circuit Models:

ECMs perform an empirical fit, where lab-data is used to determine the circuit parameters [2]. This is done with the aim of closely matching the cell voltage/current behavior. Hence, as explained by Plett, they have the same properties as other types of curve fit. With electrical models, one tries to achieve a balance between computational complexity and fidelity [37]. Zhang et al. [8], state that the most widely used battery model type in Battery Management Systems (BMSs) is the ECM.

The Enhanced Self-Correcting (ESC) model is an ECM that describes the battery cell by incorporating an ideal voltage-source in series with a resistor, RC-network, and a so-called hysteresis component [3]. The order of a linear ECM (in absence of non-linear elements) is determined by the number of RC-networks in the model [8]. Figure 2 shows the ESC.

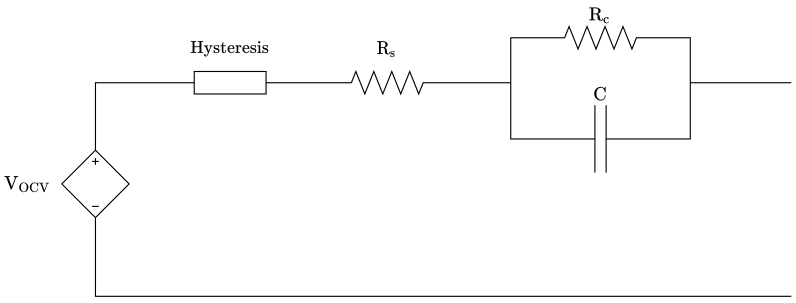

Figure 2: The Enhanced Self-Correcting (ESC) model [2].

Zhang et al. [8] mentions the Linear Parameter Varying (LPV) ECM. Here, operating-condition-dependant parameters can be captured. They argue that with this model, it is easy to configure and identify the parameters, rendering it very appealing to engineers.

In a study conducted by Hu et al. [38], 12 different ECMs were compared for various load profiles. The model generalizability between cells was also tested. Here, generalizability refers to the model's performance for a cell that is different from the one which it had its parameters adjusted for. The tests were repeated for two different cell chemistries, namely $LiFePO_4$ and LiNMC. The study found that:

- For the LiNMC chemistry, the *first-order RC model* is preferred.
- For the $LiFePO_4$ chemistry, the *first-order RC model with one state hysteresis* is preferred.
- In terms of generalizability, the *first-order RC model with one state hysteresis* is preferred for both chemistries.

In [2], Plett highlights weaknesses of the ECM. An ECM can only predict input/output (current/voltage) behavior. In contrast to high-fidelity electrochemical models, ECMs cannot accurately predict internal electrochemical states. This, for example, hampers the ability to predict and minimize future ageing. Plett believes that future applications will need to account for the electrochemical dynamics.

2.1.2 Parameter Interdependencies

There are various parameter- and state-interdependencies in a cell. These can be crucial to recognize in order to understand battery behavior. The text below introduces some of the most significant ones:

- Interdependencies related to OCV:
  - *State-of-Charge (SOC)*:
    There is a static non-linear relationship between the OCV and SOC [6]. This dependency can vary between different chemistries. As an example, the $LiFePO_4$ cells exhibit a roughly constant OCV for mid SOC-levels, while a more dynamic behavior can be observed for low and high SOC-levels. The OCV dynamics has a direct relation to the SOC derivative and can be calculated as [39]

    $$\dot{V}_{\text{OCV}} = \frac{I}{C_0}, \quad C_0 = 3600Q\frac{d\text{SOC}(V_{\text{OCV}})}{dV_{\text{OCV}}},$$

    where I is the current, and C_0 is the effective capacitance.
  - *Temperature*:
    The OCV-SOC relationship can be influenced by temperature [40]. Hence, temperature differences can lead to a different OCV at the same SOC level. In [40], one can observe that there is a general decrease in OCV for increasing temperature.
- Interdependencies related to SOC:
  - *Capacity*:
    The SOC of battery a cell can be calculated as [41]

    $$\text{SOC}(t) = \text{SOC}(0) + \frac{1}{Q}\int_0^t \eta \cdot I(\tau)d\tau,$$

    where the current I is positive on charge and negative for discharge. This clearly demonstrates the dependency of SOC on the nominal capacity Q.

- *Temperature*:
  Zhang et al. [8] explains that the capacity increases with temperature.
  In [42], one can observe decaying SOC levels with temperature.

- *Current*:
  As explained in [8], with slower and less dynamic discharge currents the capacity becomes larger.

- Interdependencies related to impedance:

  - *Temperature*:
    In work done by Lebkowski [43], one can observe a general decrease in battery resistance with increasing temperature. This, as explained in [8], is due to electrons getting excited.

  - *State-of-Charge (SOC)*:
    Wang et al. [44] has investigated the relationship between resistance and SOC at room-temperature. There is a general increase in resistance with decreasing SOC. However, a pronounced increase in resistance can be observed for very high SOC-levels.

  - *Load dynamics*:
    Using Electrochemical Impedance Spectroscopy (EIS), Bruen and Marco [39] have tested the impedance of lithium-ion batteries. Here, a general decrease in resistance can be observed for increasing current frequencies.

2.1.3 Battery-cell Ageing

To determine the State-of-Health (SOH) usually metrics pertaining to capacity and power are investigated, namely capacity fade (SOH_E) and power fade (SOH_P) [7]. These metrics are calculated based on the capacity and resistance of the cell, respectively. A cell is commonly considered to be at its End-Of-Life (EOL), when its total capacity has decreased by 20% and resistance has doubled.

In work conducted by Wikner [45], the effects of various parameters such as temperature, Depth-of-Discharge (DOD) and SOC has been investigated in relation to battery ageing. The ageing was considered both during cycling and storage.

- CC-CV tests were performed to compare the effects of different DOD-levels on the battery health. Two SOC ranges were investigated: 0-90% and 80-90%. The range allowing for lower SOC-levels, accelerated the rate of ageing; both increasing the resistance and decreasing the capacity.

- She studied the affects of current-rate by conducting cycling-tests at various C-rates. Capacity fade and resistance increased at higher C-rates. At the highest, the battery-cell degraded to the EOL performance within 100 cycles.

- CC-CV tests were also performed at various temperatures to investigate the effects during cycling. The study revealed that temperature has an impact, accelerating both forms of ageing with increasing temperature.

Moreover, Pastor-Fernandez et al. [7], observed a linear relationship between the two forms of ageings discussed above (SOH_E and SOH_P). They argue that either of them could be calculated based on the other.

2.2 Thermal Dynamics

Thermodynamics describe the kinetic and potential energy in relation to the heat a system can produce [46]. Heat can be transferred in three ways: conduction, convection and radiation [4]:

I. *Conduction* is the transfer of heat through molecular collision. At the collision of a high energy molecule (hence high temperature), with a low energy molecule, energy is transferred to the lower one, increasing its temperature.

II. *Convection* describes the transfer of heat between a solid and a fluid. This is not fundamentally different from conduction, but there is a need to describe that the fluid is in motion. Convection can be further divided into *free* and *forced* convection depending on whether or not there is an external influence, such as a pump forcing fluid motion.

III. *Radiation* is the transfer of energy through electromagnetic radiation induced by temperature difference. Here, no material medium is needed and the transfer can occur in a vacuum.

The relation between temperature rate of change, and heat in an object with thermal capacitance C is given by [47]

$$C\frac{dT}{dt} = q_1 - q_2,$$

where q_1 and q_2 are the heat in- and out- flow rates, and T is the temperature of the object. Furthermore, the rate of heat transfer, q, can be calculated as [47]

$$q = \frac{T_1 - T_2}{R},$$

where R is the resistance against q and $T_1 - T_2$ describes the temperature difference.

2.2.1 Thermal Dynamics in Batteries

The operating temperature of a battery is determined by two factors: Electrochemical reactions inside the battery and the environment [48]. The reliable operating temperature can vary between different lithium-ion chemistries [32]. For example, the $LiFePO_4$ and NCA chemistries can be charged at 0°C to 45°C and discharged at −20°C to 55°C, while for LTO the minimum charge temperature can decrease to −30°C.

Charging under low ambient temperatures may introduce a chemical side-effect called lithium plating [49]. This can partly be reversed by subsequent discharge. The irreversible part may result in capacity fade and serve as a safety hazard due to potential internal short-circuiting.

Thermal runaway is a failure, in which the system has lower effective cooling compared to the heat generation [50]. This state can be triggered by various abusive usages of the battery such as over- charging/discharging and exposing it to high temperatures [51]. Thermal runaway can lead to release of flammable and toxic materials [52].

2.2.2 Thermal Modelling of Batteries

The two largest heat generating factors within a cell are related to chemical reactions and different kind of polarizations [53]. These factors are termed reversible (entropic) and irreversible heat generation, respectively. The total heat generation, q, in the cell can be calculated as

$$q = \underbrace{I \cdot (V_t - V_{\text{OCV}})}_{q_{\text{Irreversible}}} + \underbrace{IT \cdot \left(\frac{\partial V_t}{\partial T}\right)_P}_{q_{\text{Reversible}}},$$

where V_{OCV} is the OCV, V_t is the terminal voltage, and I and T are the current and temperature, respectively.

Viswanathan et al. [54] found that the reversible heat is in-fact a large part of the total heat generation. Bandhauer et al. [55], found that the amount of reversible heat generation depends both on the temperature and the current-rate, where the contribution is largest at higher temperatures and lower rates.

Smith and Wang [56] investigated total heat generation during several dynamic load-profiles for HEVs. They found that aggressive load-profiles, favored irreversible heat as the dominant component. Moreover, some lithium-ion chemistries can have a larger entropy change than others [54]. For instance, it is much lower for $LiFePO_4$ compared to $LiCoO_2$.

In [37], Lin et al. introduces a coupled electrothermal battery model for cylindrical batteries. Here, an ECM and a two-state thermal model estimating the core and surface temperature, interact by a two-way coupling. The model calculations can be divided into two steps:

I. In the first step, SOC and voltage is calculated using the present state and parameter values. The heat generation is then determined through the voltage loss on the electrical components in the ECM as

$$q = I \cdot (V_{\text{OCV}} - V_t).$$

II. In the second step, the heat generation and ambient temperature is used to calculate the core and surface temperature. The core temperature can then be used to update the temperature dependent parameters in the electrical model.

To model the thermal interaction between batteries, LeBel et al. [24], introduces an electrothermal model where a 1D thermal network is used to determine cell temperatures through the thermal interaction to adjacent cells.

2.3 Battery Packs

Cells may need to be connected in series and/or parallel in order to supply the demanded voltage and current [2]. A *battery module* is a group of cells connected in series and/or parallel. In the extreme cases, they are all in parallel (Parallel-Connected Module (PCM)) or all in series (Series-Connected Module (SCM)). A *battery-pack* consists of battery modules connected in series and/or parallel.

Usually, cells in parallel are assumed to have homogeneous properties [24], while cells in series are assumed to be the ones requiring energy balancing [39]. Since individual cell

currents are typically not measured, differences in cell currents are not detected. Cell currents can cause differences in heat generation, degradation and SOC.

2.3.1 Causes of Heterogeneity

Resistance and capacity can vary even in new cells due to manufacturing variations [24]. Gong et al. explains that complications such as operator errors and chemical impurities can lead to differences in capacity and cell characteristics [23]. They also present differing operating conditions and environments as contributing factors for cell inconsistencies.

In [39], Bruen and Marco evaluate the resistance caused by parallel connections. Four cells are connected in parallel, with only the first cell connected to the load. The study found that there was a lower charge throughput of the cell furthest from the load, while some cells saw a higher peak current.

2.3.2 Effects of Heterogeneity

Brand et al. [57] demonstrates current distribution between two parallel cells in simulation and compares the result to experimental data. The investigation is divided into two cases, one with differing resistance and one with differing capacity:

- ΔC Scenario: The capacity of Cell 1 is a third higher.
- ΔR Scenario: The resistance of Cell 2 is a third higher.

A charge current of 3A was applied for 1000s on the parallel connection. Simulation shows that:

In the case of uneven capacities, the current through the cells are initially equal. However, since Cell 2 has a lower capacity, it charges faster. Hence the OCV increases faster. To maintain the same terminal voltage on both cells as constrained by the parallel connection, Cell 1 needs a larger current. After some time, a constant OCV and a current difference is established.

In the case of uneven resistances, the currents are initially split unevenly according to the current divider. This uneven current distribution leads to a faster charge of Cell 1, hence a faster increase in OCV. The increase in OCV leads to the equalization of cell currents, and after some time an OCV difference is established.

Brand et al. explains that the current distribution for the experimental results deviate from the rules of thumb.

In work by Pastor-Fernandez et al. [7], they investigate the behavior of four unevenly aged cells in parallel. An initial difference between the least and most aged cell in terms of SOH_P and SOH_E, was set to 45% and 40%, respectively. The study found that the initial differences between the cells converged to 30% and 10% after 500 cycles. To evaluate the active factors, they consider SOC, current, temperature, charge-throughput and thermal energy.

In the previously mentioned paper by Bruen and Marco [39], they observed that after a step-

current, the currents between the cells sometimes diverged and other times converged. They explain that this behavior is related to the magnitude of the current. If the current is small, then the self-balancing nature is prominent and the SOCs for the cells converge.

Note that, the cause and effect of heterogeneity has been explained using battery cells. Henceforth, unless stated otherwise, these theories are assumed to hold between battery-packs.

2.4 Battery Management System

According to Lu et al. [32], there is no consensus on the definition of a Battery Management System (BMS). They adopt the view that the BMS is any system that manages the battery. The BMS is said to be a key element for a reliable usage of the batteries in EVs [6].

The battery management system monitors battery current, voltage and temperature [6]. This enables the system to perform various different tasks such as cell-balancing, thermal management, ensuring battery safety and estimation of battery SOC/SOH.

2.5 State-of-Charge Estimation

It is unmanageable to compute the SOC of every single cell in a large battery-pack [58]. Zhang et al. explains that the intricacy of SOC estimation for a battery-pack is due to three factors: limitations in measurement, complex physics and the computational cost. Nonetheless, lithium-ion cells are sensitive to over-charging/discharging, and accurate estimation can prolong battery service life [59].

Another aspect of SOC estimation is that the term "battery-pack SOC" is ill-defined, and Plett goes as far as to say that the term should not be used [2]. He illustrates the complication through two series-connected cells with different SOCs, one at 100% and the other at 0%. He explains that, in this case you cannot discharge the cells without over-discharging one, nor charge the cells without over-charging one. Hence defining the charge as 0% or 100% is not meaningful, and using the average (50%) is even worse since that would indicate that the cells can be charged *and* discharged, but in reality neither is possible.

To estimate the SOC of a single cell, Plett has presented both the *Extended Kalman Filter (EKF)* [60] and the *Sigma Point Kalman Filter (SPKF)* [61] as two possible methods. Zhang et al. has in [58] proposed a method of SOC estimation where a so-called interval observer is used for estimating the SOC of parallel-connected cells. The scalability of the approach is presented as a major feature. Several of the same authors have also contributed to [59], where descriptor system theory is used.

2.6 Power Estimation

State-of-Power (SOP) estimation refers to the amount of available power (to accept or deliver) over a certain time horizon [14]. This is in-fact, according to Farmann and Sauer [25], one of the most challenging tasks of the BMS. However, they explain that an accurate prediction can both optimize battery performance and extend its lifetime.

There are several different aspects that can influence the power capability [14]. One of which is the cell-to-cell variation in impedance, capacity and temperature distribution. The power-limitation is mainly related to the temperature, SOC, voltage and current. Furthermore, power-fade is mainly influenced by the increasing impedance. In a vehicle application, this influences the acceleration and charging.

The present SOP estimation algorithms can be divided into two groups [25]:

I. Static battery interdependencies are used to estimate the SOP with so-called *Characteristic Maps (CM)*. SOC, temperature and power-duration are generally included as states/parameters utilized for the scheme.

II. Algorithms utilizing an ECM to estimate SOP.

In [62], Wik et al. introduces a power estimation technique based on ECM. It is argued to be very robust, and the probability of exceeding voltage limits is said to be marginal. The proposed algorithm is formulated in respect of maximum charge/discharge current. Essentially, a maximum current for a certain time-horizon is determined based on the voltage limit for the system.

Another SOP prediction algorithm using ECM (Randles circuit) is proposed by Anderson et al. [63]. This model utilizes an Extended Kalman Filter (EKF) to predict model parameters and RC-voltages.

2.7 The Model Predictive Framework

Model Predictive Control (MPC) is a control algorithm that can be solved online by determining inputs based on prediction of future behavior, while ensuring stability [64]. The architecture of MPC can be illustrated as Figure 3:

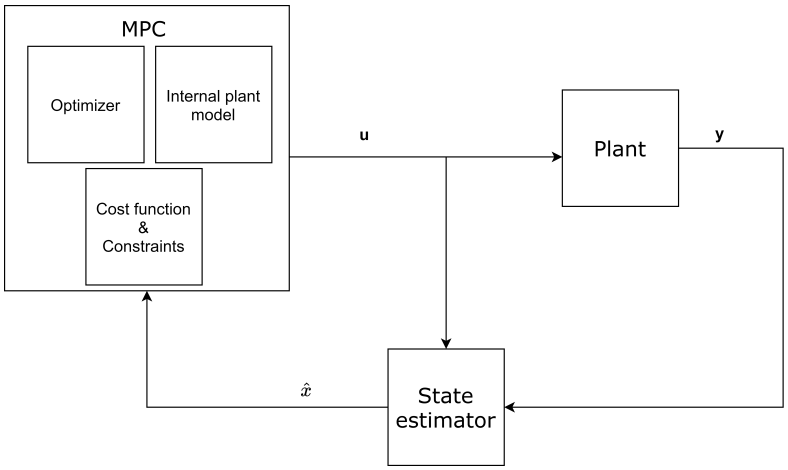

Figure 3: The MPC architecture [65].

MPC allows for administration of constraints and disturbances [66]. However, there are also several disadvantages of MPC as it has both high algorithmic and computational complexity [67]. Furthermore, its performance is highly dependant on plant-model accuracy [68].

2.7.1 Receding Horizon Controller (RHC)

Receding Horizon Control (RHC) is a feedback-based control scheme [69]. Here, at each time-step, the controller determines control actions for a fixed time-horizon, but only applies the first action of the plan. The next time-step, the horizon is shifted one step ahead and the process repeated. This is a nonlinear strategy that iteratively solves an optimization problem.

Optimization problem formulation:
Using [70] as a template, for a set of differential equations;

$$\dot{\mathbf{x}} = \mathbf{f}(\mathbf{x}(t), \mathbf{u}(t)), \quad \mathbf{x}(0) = \mathbf{x}_0,$$

with the state-and input-constraints $\mathcal{X} \subseteq \mathbb{R}^n, \mathcal{U} \subseteq \mathbb{R}^m$. The optimal control problem can be formulated as

$$\min_{\mathbf{u}} J(\mathbf{x}(t_0), \mathbf{u})$$

$$\begin{aligned} \text{Subject to:} \quad & \dot{\bar{\mathbf{x}}}(\tau) = \mathbf{f}(\bar{\mathbf{x}}(\tau), \bar{\mathbf{u}}(\tau)), \quad \bar{\mathbf{x}}(t_0) = \mathbf{x}(t_0) \\ & \bar{\mathbf{u}}(\tau) \in \mathcal{U}, \quad \forall \tau \in [t_0, t_0 + T_c] \\ & \bar{\mathbf{u}}(\tau) = \bar{\mathbf{u}}(\tau + T_c), \quad \forall \tau \in [t_0 + T_c, t_0 + T_p] \\ & \bar{\mathbf{x}}(\tau) \in \mathcal{X}, \quad \forall \tau \in [t_0, t_0 + T_p], \end{aligned}$$

where J is the cost-function and T_p and T_c are the prediction and control horizons, respectively. The bar denotes that the variables are used inside the controller as opposed to being states of the real system. There are also some additional assumptions made for the input- and state-constraints.

Time-horizons:
The controller predicts the behavior over a *prediction horizon* (T_p) and determines the input over a control horizon (T_c) [70]. The relation between them is $T_c \leq T_p$. Beyond the control horizon, the control values can be assigned as the latest control horizon value.

It is desirable to maintain a small horizon, as this results in a lower computational cost when performing the on-line optimization [70]. However, this is not without liabilities, as when a finite prediction horizon is used, predicted open-loop trajectories will disagree with the real trajectory.

2.7.2 State Estimators

The MPC formulation above assumes that the states are available from measurements [70]. This is generally not true and a state estimator (observer) needs to be included. In this case, you need to determine an observer type, as well as consider the observer stability properties.

2.7.3 Different MPC Schemes

An MPC scheme may be categorized as either linear or non-linear based on the system dynamics, constraints and objective function. Linear MPC allows for formulating the resulting optimization problem as one efficiently solved by quadratic programming [71].

Non-linear MPC requires more computation due to iterative linearization and may only arrive at an approximate solution [72]. Beyond these categories, there are variants addressing different aspects of the control scheme. Below, some examples are provided:

I. *Adaptive MPC* is a control scheme which addresses the aspect of reliance on plant model accuracy [73]. This is achieved by using input-output data to adjust model parameters.

II. *Robust MPC* is a conservative control strategy that deals with uncertainty in the constraints, system model or objective function. It aims to guarantee that despite uncertainties, the predicted sequence of states and control actions satisfy the constraints and minimizes the "worst-case" cost [74].

III. *Economic MPC* is a control scheme which alters the objective function to simultaneously perform economic process optimization and process control [75]. With this method, economy-related information is incorporated explicitly in the objective function, rather than embedded in set-points [76].

2.7.4 MPC for Batteries

Using economic non-linear MPC, Zou et al. [28] investigates the power-capability of lithium-ion batteries. They use a high-fidelity model capturing both non-linear electrical and thermal dynamics. They're able to estimate the power-capability with errors subsiding 0.2%. The controller is also able to protect the battery from undesirable reactions.

Some of the same authors also published a paper [77], in which an electrochemical-thermal Linear Time Varying (LTV) model is used for fast charging through an MPC-scheme. The authors suggest that this scheme is superior to CC-CV and MCC as it can charge faster while protecting the battery from side-reactions.

In [78], Xavier and Trimboli use MPC to construct a CC-CV fast-charging profile. The authors state that the controller displays an acceptable performance. The paper investigates the effect of the prediction and control horizons. Their simulation suggests that the control horizon makes no apparent difference on the SOC-performance. However, the prediction horizon has an influential effect.

3 Simulation Models

This chapter elaborates on the MATLAB/Simulink and Simcenter Amesim models used for the sensitivity analysis in the upcoming chapter, Chapter 4. Some details may be omitted due to confidentiality.

3.1 MATLAB/Simulink Model

The MATLAB/Simulink model can be divided into two parts: a thermal and an electrical part. The thermal part is coupled with the electrical model in a state-space description.

The complete model consists of six parallel-connected packs. Each pack has n_p strings in parallel, where each string has n_s cells in series. For computational efficiency, each pack is represented by *a single* cell. The computations for both the electrical- and the thermal model are then performed on the cell-scale. To then observe the system on an ESS-level, the model is scaled with constants. Cell-to-cell interactions within packs are then undetected, and only pack electrical interactions are captured. A rough sketch is presented in Figures 4 and 5.

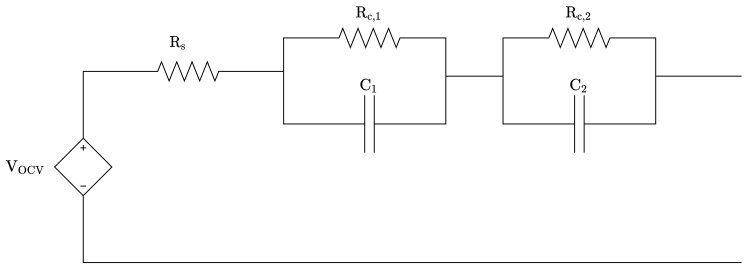

Figure 4: The second order RC model used in the analysis.

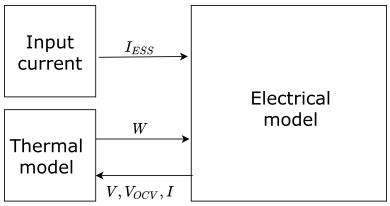

Figure 5: The interaction between the thermal and electrical models.

More specifically, the system is described by an LPV state-space model based on a second order ECM with hysteresis

$$\dot{x}(t) = A(p)x(t) + B(p)u(t)$$
$$y(t) = C(p)x(t) + D(p)u(t).$$

The state-vector contains five states for each cell, while the input-vector contains the total demanded current (I_{dem}) and a quantity related to the thermal dynamics in each cell (W). Assuming that N cells are connected in parallel

$$x(t) = \begin{bmatrix} x_1(t) \\ x_2(t) \\ \vdots \\ x_N(t) \end{bmatrix}, \quad x_i(t) = \begin{bmatrix} V_{RC1,i}(t) \\ V_{RC2,i}(t) \\ V_{\text{OCV},i}(t) \\ \text{SOC}_i(t) \\ T_{c,i}(t) \end{bmatrix}, \quad u(t) = \begin{bmatrix} I_{\text{dem}}(t) \\ W_1(t) \\ \vdots \\ W_N(t) \end{bmatrix}.$$

The model allows for custom current-profiles and individual initialization of cells' SOC, temperature and SOH. Furthermore, the model allows for specification of the number

of cells in series and parallel. All packs have the same configuration and all cells in a pack are identical. However, cell-specification between packs can differ. The model used in the sensitivity analysis consists of six packs in parallel. The model structure for two packs is presented in Figure 6.

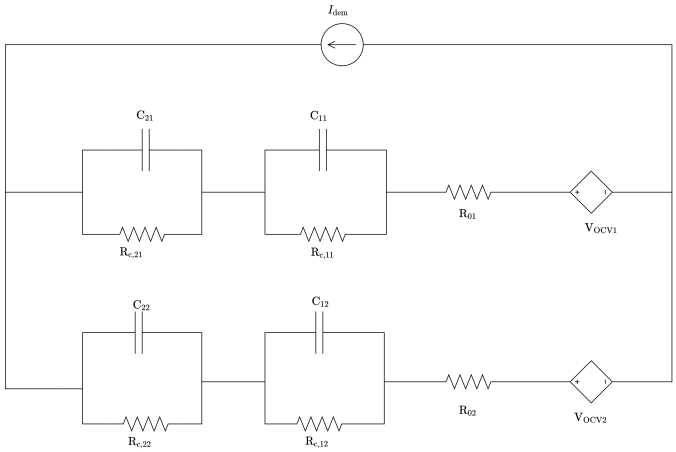

Figure 6: Two parallel-connected battery cells (or packs).

The state-space model for two packs in parallel is described by

$$\dot{x} = A(p)x(t) + B(p)u(t)$$
$$y = C(p)x(t) + D(p)u(t),$$

where

$$A = \begin{bmatrix} A_{11} & A_{12} \\ A_{21} & A_{22} \end{bmatrix}, \quad B = \begin{bmatrix} B_1 \\ B_2 \end{bmatrix}$$

$$C = \frac{1}{\Omega}\begin{bmatrix} -1 & -1 & -1 & 0 & 0 & 1 & 1 & 1 & 0 & 0 \\ 1 & 1 & 1 & 0 & 0 & -1 & -1 & -1 & 0 & 0 \end{bmatrix}, \quad D = \frac{1}{\Omega}\begin{bmatrix} R_{02} & 0 & 0 \\ R_{01} & 0 & 0 \end{bmatrix}$$

$$A_{11} = \frac{1}{\Omega}\cdot\begin{bmatrix} \frac{R_{01}+R_{02}+R_{11}}{R_{11}C_{11}} & \frac{1}{C_{11}} & \frac{1}{C_{11}} & 0 & 0 \\ \frac{1}{C_{21}} & \frac{R_{01}+R_{02}+R_{21}}{R_{21}C_{21}} & \frac{1}{C_{21}} & 0 & 0 \\ \frac{1}{C_{01}} & \frac{1}{C_{01}} & \frac{1}{C_{01}} & 0 & \Omega\cdot a_{\tau 1}\frac{\partial V_{\mathrm{OCV1}}}{\partial T_1} \\ \frac{\eta_1}{3600Q_1} & \frac{\eta_1}{3600Q_1} & \frac{\eta_1}{3600Q_1} & 0 & 0 \\ 0 & 0 & 0 & 0 & \Omega\cdot a_{\tau 1} \end{bmatrix}, \quad A_{12} = -\frac{1}{\Omega}\begin{bmatrix} \frac{1}{C_{11}} & \frac{1}{C_{11}} & \frac{1}{C_{11}} & 0 & 0 \\ \frac{1}{C_{21}} & \frac{1}{C_{21}} & \frac{1}{C_{21}} & 0 & 0 \\ \frac{1}{C_{01}} & \frac{1}{C_{01}} & \frac{1}{C_{01}} & 0 & 0 \\ \frac{\eta_1}{3600Q_1} & \frac{\eta_1}{3600Q_1} & \frac{\eta_1}{3600Q_1} & 0 & 0 \\ 0 & 0 & 0 & 0 & 0 \end{bmatrix}$$

$$A_{21} = -\frac{1}{\Omega}\begin{bmatrix} \frac{1}{C_{12}} & \frac{1}{C_{12}} & \frac{1}{C_{12}} & 0 & 0 \\ \frac{1}{C_{22}} & \frac{1}{C_{22}} & \frac{1}{C_{22}} & 0 & 0 \\ \frac{1}{C_{02}} & \frac{1}{C_{02}} & \frac{1}{C_{02}} & 0 & 0 \\ \frac{\eta_2}{3600Q_2} & \frac{\eta_2}{3600Q_2} & \frac{\eta_2}{3600Q_2} & 0 & 0 \\ 0 & 0 & 0 & 0 & 0 \end{bmatrix}, \quad A_{22} = \frac{1}{\Omega}\cdot\begin{bmatrix} \frac{R_{01}+R_{02}+R_{12}}{R_{12}C_{12}} & \frac{1}{C_{12}} & \frac{1}{C_{12}} & 0 & 0 \\ \frac{1}{C_{22}} & \frac{R_{01}+R_{02}+R_{21}}{R_{22}C_{22}} & \frac{1}{C_{22}} & 0 & 0 \\ \frac{1}{C_{02}} & \frac{1}{C_{02}} & \frac{1}{C_{02}} & 0 & \Omega\cdot a_{\tau 2}\frac{\partial V_{\mathrm{OCV2}}}{\partial T_2} \\ \frac{\eta_2}{3600Q_2} & \frac{\eta_2}{3600Q_2} & \frac{\eta_2}{3600Q_2} & 0 & 0 \\ 0 & 0 & 0 & 0 & \Omega\cdot a_{\tau 2} \end{bmatrix}$$

$$B_1 = \frac{1}{\Omega}\begin{bmatrix} \frac{R_{02}}{C_{11}} & 0 & 0 \\ \frac{R_{02}}{C_{21}} & 0 & 0 \\ \frac{R_{02}}{C_{01}} & \Omega\frac{\partial V_{\mathrm{OCV},1}}{\partial T_1} & 0 \\ \frac{\eta_1\cdot(R_{02})}{3600Q_1} & 0 & 0 \\ 0 & \Omega\cdot b_{\tau 1} & 0 \end{bmatrix}, \quad B_2 = \frac{1}{\Omega}\begin{bmatrix} \frac{R_{01}}{C_{12}} & 0 & 0 \\ \frac{R_{01}}{C_{22}} & 0 & 0 \\ \frac{R_{01}}{C_{02}} & 0 & \Omega\frac{\partial V_{\mathrm{OCV},2}}{\partial T_2} \\ \frac{\eta_2\cdot R_{01}}{3600Q_1} & 0 & 0 \\ 0 & 0 & \Omega\cdot b_{\tau 2} \end{bmatrix}.$$

and

- $\Omega = R_{01} + R_{02}$.
- η_1 and η_2 denote the Coulombic efficiency of pack 1 and 2, respectively.
- Q_1 and Q_2, denote the capacity of pack 1 and 2, respectively.
- T_1 and T_2, denote the temperature of pack 1 and 2, respectively.

3.1.1 Electrical Model

The electrical part is adapted for cylindrical battery cells based on lithium-ion chemistry, and uses lab-based data tables to aid in the dynamic description.

The time-varying matrices:
The state-space matrices A, B, C and D can vary with time through their dependency on the parameters R_0, R_1, R_2, C_1 and C_2. The parameter values are in turn calculated through look-up tables associated to temperature, SOC and current. R_0 is dependent on temperature and SOC, while the remaining parameters also include a dependency on current. There are five temperature-, six current- and 47 SOC-indices for the tables. For intermediate values, the algorithm performs interpolation.

The OCV Jacobians appear explicitly in the matrices. These are computed numerically offline. The calculations use forward and backward differentiation and stores the values in look-up tables. Again, interpolation is used for intermediate values. These derivatives are divided into charge- and discharge cases, but the model uses an average of the two.

$$\frac{\partial V_{\mathrm{OCV},i}}{\partial T_i} = \begin{cases} \dfrac{V_{\mathrm{OCV}_i}(k+1) - V_{\mathrm{OCV}_i}(k)}{T_i(k+1) - T_i(k)}, & \text{if } k = 1 \\ \dfrac{V_{\mathrm{OCV}_i}(k) - V_{\mathrm{OCV}_i}(k-1)}{T_i(k) - T_i(k-1)}, & \text{otherwise} \end{cases} \qquad \frac{\partial V_{\mathrm{OCV},i}}{\partial \mathrm{SOC}_i} = \begin{cases} \dfrac{V_{\mathrm{OCV}_i}(k+1) - V_{\mathrm{OCV}_i}(k)}{\mathrm{SOC}_i(k+1) - \mathrm{SOC}_i(k)}, & \text{if } k = 1 \\ \dfrac{V_{\mathrm{OCV}_i}(k) - V_{\mathrm{OCV}_i}(k-1)}{\mathrm{SOC}_i(k) - \mathrm{SOC}_i(k-1)}, & \text{otherwise} \end{cases}$$

State-of-Health (SOH):
The SOH of the cells is modeled through capacity fade ($\mathrm{SOH_E}$) and resistance increase ($\mathrm{SOH_P}$). The resistance increase affects all resistive components in the cell. The ageing is modeled as a *constant* scaling, hence does not change during run-time in the simulations.

3.1.2 Thermal Model

The thermal model describes internal heat generation and convection between the cell and both a coolant and ambient temperature, i.e. both forced and free convection is modeled. Recall the equation for temperature dynamics of an object, and the equation for rate of heat transfer

$$C_c \frac{dT_c}{dt} = q_c - \frac{T_c - T_a}{R_{ca}} - \frac{T_c - T_f}{R_{cf}}, \quad q_c = I \cdot (V_{\mathrm{OCV}} - V_T),$$

where:

- T_c is the cell temperature.
- T_a and T_f are the ambient and coolant temperatures, respectively.
- R_{ca} and R_{cf} are the thermal resistances, cell-ambient and cell-coolant, respectively.
- q_c is the heat generated in the cell.
- C_c is the thermal capacity of the cell.

Re-writing this equation

$$\dot{T}_c = \frac{1}{C_c}\left(q_c - \frac{T_c - T_a}{R_{ca}} - \frac{T_c - T_f}{R_{cf}}\right) \Leftrightarrow$$

$$\Leftrightarrow \dot{T}_c = \underbrace{\frac{1}{C_c}q_c + \frac{1}{C_c R_{ca}}T_a + \frac{1}{C_c R_{cf}}T_f}_{W} - T_c\left(\frac{1}{C_c R_{cf}} + \frac{1}{C_c R_{ca}}\right).$$

The quantity W is the output from the thermal model. However, it does not fully describe the heat generation. This is accomplished in the complete state-space description. Note that the thermal model does not include the thermal interaction between cells.

The user can specify the rate of coolant flow individually for each pack. This changes the heat-transfer resistance R_{cf} of the coolant. There are three coolant flow-rate indices from which intermediate values are interpolated.

3.2 Simcenter Amesim Model

The Simcenter Amesim setup should resemble the MATLAB/Simulink one to obtain comparable results in the final analysis. Look-up tables and parameter values from the aforementioned framework is provided to the Simcenter Amesim model. Figure 7 is a representative figure of the Simcenter Amesim model.

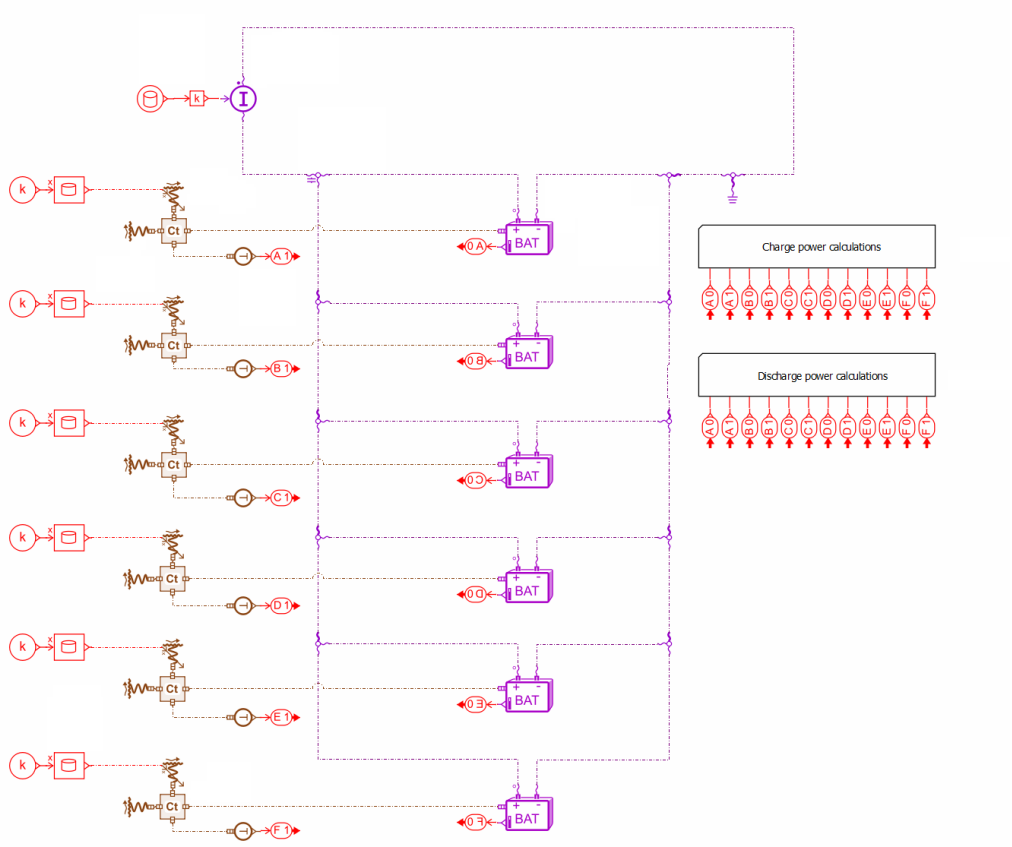

Figure 7: Representative figure of the Simcenter Amesim model.

The battery-pack modules are configured to include

- second-order RC models with dynamic parameters.
- OCV-temperature dependency.
- hysteresis modelling.
- static ageing through capacity fade and resistance increase.

Variation between packs is feasible through parameter manipulations. The thermal part is configured to include convection, both through a coolant and ambient temperature. This model includes reversible heat generation, which is a significant difference from the MATLAB/Simulink model.

For further details and explanations about the Simcenter Amesim model, please refer to Appendix C. This is especially recommended for readers unfamiliar with the Simcenter Amesim framework.

3.3 Power Estimation

The power estimation is performed through a look-up table dependent on temperature, SOC and time-horizon. The given time-horizons are: 2, 10 and 30 seconds. The tables are also divided into charge and discharge cases.

The tables specify single cell current-limits. Hence to obtain the power-limit, one can make an approximation in which the cell nominal voltage is multiplied.

3.4 Model Comparison

To compare the pack-models of the frameworks, let us conduct a test on two parallel-connected packs. Important measurements include: SOC, temperature and current distribution between the packs. In these tests Battery-Pack (BP) 1 is aged through capacity fade (-10%) and resistance increase ($+50\%$), which will cause varying current-split between the two packs. The applied total current is shown in Figure 8 and the resulting SOC, temperature and current-split are shown in Figures 9-11.

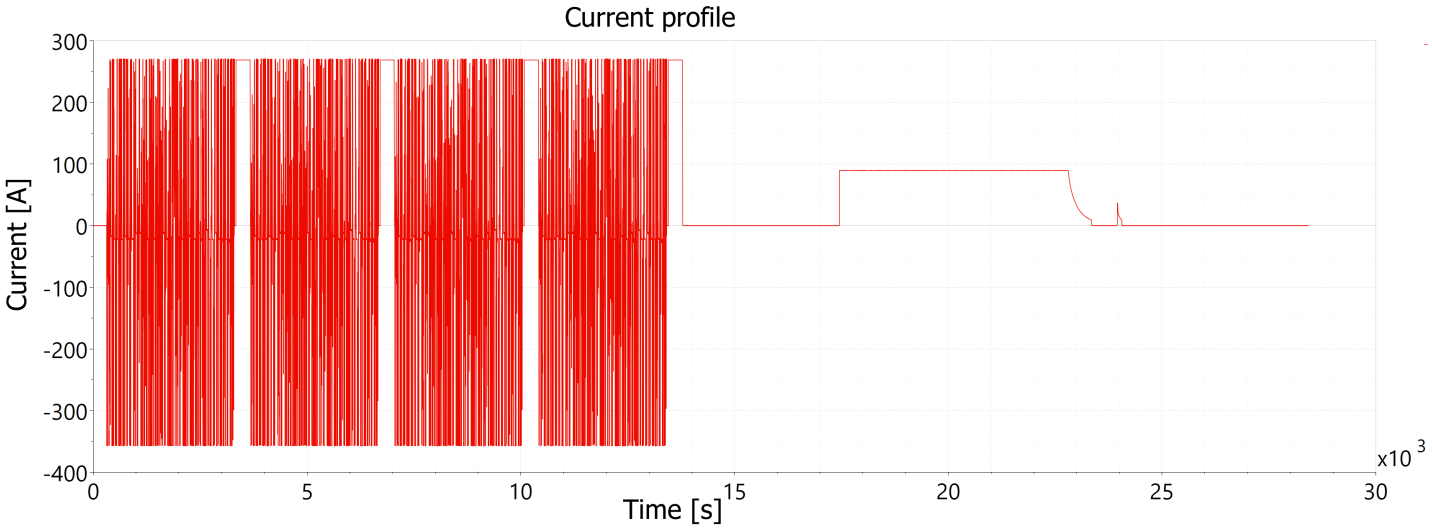

Figure 8: Dynamic current load-profile.

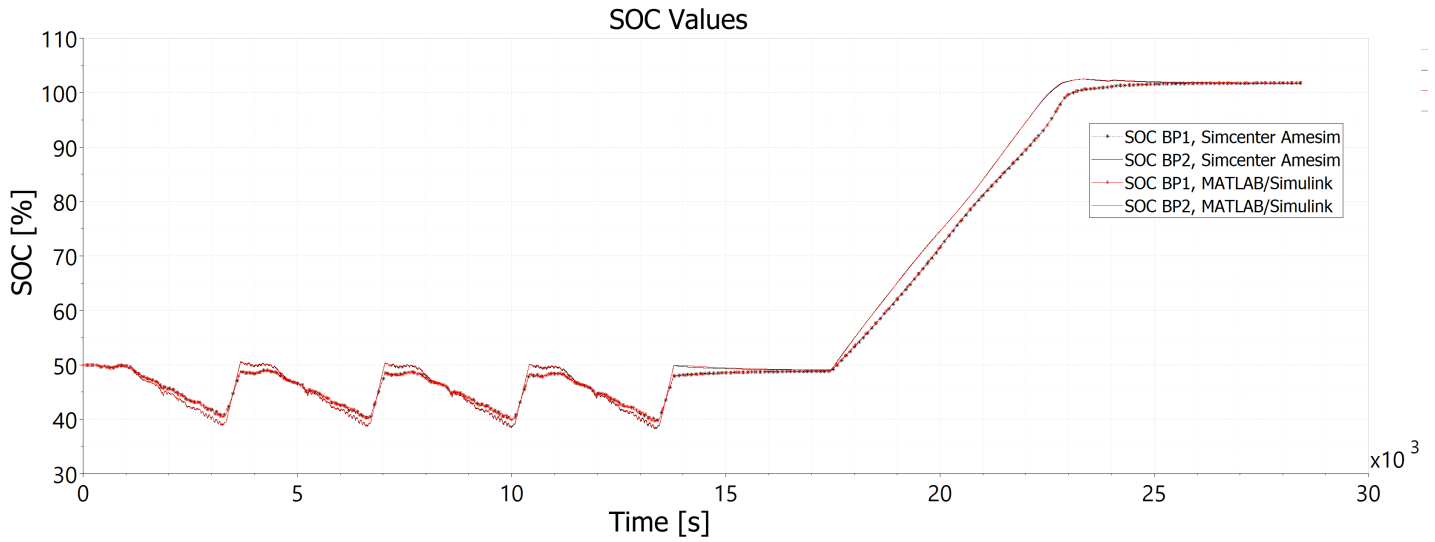

Figure 9: SOC of the models with dynamic load-profile and aging of pack 1.

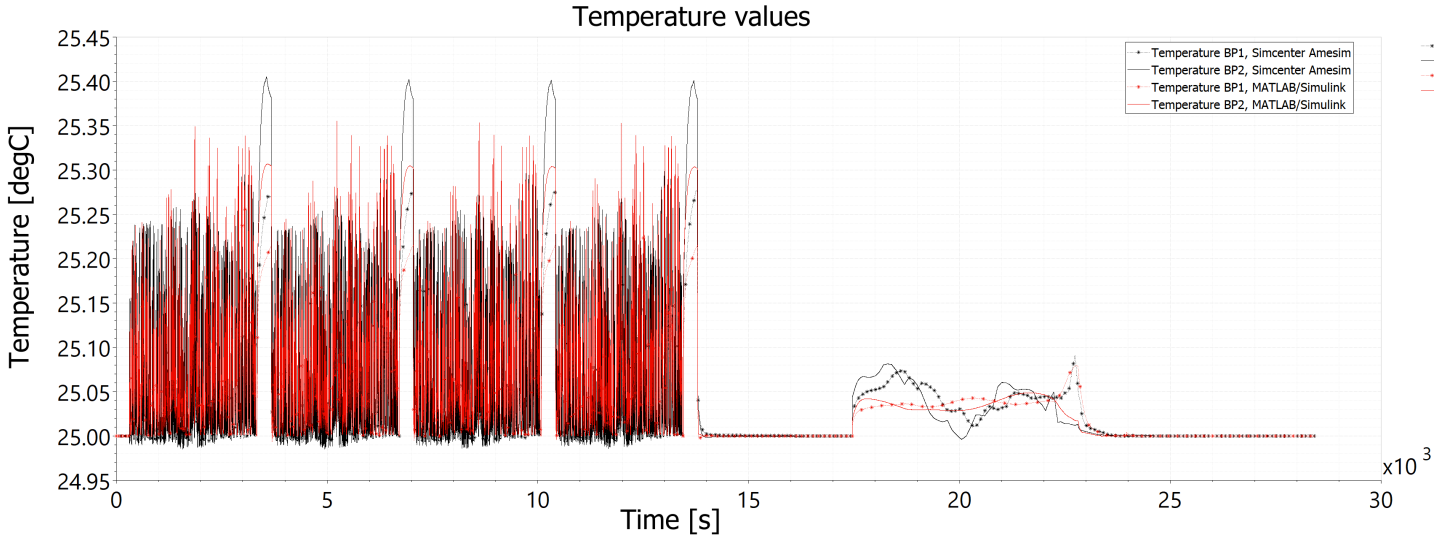

Figure 10: Temperature of the models with dynamic load-profile and aging of pack 1.

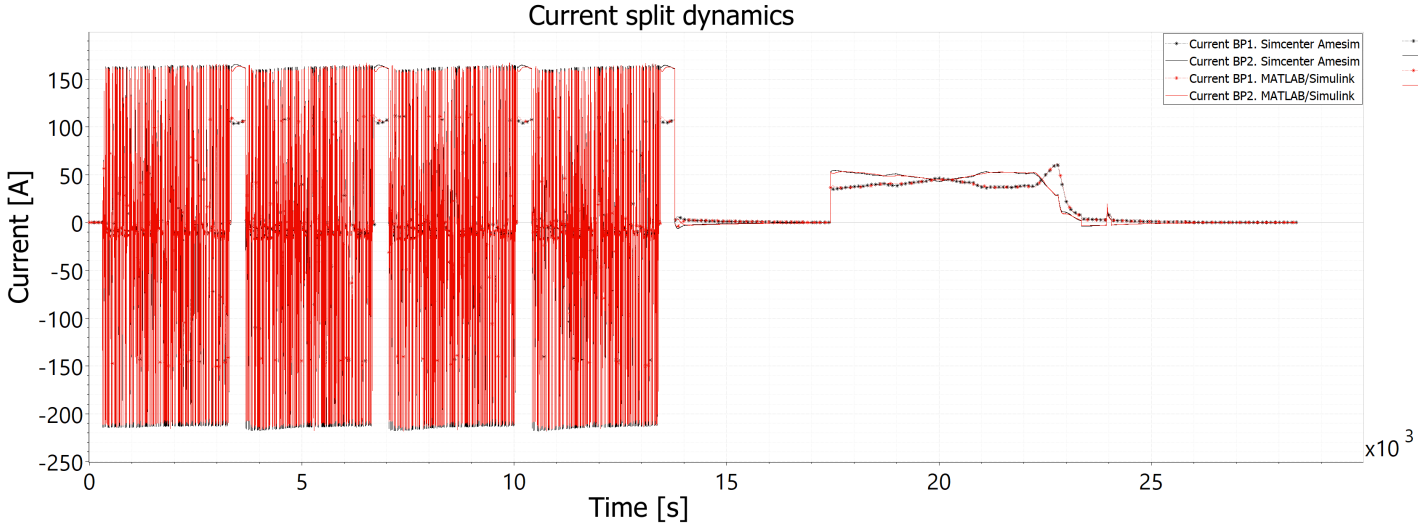

Figure 11: Current distribution of the models with dynamic load-profile and aging of pack 1.

There is a clear difference between the Simcenter Amesim and MATLAB/Simulink results. The differences are large enough to not be explained by different solvers or factors alike. The discrepancy can partly be explained by the two different thermal models in use, as the MATLAB/Simulink model does not model the entropic heat generation. This test is conducted with a Plug-in Hybrid Electric Vehicle (PHEV) drive-cycle. Hence, the reversible heat can be expected to be small, and even larger differences can be assumed for EV cycles (see Chapter 2.2.2).

4 Sensitivity Analysis

The sensitivity analysis aims to investigate the effect of battery-pack state/parameter heterogeneity on SOP. Influential states and parameters are discovered by varying them individually, and observing the effect on the SOP estimation.

Here, the sensitivity analysis is performed in two different frameworks: MATLAB/Simulink and Simcenter Amesim. Hence, this chapter includes two subsections where respective study is elaborated upon. Before that, we present the general procedure common for both methods.

4.1 General Outline

The analysis investigates the following state/parameter influence on the power-capability:

- Ageing through capacity fade and resistance increase.
- Coolant flow-rate.
- Coolant temperature.
- Initial temperature.
- Initial SOC.

The power-capability is considered for six parallel-connected battery-packs and three different time-horizons: 2, 10, and 30 seconds. The analysis is conducted with the load-profile shown in Figure 12, based on an EV drive-cycle.

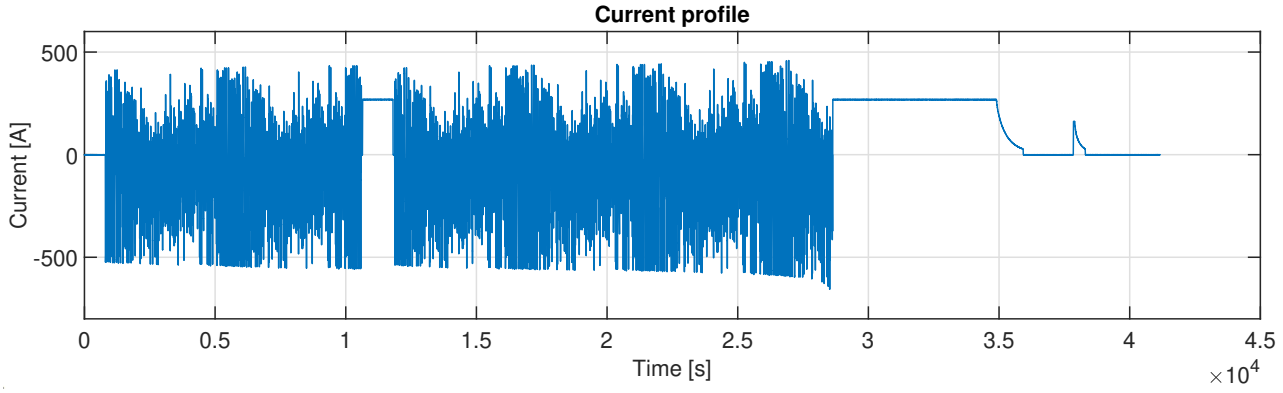

Figure 12: Current load-profile used in the sensitivity analysis.

All initial temperatures have nominal value of 25°C, and nominal SOC set to 70%. The pack is considered to be at its EOL at 80% capacity and 200% resistance. Hence in the analysis below, the packs are at their EOL values at 0% SOH.

Symbol	*Description*	*Values*
SOH_C	Ageing through capacity fade	[75%, 50% 25%, 0%]
SOH_R	Ageing through resistance increase	[75%, 50% 25%, 0%]
$V_{Coolant}$	Coolant flow rate	[80%, 90%, 110%, 120%]
$T_{Coolant}$	Coolant temperature	[21°C, 23°C, 27°C, 29°C]
T_0	Initial temperature	[21°C, 23°C, 27°C, 29°C]
SOC_0	Initial SOC	[63.0%, 66.5%, 73.5%, 77.0%]

Table 1: Table describing the parameters/states that are varied.

In the plots below and in the related appendices, *Battery-Pack 1* refers to the pack that experiences the heterogeneities. The remaining five packs are assumed to have identical behavior, hence an *"Equivalent pack"* is used to represent them.

4.2 Sensitivity Analysis using MATLAB/Simulink

For the general outline described above, the MATLAB/Simulink simulations show the following results. This chapter only presents results regarding Battery-Pack 1 (BP1) at $\Delta t = 2$ (time-horizon). Figures 13-17 show the difference in power-capability when varying the five states/parameters individually. The difference is obtained by subtracting the nominal value from the result. Please refer to Appendix A for the complete analysis.

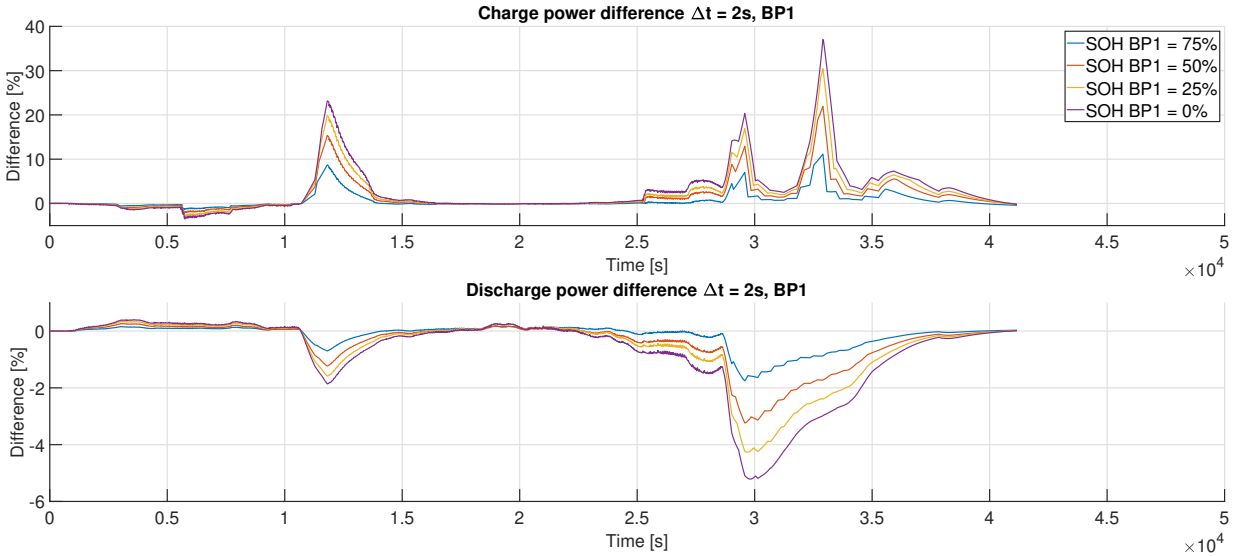

Figure 13: Difference from nominal SOP for 0, 25, 50 and 75% SOH using a 2s time-horizon for both charge and discharge case; MATLAB/Simulink framework.

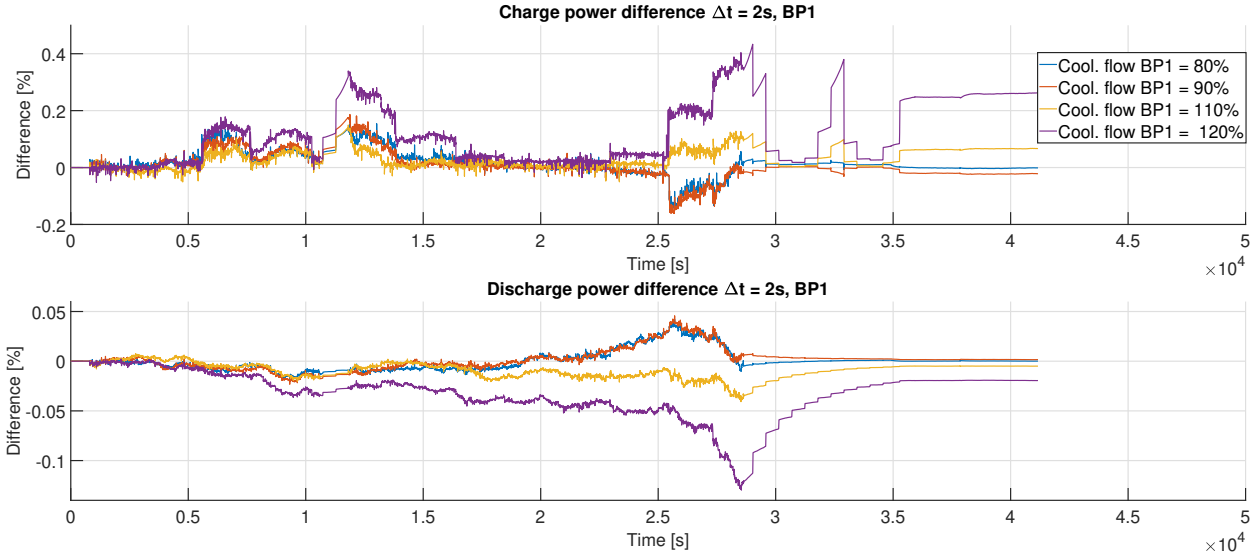

Figure 14: Difference from nominal SOP for 80, 90, 110 and 120% coolant flow-rate using a 2s time-horizon for both charge and discharge case; MATLAB/Simulink framework.

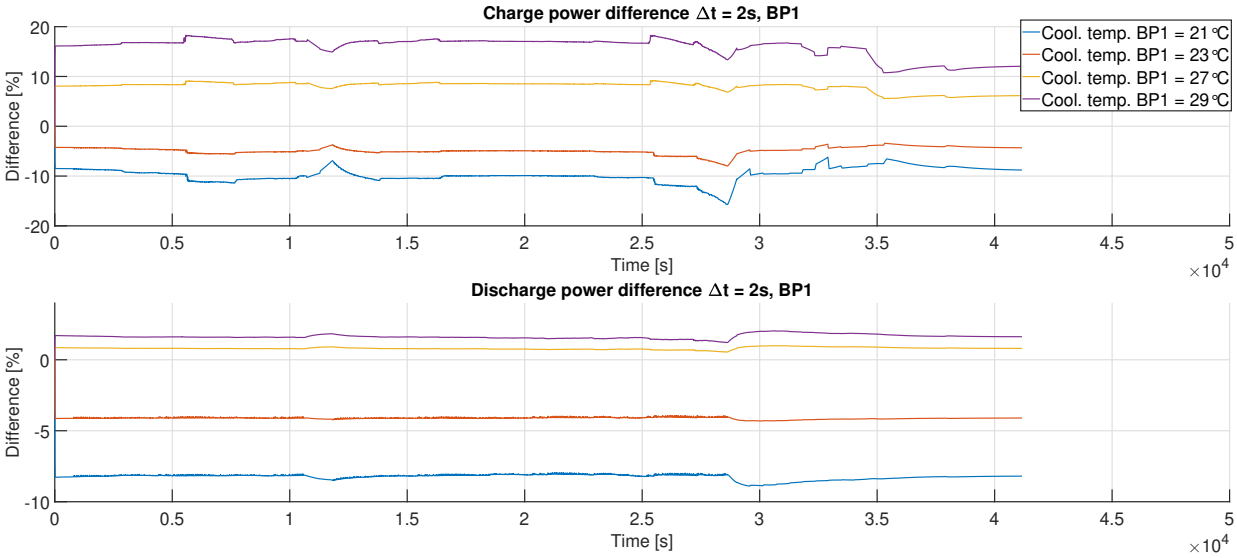

Figure 15: Difference from nominal SOP for 21, 23, 27 and 29 °C coolant temperature using a 2s time-horizon for both charge and discharge case. Nominal packs at nominal coolant temperature 25°C; MATLAB/Simulink framework.

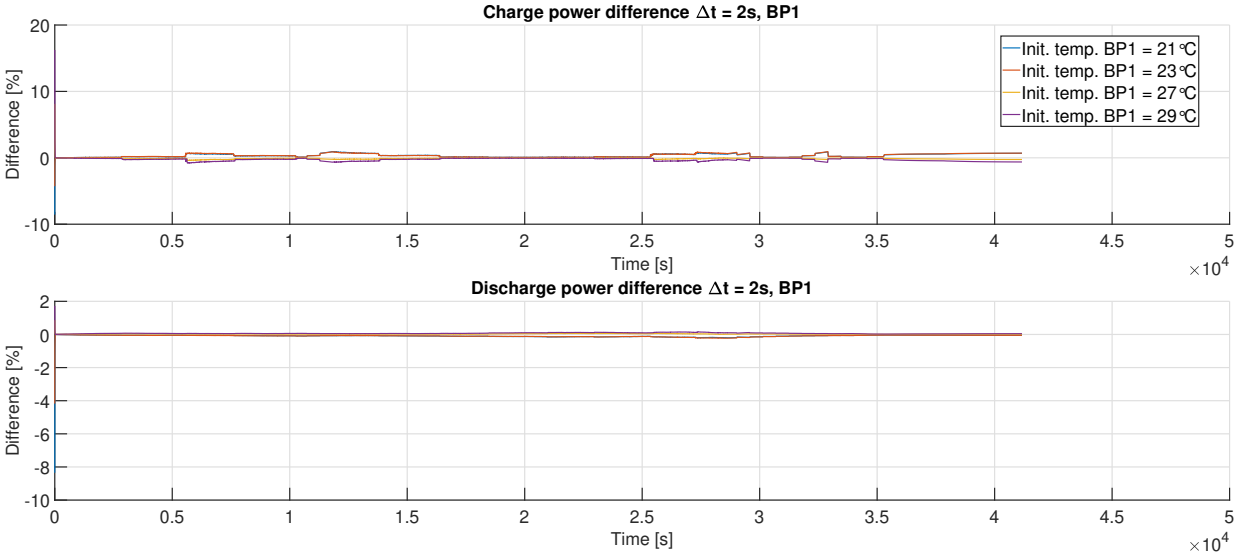

Figure 16: Difference from nominal SOP for 21, 23, 27 and 29 °C initial temperature using a 2s time-horizon for both charge and discharge case. Nominal packs at nominal initial temperature 25°C; MATLAB/Simulink framework.

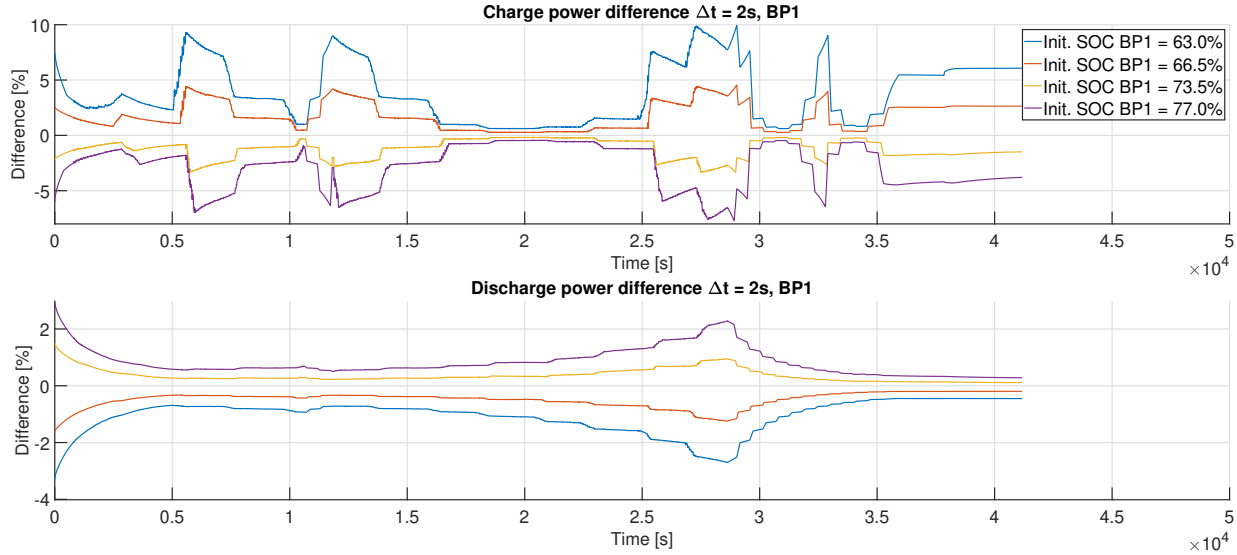

Figure 17: Difference from nominal SOP for 63.0, 66.5, 73.5 and 77% initial SOC using a 2s time-horizon for both charge and discharge case. Nominal packs at nominal initial SOC 70%; MATLAB/Simulink framework.

4.3 Sensitivity Analysis using Simcenter Amesim

For the general outline described above, the Simcenter Amesim simulations show the following results. This chapter only presents results regarding Battery-Pack 1 (BP1) at $\Delta t = 2$ (time-horizon). Figures 18-22 show the difference in power-capability when varying the five states/parameters individually. The difference is obtained by subtracting the nominal value from the result. Please refer to Appendix B for the complete analysis.

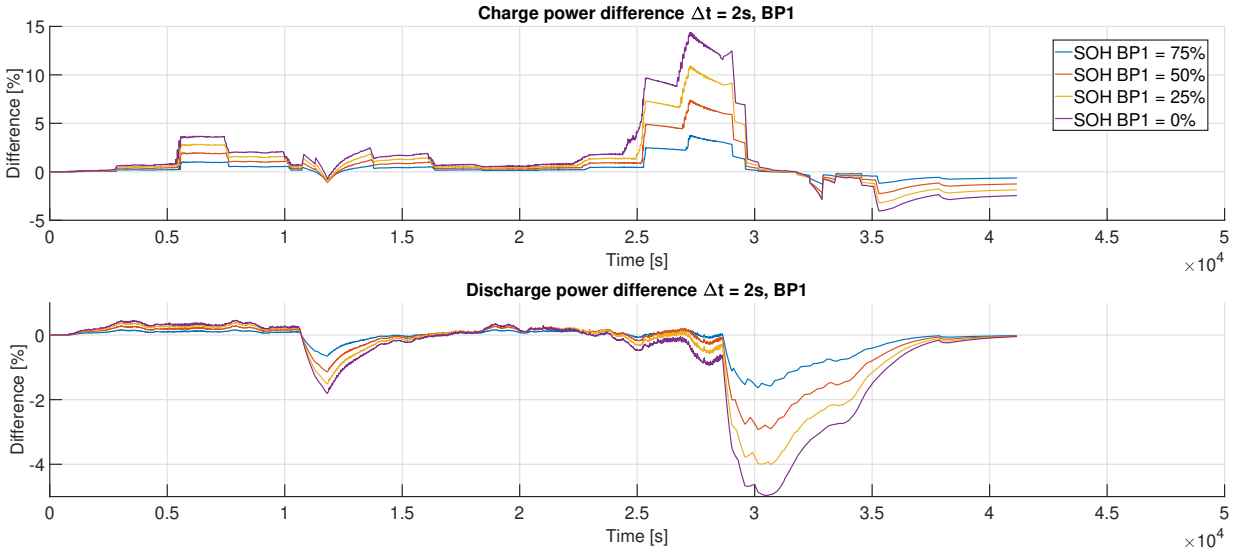

Figure 18: Difference from nominal SOP for 0, 25, 50 and 75% SOH using a 2s time-horizon for both charge and discharge case; Simcenter Amesim framework.

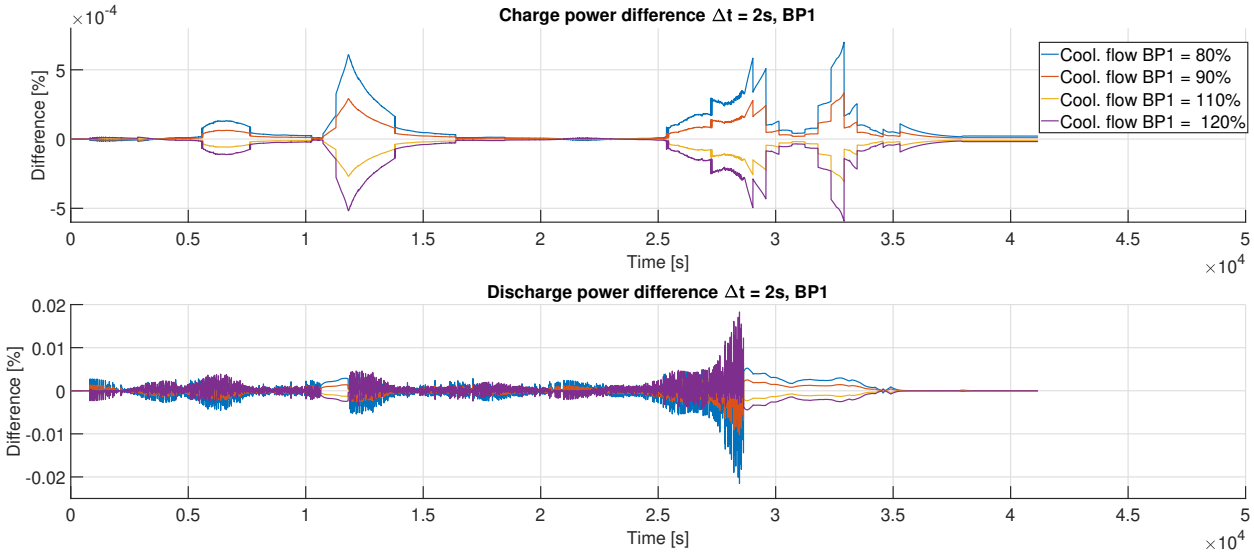

Figure 19: Difference from nominal SOP for 80, 90, 110 and 120% coolant flow-rate using a 2s time-horizon for both charge and discharge case; Simcenter Amesim framework.

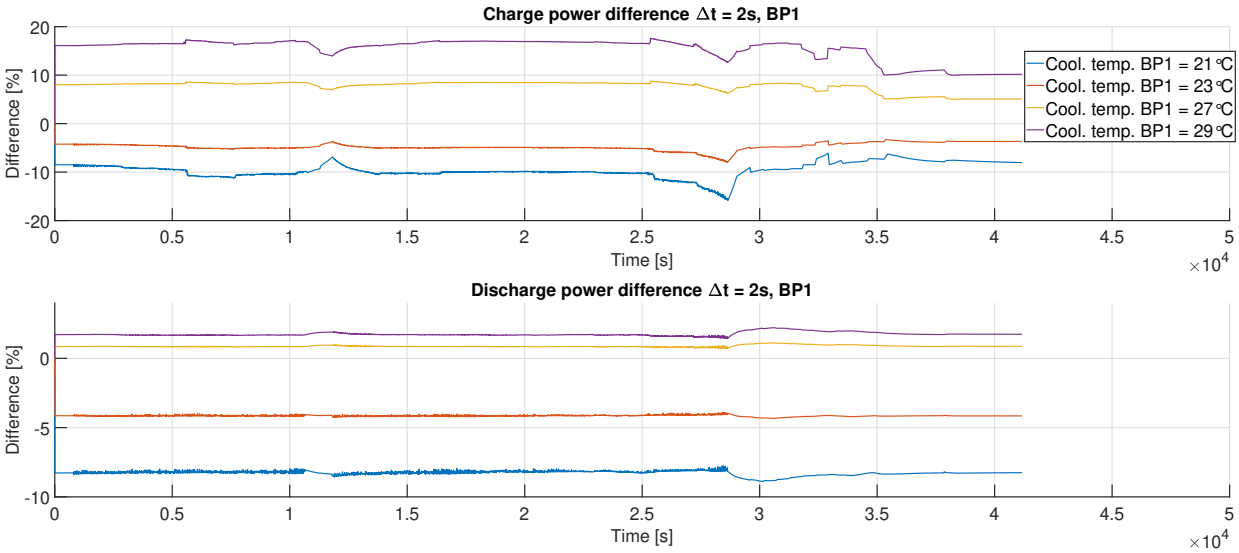

Figure 20: Difference from nominal SOP for 21, 23, 27 and 29 °C coolant temperature using a 2s time-horizon for both charge and discharge case. Nominal packs at nominal coolant temperature 25°C; Simcenter Amesim framework.

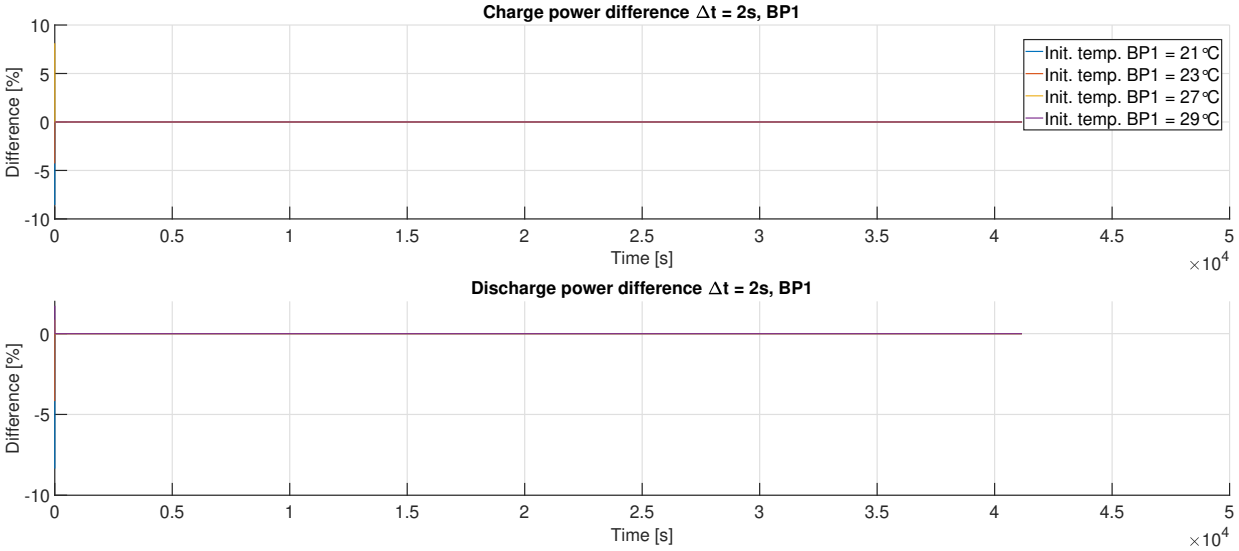

Figure 21: Difference from nominal SOP for 21, 23, 27 and 29 °C initial temperature using a 2s time-horizon for both charge and discharge case. Nominal packs at nominal initial temperature 25°C; Simcenter Amesim framework.

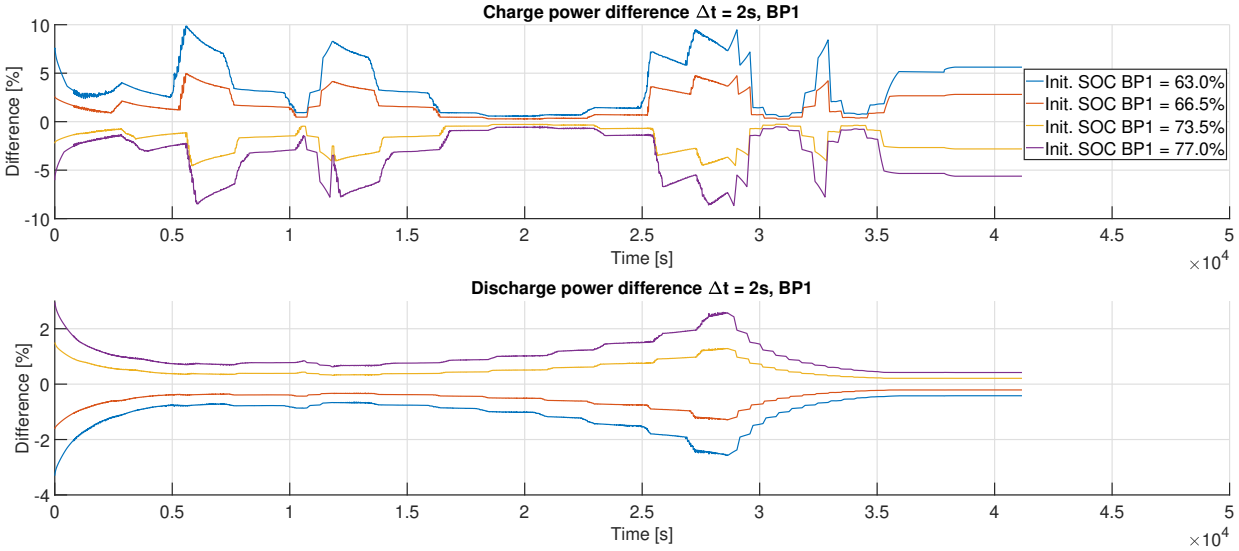

Figure 22: Difference from nominal SOP for 63.0, 66.5, 73.5 and 77% initial SOC using a 2s time-horizon for both charge and discharge case. Nominal packs at nominal initial SOC 70%; Simcenter Amesim framework.

4.4 Analysis and Conclusions

The results show that the two frameworks exhibit some similar and some dissimilar behavior. This should be expected, as explained in Chapter 3, the MATLAB/Simulink model does not include entropic heat generation. Since the power-calculations are directly related to the temperature, this can cause substantial effects, especially for an EV load cycle as used here (see Chapter 2.2.2).

One then needs to determine if the MATLAB/Simulink framework exhibits appropriate accuracy for the given application, as this model is potentially more computationally efficient. Otherwise measures need to be taken to make the thermal model more accurate, and further tests need to be conducted.

To understand the results and behavior of the power capability, it is appropriate to investigate the temperature and SOC behavior of the packs, as the power-limits are computed based on these two quantities. Let us investigate how these evolve during the simulations. The Simcenter Amesim model is reasonably the more accurate framework, hence these results are now used in the rest of the investigation. Figures 23-27 shows the difference in temperature and SOC when the varying the five states/parameters.

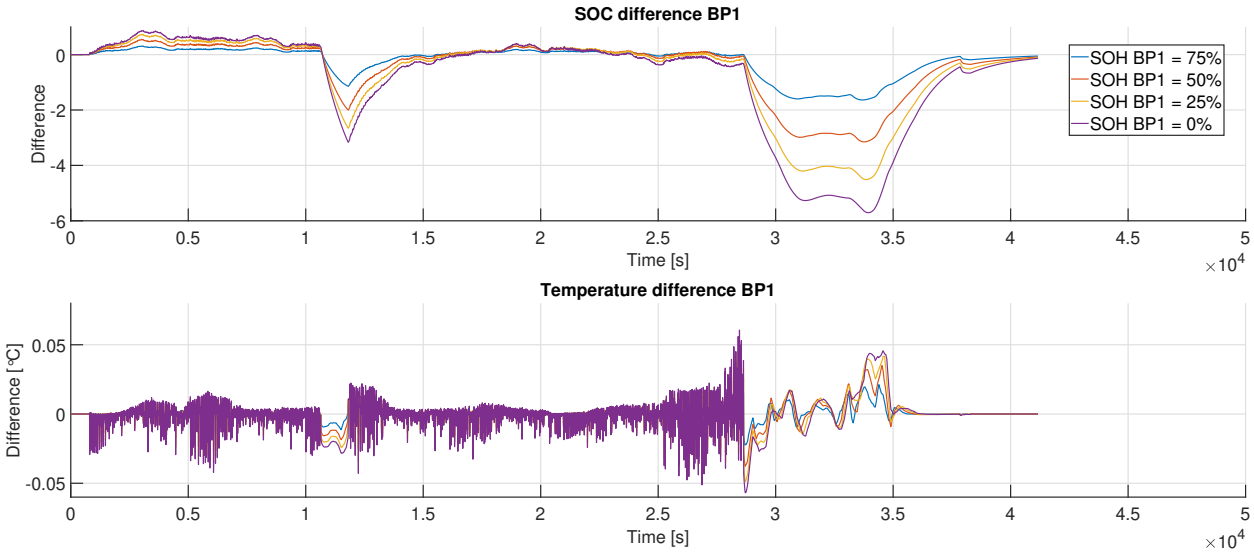

Figure 23: SOC and temperature deviation from nominal result for 0, 25, 50 and 75% SOH, in the Simcenter Amesim framework.

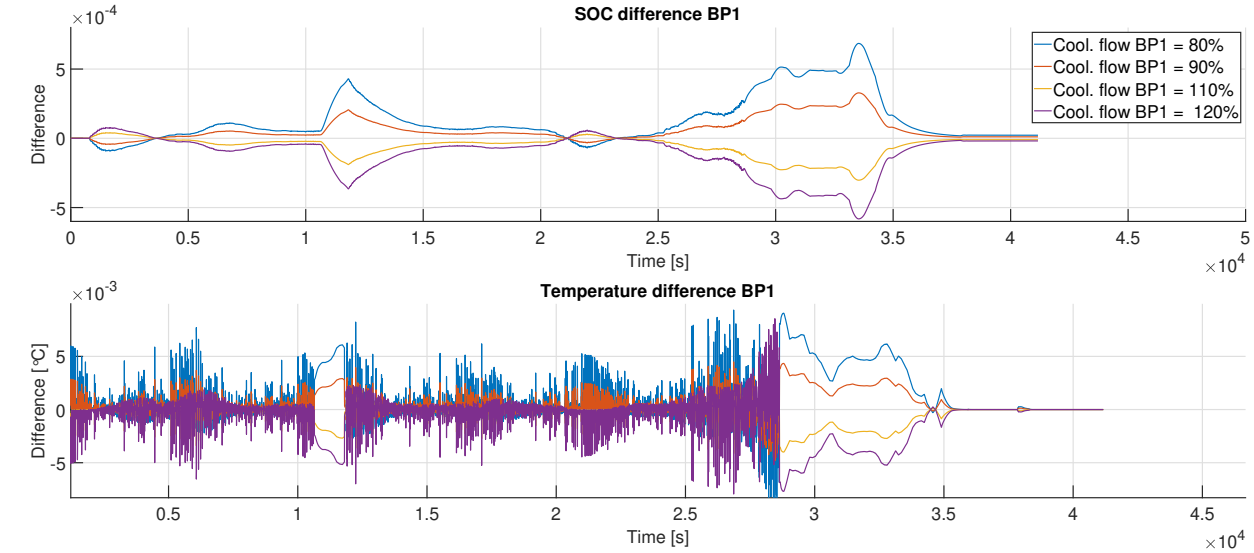

Figure 24: SOC and temperature deviation from nominal result for 80, 90, 110 and 120% coolant flow-rate, in the Simcenter Amesim framework.

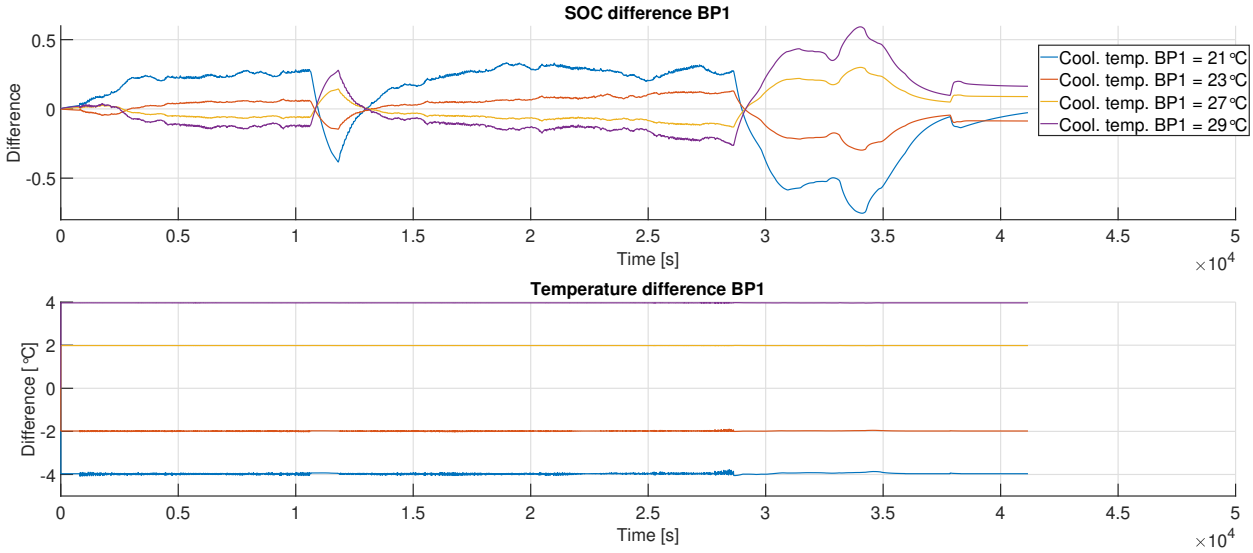

Figure 25: SOC and temperature deviation from nominal result for 21, 23, 27 and 29 °C coolant temperature. Nominal packs at nominal coolant temperature 25°C; Simcenter Amesim framework.

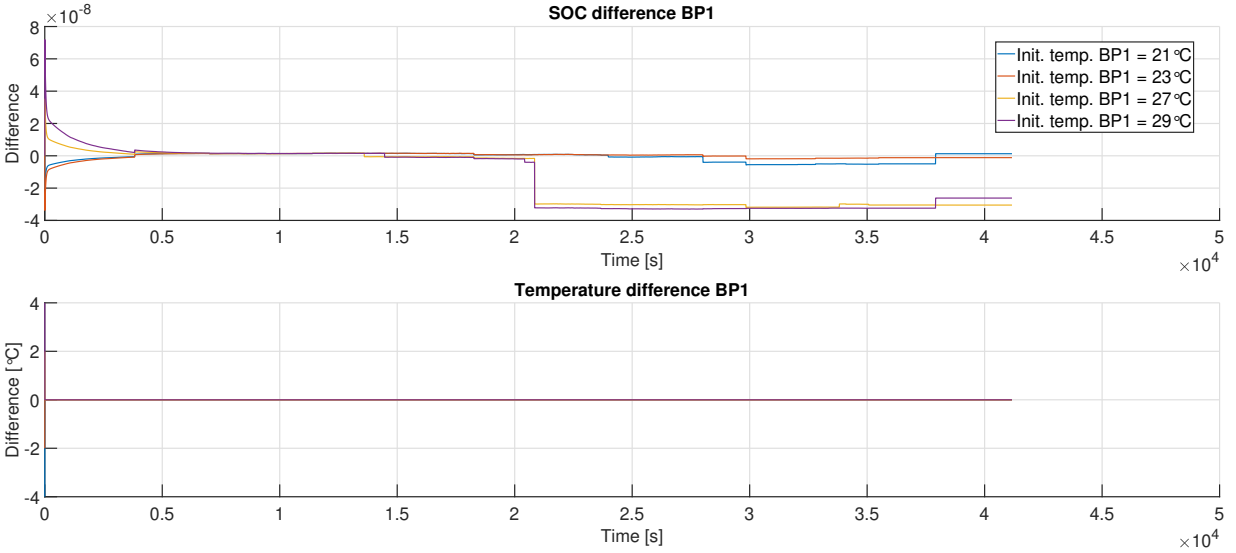

Figure 26: SOC and temperature deviation from nominal result for 21, 23, 27 and 29 °C initial temperature. Nominal packs at nominal initial temperature 25°C; Simcenter Amesim framework.

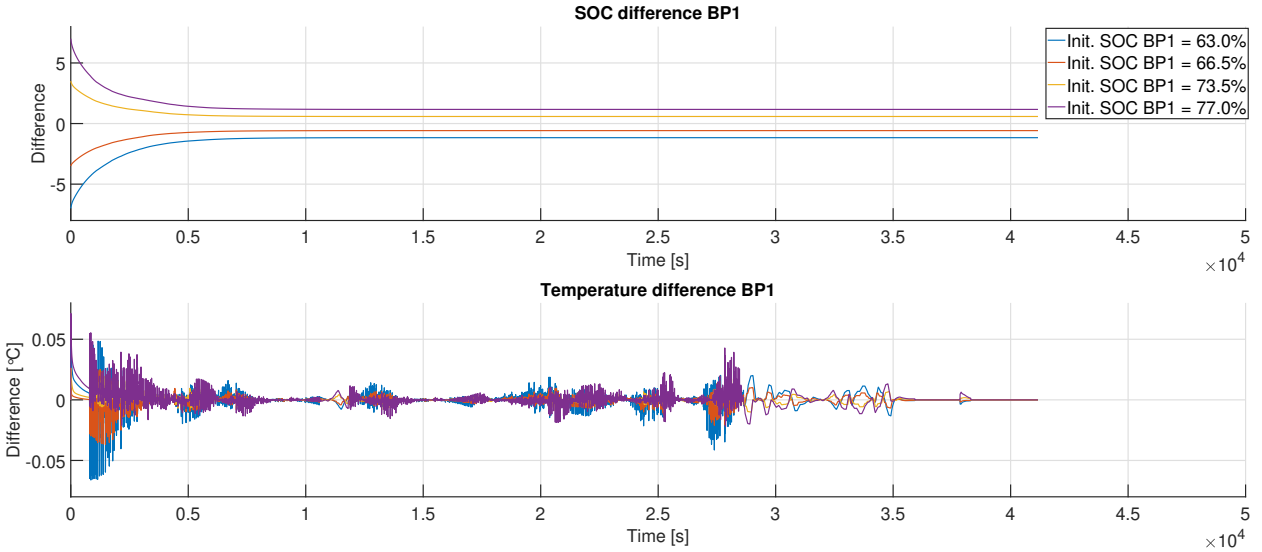

Figure 27: SOC and temperature deviation from nominal result for 63.0, 66.5, 73.5 and 77% initial SOC. Nominal packs at nominal initial SOC 70%; Simcenter Amesim framework.

From these plots one can clearly observe that if there are large temperature and/or SOC differences generated by the heterogeneity, then this can directly reflect on the power-capability of the battery-pack. Heterogeneity caused by aging (SOH), coolant temperature and initial SOC can greatly effect the power-capability.

The plots also suggest that the temperature equalization through coolant is quite effective, since the coolant temperature seems to dominate the temperature behavior. Furthermore, although restricting the coolant flow-rate affects the system, it does not have the same influence as some other heterogeneities.

Let us reflect upon each case individually:

- *SOH heterogeneity*:

  The aging of BP1 through capacity fade and resistance increase has a large effect on the discharge capability of all packs. Although there are some temperature variations in effect, the largest influence is clearly the varying SOC. When at its EOL, the pack can experience around a 6 unit SOC difference from its nominal run.

  While the effect on all packs is large, the power-capability of the aged pack is hampered to a larger degree. The peak discharge-SOP difference of the aged pack is larger for all time-horizons.

  Recall that (Chapter 2.1.3) power fade is calculated based on the resistance of the cell. Hence, most of the effect can be expected to be a result of the increasing resistance.

- *Coolant flow-rate heterogeneity*:

  The effect of coolant flow-rate variations on power-capability is small in comparison to some other parameter/state variations. This holds both during charge and discharge, and for all tested time-horizons.

  This small effect means that there is no need to investigate the differences in coolant flow-rate any further, hence it may be neglected in SOP estimations.

- *Coolant temperature heterogeneity*:

  In contrast to the first case, here the largest influence is the temperature. Because of the effectiveness of the cooling system, the temperature of the coolant dominates the temperature of the packs. Temperature affects, among other things, the internal resistance and OCV. Thus, it also affects the current distribution. A variation in SOC, although maybe small, is therefor inevitable.

  The higher coolant temperatures benefit both charge power and discharge power. Furthermore, compared to some other heterogeneities, this heterogeneity exhibits less sporadic behavior in both charge and discharge SOP for BP1.

  During prolonged charging, the discharge SOP of the nominal battery-packs seem to be negatively affected by increased temperature of BP1 (see Figure 75 in Appendix B). This may be related to the previously mentioned effect of temperature on current distribution.

- *Initial temperature heterogeneity*:

  Through the effectiveness of the cooling system in place, initial temperature variations are quite quickly recovered and the effects are therefore almost negligible. Hence, initial temperature differences can be neglected for most of the time.

- *Initial SOC heterogeneity*:

  Initial SOC difference can cause long-lasting effects on the battery system. A clear initial convergence to the nominal value can be seen in Figure 22. However, the power-capability also diverges at times. Especially, note the initial divergence of the discharge power for the nominal packs.

  Possibly due to the self-balancing effect, there is a gradual similarity in the power-capability between the heterogeneous and nominal packs. This is most noticeable in Figure 82 and Figure 83. Recall (Chapter 2.3.2) that if the load-current is large, then this can cause the SOC values of different packs to diverge, which might partly be what we are observing in these plots.

  With a positive offset on BP1, the SOC heterogeneity can provide additional charge available to the total system. This could elevate the discharge capability. Due to the aforementioned self-balancing effect, all battery-packs should experience a sustained positive discharge-SOP-offset from nominal, depending on the initial SOC of the heterogeneous BP.

  Here, the peak charge SOP-difference for BP1 decreases with increasing time-horizon. However, note that in this case also the nominal packs experience large charge SOP-differences.

In conclusion, the most significant state/parameter variations seem to be SOH, coolant temperature and SOC.

Note that, generally, when the difference in temperature against the nominal value is more significant, the two frameworks seem to produce more similar results. This may be due to the heterogeneities having a more significant effect in the heat generation than the entropic heat by itself. For the charge power with heterogeneity in the SOH, one can observe a more similar trend for the longer time-horizons 10, and 30 seconds (see Figure 44 and Figure 64).

5 Model Predictive Power Estimation

This chapter describes two Economic Model Predictive Control formulations for the power estimation of a multi-pack battery system. A simple battery model is used to represent the individual packs, which can potentially allow for high computational efficiency.

By utilizing a cell model and an associated current-split predictor, one can make predictions of the available power. The sensitivity analysis from the previous chapter, revealed that the differences in SOH (SOH_E and SOH_P), coolant temperature and initial SOC claim a significant role in the available power. Based on these insights the study assumes the following:

- There needs to be a consideration of the SOH in the model.
- The pack temperature is assumed to be constant and equal to the coolant temperature. Hence, the model does not need thermal computations or temperature as an input.
- There needs to be a consideration of the initial SOC-differences between the packs, as the self-balancing effect of the packs may not be sufficient.

Using a simple model for power estimation, will evidently lead to errors. This can cause violation of constraints or sub-optimal utilization of the battery-system. Although both are undesirable behaviors, the former may be of higher concern as it could damage the system. This is further elaborated on in the concluding remarks.

5.1 The Simplified Model

In the MATLAB/Simulink model used for the sensitivity analysis, the entire battery-pack was represented by a single cell and modeled with a second order RC-network. Here, each pack is modeled by an OCV-source in series with a resistance. For parallel-connected packs, the model is presented in Figure 28:

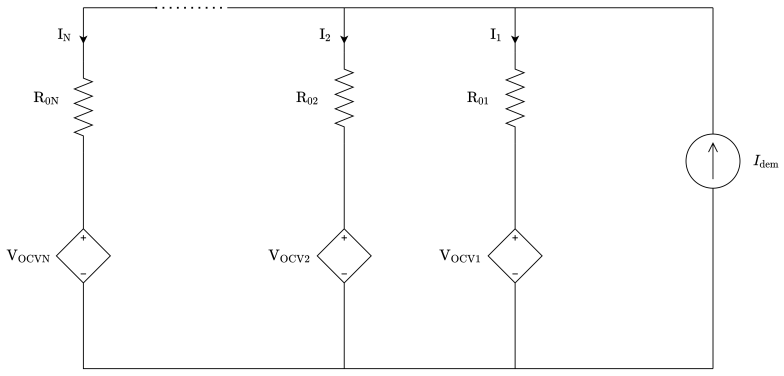

Figure 28: Simplified parallel-connected ESS model.

With the states $x_k = V_{\text{OCV}_k}$, outputs $y_k = I_k$ and input $u = I_{\text{dem}}$, the state-space description becomes

$$\dot{x}(t) = A(p)x(t) + B(p)u(t)$$
$$y(t) = C(p)x(t) + D(p)u(t).$$

The Open-Circuit-Voltage dynamics for pack k can be written as [39]

$$\dot{V}_{\mathrm{OCV}_k} = \frac{I_k}{C_{0,k}}, \quad C_{0,k} = 3600 Q_k \frac{d\mathrm{SOC}(V_{\mathrm{OCV}_k})}{dV_{\mathrm{OCV}_k}}.$$

To determine the current (I_k) received by each pack, an equation for the current distribution is needed. The current distribution in a system with two parallel-connected packs is given by [29, 30]

$$I_1 = \frac{R_{02}}{R_{01}+R_{02}} I_{\mathrm{dem}} + \frac{1}{R_{01}+R_{02}}(V_{\mathrm{OCV}_2} - V_{\mathrm{OCV}_1})$$
$$I_2 = \frac{R_{01}}{R_{01}+R_{02}} I_{\mathrm{dem}} + \frac{1}{R_{01}+R_{02}}(V_{\mathrm{OCV}_1} - V_{\mathrm{OCV}_2}).$$

The first term models the effect of resistance imbalance, while the second term captures the effect of OCV imbalance. In the case of N packs, the current distribution may be predicted as [29, 30]

$$I_k = \frac{1}{\phi} \prod_{i \neq k}^{N} R_{0i} \cdot I_{\mathrm{dem}} + \frac{1}{\phi} \sum_{i \neq k}^{N} \left((V_{\mathrm{OCV}_i} - V_{\mathrm{OCV}_k}) \cdot \prod_{\substack{j \neq k \\ j \neq i}}^{N} R_{0j} \right), \quad \phi = \sum_{k=1}^{N} \left(\prod_{i \neq k}^{N} R_{0i} \right).$$

The state-space model is now ready to be formulated for six packs

$$\dot{x} = \begin{bmatrix} \dot{V}_{\mathrm{OCV}_1} \\ \dot{V}_{\mathrm{OCV}_2} \\ \vdots \\ \dot{V}_{\mathrm{OCV}_6} \end{bmatrix} = A \cdot \begin{bmatrix} V_{\mathrm{OCV}_1} \\ V_{\mathrm{OCV}_2} \\ \vdots \\ V_{\mathrm{OCV}_6} \end{bmatrix} + B \cdot I_{\mathrm{dem}}.$$

The output is the pack-currents

$$y = \begin{bmatrix} I_1 \\ I_2 \\ \vdots \\ I_6 \end{bmatrix} = C \cdot \begin{bmatrix} V_{\mathrm{OCV}_1} \\ V_{\mathrm{OCV}_2} \\ \vdots \\ V_{\mathrm{OCV}_6} \end{bmatrix} + D \cdot I_{\mathrm{dem}}.$$

The resistances assume a constant temperature determined by the coolant, hence computed as $R_{0k} = R_{0k}(T_k, \mathrm{SOC}_k(t))$. The values are computed through look-up tables, which are provided from the more complex MATLAB/Simulink model introduced in Chapter 3. The resistances are multiplied by n_s/n_p and C_0 by n_p in order to scale them up to pack-level.

For the complete state-space description of six parallel-connected packs, with the matrices explicitly outlined, the reader is referred to Appendix D. Now that the state-space model is established, let us formulate the MPC description and the related optimization problem.

5.2 MPC Formulation

The overall structure for the power estimator can be illustrated as in Figure 29:

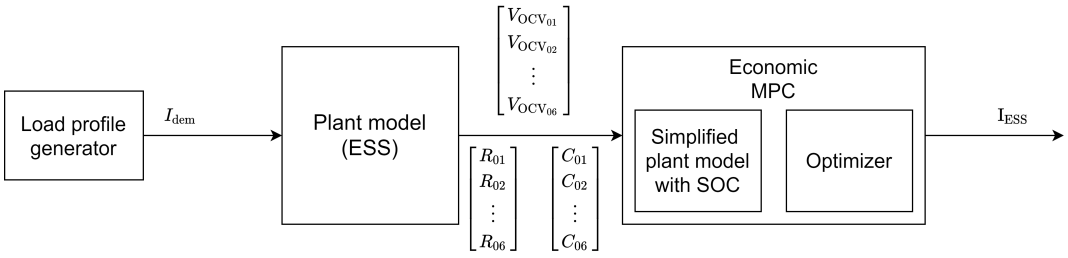

Figure 29: An overview of the plant model and power estimator.

Note that this is not a feed-back controller, but formulated as an Economic Model Predictive Control (EMPC) problem. To aid in the MPC formulation the parameters are assumed to be constant over the prediction horizon.

The objective is to maximize the charge and discharge power of the battery system over a pre-determined time-horizon. Each pack delivers the power $P_k = V_{T_k} \cdot I_k$, where V_{T_k} is the terminal voltage and calculated as

$$V_{T_k} = V_{\text{OCV}_k} + R_{0k} I_k.$$

The cost-function (J) can be formulated as

$$J = \sum_{k=1}^{N} |P_k| = \sum_{k=1}^{N} |V_{T_k} I_k|.$$

The optimization problem then becomes

$$\max_{\boldsymbol{I}_{\text{dem}}} J(\mathbf{x}(t_0), \boldsymbol{I}_{\text{dem}})$$

$$\begin{aligned}
\text{Subject to:} \quad & \dot{\boldsymbol{x}}(\tau) = A \cdot \boldsymbol{x}(\tau) + B \cdot I_{\text{dem}}(\tau), \\
& I_{\text{dem}}(\tau) = I_{\text{dem}}(t_0 + T_c), \quad \forall \tau \in [t_0 + T_c, t_0 + T_p] \\
& |I_{\text{dem}}(\tau)| \leq I_{\text{lim}}, \quad \forall \tau \in [t_0, t_0 + T_p] \\
& |y_k(\tau)| \leq y_{\text{lim}}, \quad \forall \tau \in [t_0, t_0 + T_p] \\
& V_{T_k}(\tau) \leq V_{\max}, \quad \forall \tau \in [t_0, t_0 + T_p] \\
& V_{T_k}(\tau) \geq V_{\min}, \quad \forall \tau \in [t_0, t_0 + T_p].
\end{aligned}$$

I_{lim} specifies the instantaneous current-limit for the complete ESS, while y_{lim} specifies the instantaneous current-limits for the individual packs. $V_{\min}$ and $V_{\max}$ specify the terminal voltage limits. A limit on the total system current (I_{lim}) could be relevant if parts of the system experience the full current-load e.g. potentially current conducting cables.

5.3 Simplified MPC with SOC

Recall that lithium-ion batteries are sensitive to over- charging/discharging (see Chapter 2.5). Hence, there is a motivation to also consider the SOC-limits when formulating the

MPC problem, especially for long time-horizons. The simplified model can be extended with a state for the SOC of each pack. The SOC-dynamics of pack k can be calculated as [39]

$$\dot{\mathrm{SOC}}_k = \frac{1}{3600 Q_k} \cdot I_k.$$

Adding this to the state-space description above, the extended model becomes

$$\dot{x} = \begin{bmatrix} \dot{x}_1 \\ \dot{x}_2 \\ \vdots \\ \dot{x}_6 \end{bmatrix} = A \cdot \begin{bmatrix} x_1 \\ x_2 \\ \vdots \\ x_6 \end{bmatrix} + B \cdot I_{\mathrm{dem}}, \quad x_k = \begin{bmatrix} V_{\mathrm{OCV}_k} \\ \mathrm{SOC}_k \end{bmatrix}.$$

The output of the model does not change, hence

$$y = \begin{bmatrix} I_1 \\ I_2 \\ \vdots \\ I_6 \end{bmatrix} = C \cdot \begin{bmatrix} x_1 \\ x_2 \\ \vdots \\ x_6 \end{bmatrix} + D \cdot I_{\mathrm{dem}}, \quad x_k = \begin{bmatrix} V_{\mathrm{OCV}_k} \\ \mathrm{SOC}_k \end{bmatrix}.$$

The overall structure does not change significantly. As an additional input, the controller receives the SOCs from the plant at each control-interval, as illustrated in Figure 30:

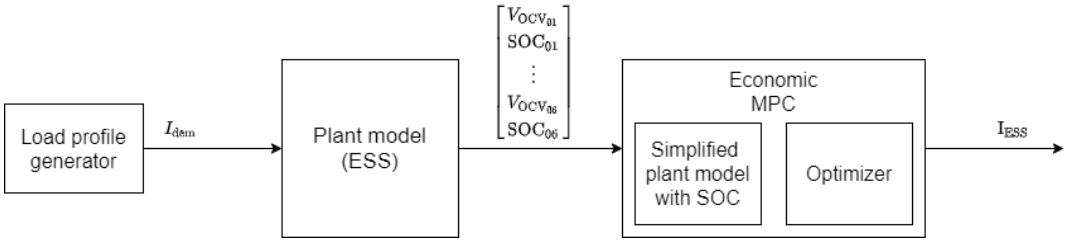

Figure 30: An overview of the plant model and power estimator with SOC included.

Again, the complete state-space matrices are not presented here. For an elaboration on the model and the matrices explicitly outlined, the reader is referred to Appendix D. The optimization problem can also include SOC constraints. The resulting optimization problem is very similar to the previous

$$\max_{\boldsymbol{I}_{\mathrm{dem}}} J(\mathbf{x}(t_0), \boldsymbol{I}_{\mathrm{dem}})$$

$$\begin{aligned}
\text{Subject to:} \quad & \dot{\boldsymbol{x}}(\tau) = A \cdot \boldsymbol{x}(\tau) + B \cdot I_{\mathrm{dem}}(\tau), \\
& I_{\mathrm{dem}}(\tau) = I_{\mathrm{dem}}(t_0 + T_c), \quad \forall \tau \in [t_0 + T_c, t_0 + T_p] \\
& |I_{\mathrm{dem}}(\tau)| \leq I_{\mathrm{lim}}, \quad \forall \tau \in [t_0, t_0 + T_p] \\
& |y_k(\tau)| \leq y_{\mathrm{lim}}, \quad \forall \tau \in [t_0, t_0 + T_p] \\
& V_{T_k}(\tau) \leq V_{\mathrm{max}}, \quad \forall \tau \in [t_0, t_0 + T_p] \\
& V_{T_k}(\tau) \geq V_{\mathrm{min}}, \quad \forall \tau \in [t_0, t_0 + T_p] \\
& \mathrm{SOC}_k(\tau) \leq \mathrm{SOC}_{\mathrm{max}}, \quad \forall \tau \in [t_0, t_0 + T_p] \\
& \mathrm{SOC}_k(\tau) \geq \mathrm{SOC}_{\mathrm{min}}, \quad \forall \tau \in [t_0, t_0 + T_p].
\end{aligned}$$

Extending the model, will naturally lead to higher computational complexity, hence a slower controller. One can note that the SOC state becomes relevant only at the limits. The controller can then be optimized by only using the SOC-states when close to the limits, thereby switching between the simplified model and this extended model during run-time.

The SOC problem may also be solved external to the EMPC. In a conservative approach, the pack with the lowest/highest SOC determines the maximum allowable current from/to the system. This assures that the pack does not over-charge/discharge.

A third way to reduce the complexity is by noting the symmetry between the OCV and SOC entries in the state-dynamics (see Appendix D). The entries simply differ by a factor. This observation could be utilized for a more generic state-space model, and use factors to calculate the state-dynamics of interest.

Note that, since the inclusion of SOC as a state does not change the electrical model, the MPC-formulation has not changed significantly. However, including additional model-components such as an RC-network will influence the current-split dynamics and change the formulation in a more substantial way, and potentially lead to higher computational complexity.

5.4 Experimental Setup

The results are divided into two main cases, one where the EMPC acts only as a predictor of the maximum allowable charge current, and a second case where the output of the EMPC is used as input for the plant model. Since the cases involve charging, the lower current-rate limit is set to 0. The voltage limits are set to about 510 and 760V. The ESS current-limit is 95% of the sum of all pack limits. The MATLAB/Simulink model used in the sensitivity analysis, is here used as the plant model.

Case 1: Only prediction
The current load-profile presented in Figure 31, allows for a fairly deep charge phase. This may provide some meaningful analysis when comparing the two EMPCs.

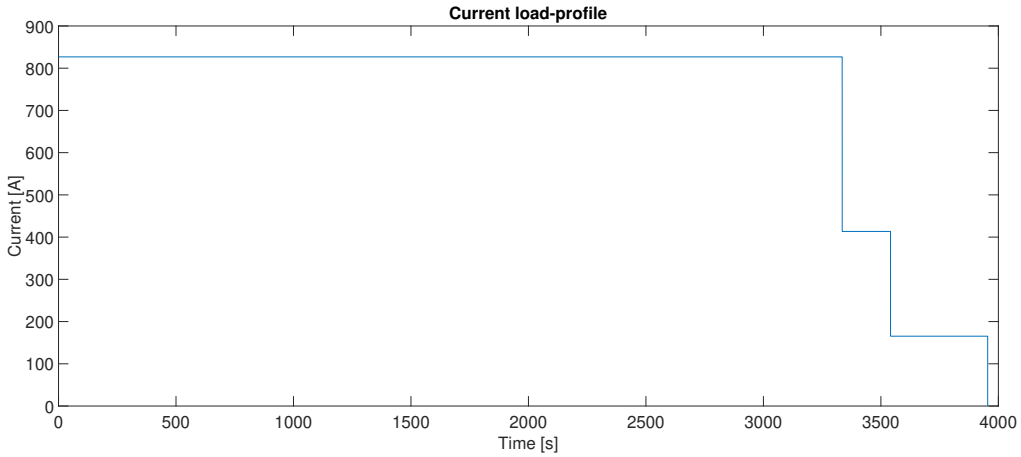

Figure 31: The current load-profile used in the MPC-test.

The upper current-rate limit for the packs is given as their nominal 2C-rates. The packs are allowed to charge fully, hence $\mathrm{SOC}_{\max} = 100\%$. Furthermore, Battery-Pack (BP) 1 is aged through capacity fade (90%) and resistance increase (130%). The ageing should allow for uneven current distribution, hence more interesting results.

The selected prediction-horizon is 10s, while the control-horizon and sampling time is set to 1s.

Case 2: Feedback control

The predicted maximum allowable current from the controller, is now connected as the input current to the plant model. This allows us to investigate whether constraints are being violated, or if the battery system is charged at a sub-optimal rate. The packs are charged between 10% and 90%. Only the EMPC without SOC constraints is tested.

5.5 Results

For the experimental setups described above, the following results are obtained. *Note that the black dotted lines in the plots mark limits.*

Case 1: Only prediction:

Figure 32 shows the SOC evolution of the packs.

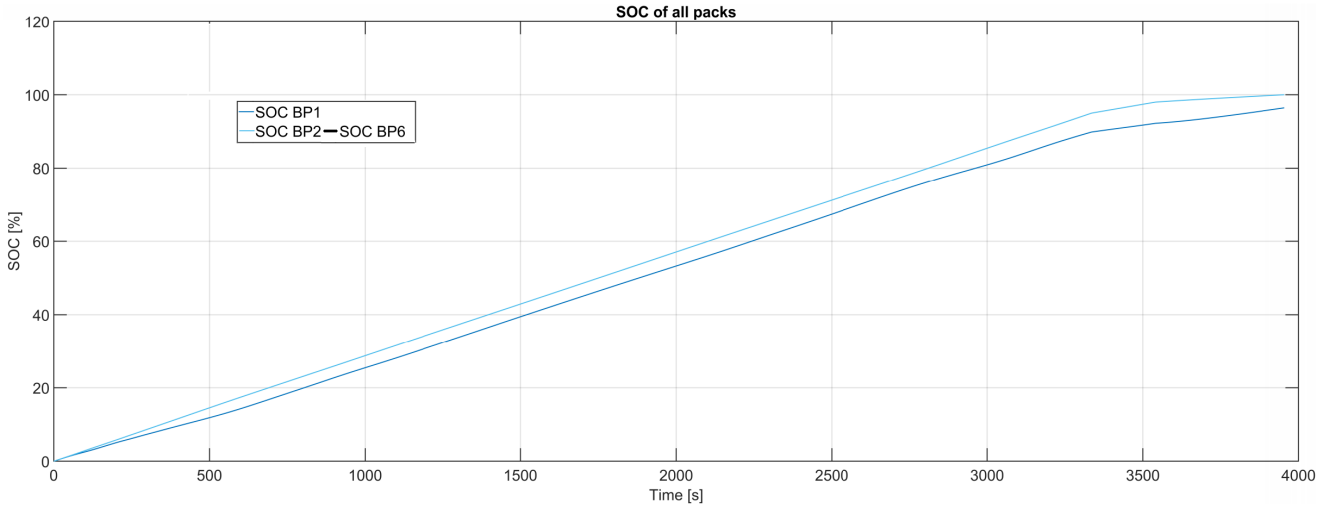

Figure 32: The SOC of the plant-model packs when using a current load-profile.

Figures 33 and 34 show the result when SOC-limits are *not* part of the EMPC formulation.

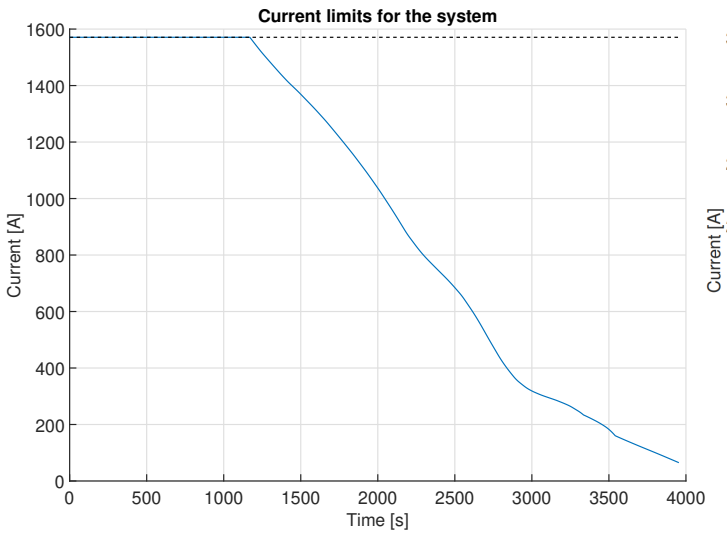

Figure 33: The maximum allowable charge current to the entire system, using MPC with constraints on terminal voltage, nominal 2C current-rate limit and a 10s time-horizon.

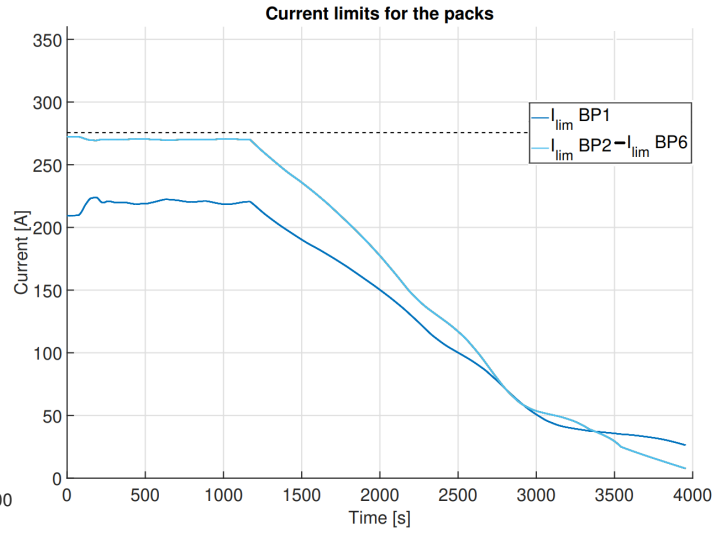

Figure 34: The maximum allowable charge current to each pack, using MPC with constraints on terminal voltage, nominal 2C current-rate limit and a 10s time-horizon.

Figures 35 and 36 show the result when SOC-limits *are* part of the EMPC formulation:

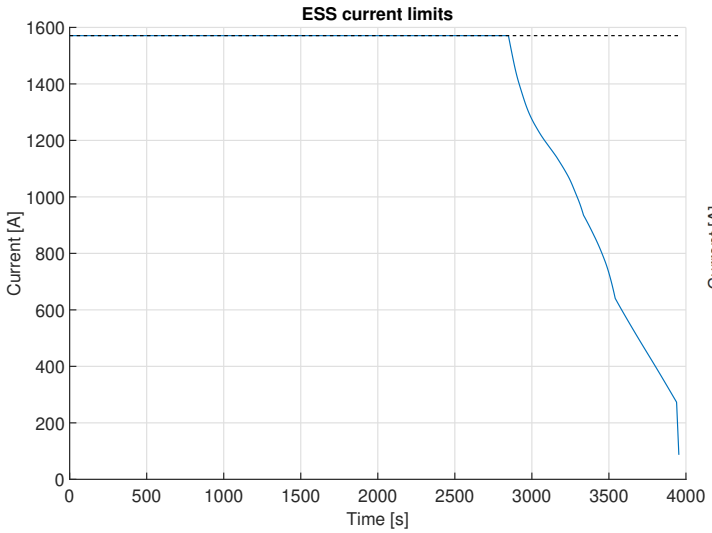

Figure 35: The maximum allowable charge current to the entire system, using MPC with constraints on terminal voltage, SOC, nominal 2C current-rate limit and 10s time-horizon.

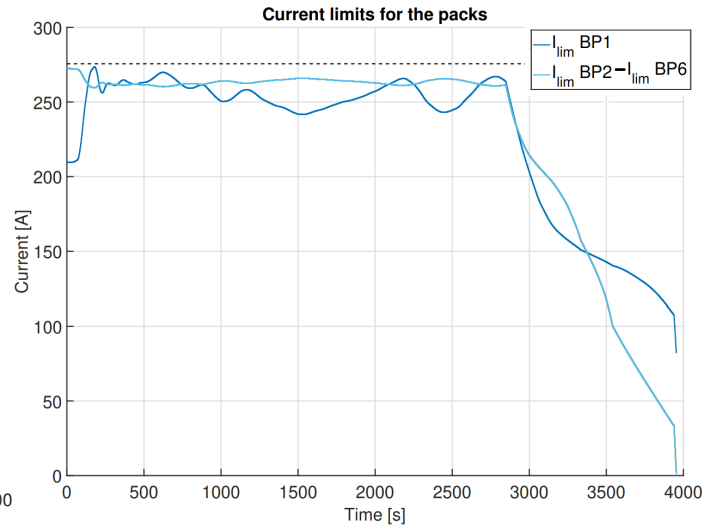

Figure 36: The maximum allowable charge current to each pack, using MPC with constraints on terminal voltage, SOC, nominal 2C current-rate limit and 10s time-horizon.

Case 2: Feedback control:

Figures 37-40 show the results of using the previous terminal voltage limit and a 2C current-rate limit, when allowing the EMPC to charge the batteries from 10% to 90%.

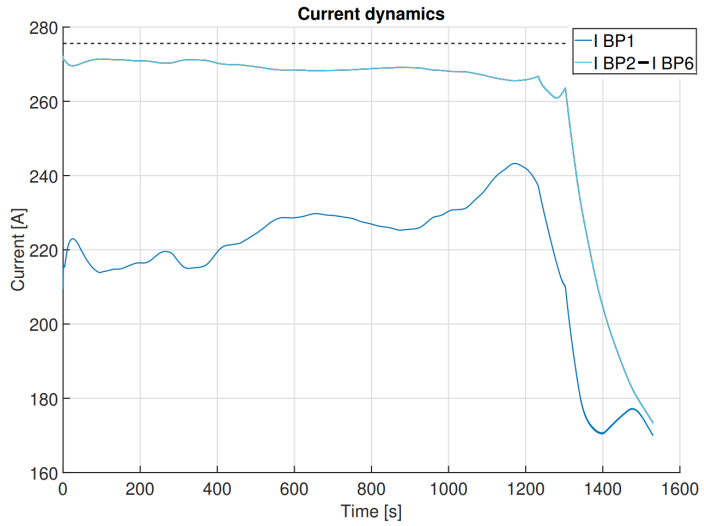

Figure 37: The current to each pack when charging, using MPC with constraints on terminal voltage, nominal 2C current-rate limit and a 10s time-horizon.

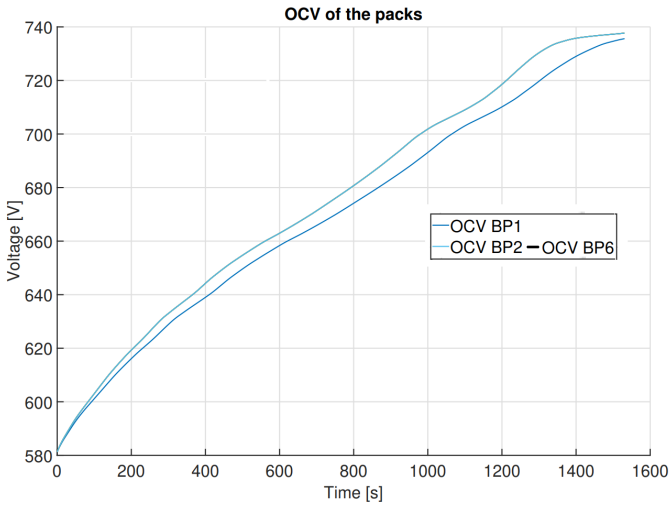

Figure 38: The pack OCVs when charging, using MPC with constraints on terminal voltage, nominal 2C current-rate limit and a 10s time-horizon.

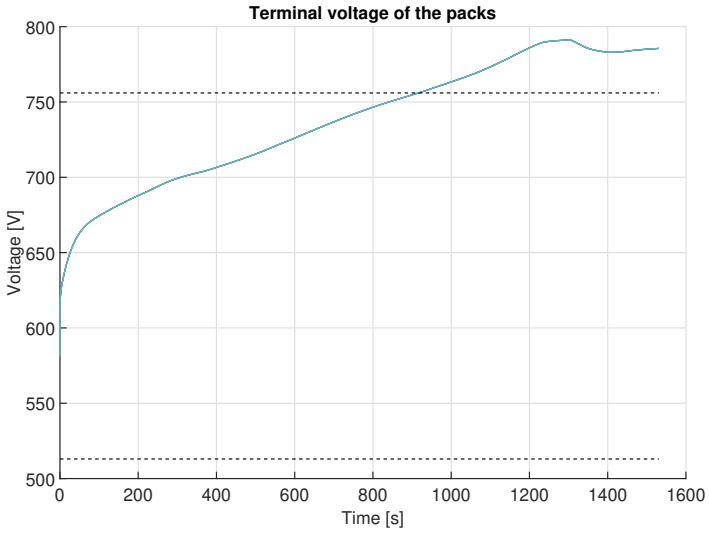

Figure 39: The pack terminal voltage when charging, using MPC with constraints on terminal voltage, 2C current-rate limit and a 10s time-horizon.

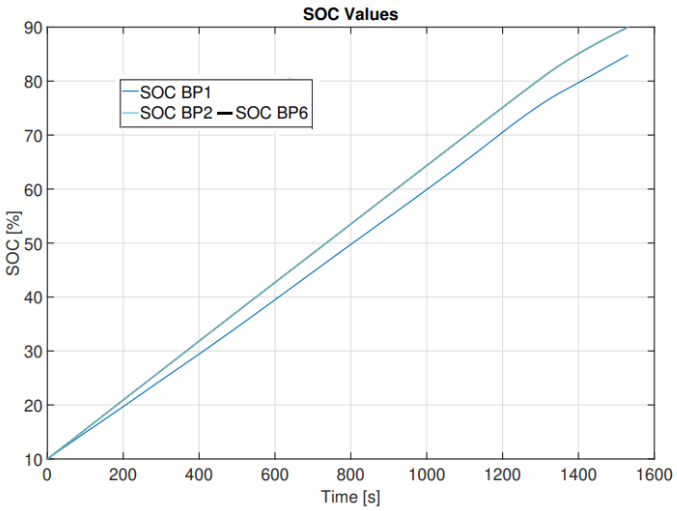

Figure 40: The pack SOC when charging, using MPC with constraints on terminal voltage, nominal 2C current-rate limit and a 10s time-horizon.

5.6 Discussion

When in prediction mode, the EMPCs output seem to respect the charge-constraints specified in the formulation. Especially, note that when SOC-limits are introduced, the EMPC lowers the maximum allowable charge current as the packs approach a fully charged state. However, adding the SOC as a state proved to have a very noticeable effect on the computation/simulation time, hence if the SOC-states are not necessary for other calculations but SOC-limits, it is recommended to try the other methods, as discussed in Chapter 5.3.

When using the EMPC as a feedback-controller, it is clear that terminal voltage constraints may be violated (see Figure 39) using this simple model, possibly caused by the simplification. A solution may be to manipulate the resistance used inside the model. Recall that the terminal voltage is calculated as

$$V_T = V_{\mathrm{OCV}_k} + R_k \cdot I_k.$$

Here, there are two options to explore in aim of preventing the violation of constraints; either increase the resistance, or scale the output from the EMPC. Note that the terminal voltage constraint is not always violated. Scaling the output from the EMPC may be too conservative, as this would always affect the delivered current, despite existing margin from limits.

Let us instead look at the resistance. Since there is a violation of the upper terminal voltage limit, scaling the resistance by a factor of > 1 should mitigate these effects. Figure 41 shows the terminal voltage evolution when testing to scale the resistance by a factor of 4.

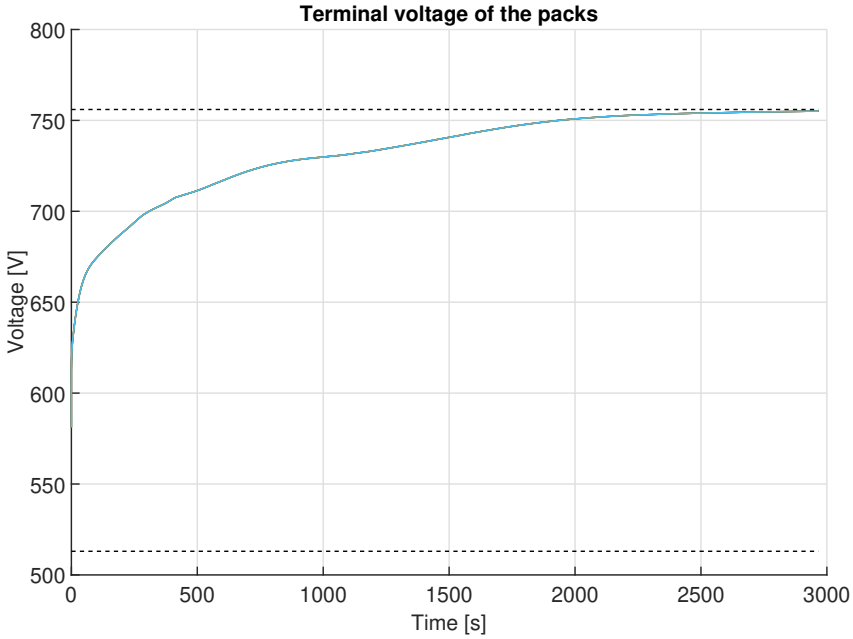

Figure 41: The terminal voltage when charging, using MPC with resistance scaling and constraints on terminal voltage, nominal 2C current-rate limit and a 10s time-horizon.

To test the generalizability, let us see if this scaling also holds for higher charge current-limits. Figures 42 and 43 show the terminal voltage evolution for nominal 2.5 and 3-C-rate, respectively.

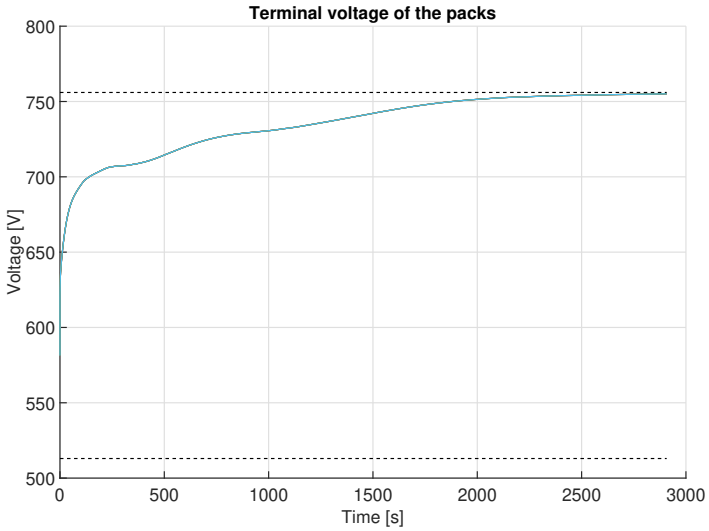

Figure 42: The terminal voltage when charging, using MPC with resistance scaling and constraints on terminal voltage, nominal 2.5C current-rate limit and 10s time-horizon.

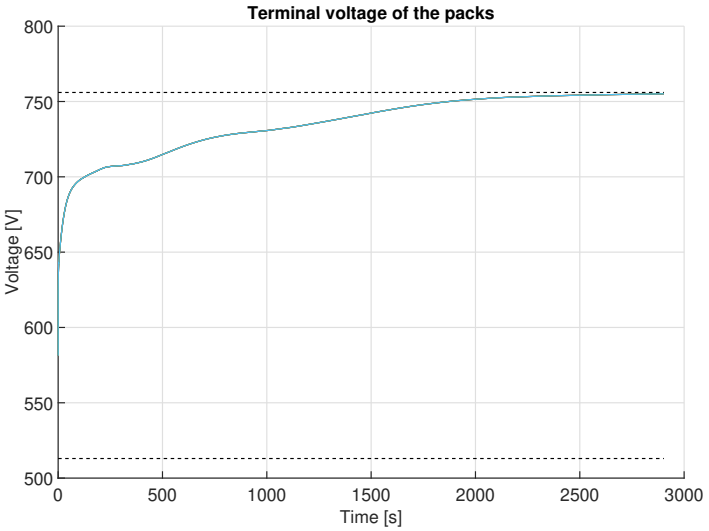

Figure 43: The terminal voltage when charging, using MPC with resistance scaling and constraints on terminal voltage, nominal 3C current-rate limit and 10s time-horizon.

The system seems to no longer violate the upper terminal voltage constraint for the charging window. However, the system now works in a sub-optimal state and the charging can take a longer time, since the currents no longer can be as large.

Note that, here only the current-split between the batteries are calculated. To obtain the actual delivered power, one needs to multiply the pack currents with the terminal voltage and sum the results.

6 Conclusion and Future Work

The work is mainly divided into two parts, sensitivity analysis and model-predictive power estimation. This final chapter is also divided into two parts discussing results, shortcomings and possible future work of the two main topics, separately.

6.1 Conclusions Sensitivity Analysis

The sensitivity analysis was conducted using two different frameworks: MATLAB/Simulink and Simcenter Amesim. Although there were many similarities between the models, there was a significant difference in the thermal part. The MATLAB/Simulink framework neglected the entropic heat generation. Recall that the entropic heat generation seems to be an important aspect for low currents (see Chapter 2.2.2). As the batteries studied in the sensitivity analysis are meant for Electric-Vehicles, lower rates might be the actual use-case; hence arguing for inclusion of this effect.

The Simcenter Amesim model was chosen for further analysis due to its assumed higher accuracy. The SOP was estimated using look-up tables dependent on SOC, temperature and time-horizon. The study found that differences in

- ageing
- initial SOC
- coolant temperature

may have significant effects on the SOP, while effects of heterogeneity w.r.t initial temperature and coolant flow-rate are of less significance for the power estimation.

As explained in Chapter 2.1.3 and repeated in Chapter 4.4, power-fade is usually calculated based on the resistance. Hence, the majority of the effect of ageing on the SOP may be attributed to the increased resistance, i.e. $\mathrm{SOH_P}$.

There are several aspects of the analysis that could be improved, and things that can be added to further increase the accuracy. Although the model is based on an experimental characterization, there has not been a lab-validation. This is arguably the most significant flaw. Lab results could potentially be used to further tune parameters, and reassure that significant physical phenomena are not neglected. Furthermore, future work could investigate the following:

- Effects of heterogeneity when several packs are manipulated w.r.t the nominal values.
- A more accurate SOP-estimation algorithm.
- Using different current load-profiles.

6.2 Conclusions Model Predictive Power Estimation

The results from the sensitivity analysis could be utilized in formulating an EMPC for the estimation of SOP. A simplified model was used as the EMPC plant-model, which has the potential of lowering computational complexity. The study found that, although adding SOC as a state could benefit safe operation of the batteries, it can lead to higher computational complexity.

The EMPC violated the plant terminal voltage constraint within the given charging window, this may be due to the model used in the EMPC. To mitigate these effects

we propose a solution where the internal resistance used in the EMPC is increased. However, this may lead to sub-optimal utilization, but could keep the batteries safer.

Because of the drawbacks, this EMPC may be better used as a back-up controller to a more refined estimator that utilizes a more complex model. If the more complex estimator fails, this could potentially provide a temporary *conservative* estimate.

Below are some suggestions for future work:

- Comparison of the simple model against a high fidelity model, to determine the error margins in SOP estimation.
- Lab experiments to test the proposed power estimator.
- Exploration of parameter tuning, such as time-horizon.

Depending on the computation power available one might instead use a more refined simple model, which includes a RC-network. However, increasing model complexity and thereby computation load, could result in the need for better hardware and higher manufacturing costs. One of the key barriers to wide-spread adoption of EVs is the high purchasing price [79]. Hence, further exploration of computationally efficient power estimation algorithms is merited.

Bibliography

[1] Matthew T. Lawder et al. “Battery Energy Storage System (BESS) and Battery Management System (BMS) for Grid-Scale Applications”. In: *Proceedings of the IEEE* 102.6 (2014), pp. 1014–1030. DOI: https://doi.org/10.1109/JPROC.2014.2317451.

[2] Gregory Plett. *Battery Management Systems, Volume II: Equivalent-Circuit Methods Equivalent-Circuit Methods*. Artech House, 2016. ISBN: 9781630810283. URL: https://ieeexplore.ieee.org/document/9100098.

[3] Gregory Plett. *Battery Management Systems, Volume I: Battery Modeling*. Artech House, 2015. ISBN: 9781630810238.

[4] P.S. Ghoshdastidar. *Heat Transfer*. 2nd ed. Oxford University Press, 2012. ISBN: 978-0-19-807997-2.

[5] Andreas Jossen. “Fundamentals of battery dynamics”. In: *"Journal of Power Sources"* 154.2 (2006), pp. 530–538. DOI: https://doi.org/10.1016/j.jpowsour.2005.10.041.

[6] Habiballah Rahimi-Eichi et al. “Battery Management System: An Overview of Its Application in the Smart Grid and Electric Vehicles”. In: *IEEE Industrial Electronics Magazine* 7.2 (2013), pp. 4–16. DOI: https://doi.org/10.1109/MIE.2013.2250351.

[7] C. Pastor-Fernandez et al. “A Study of Cell-to-Cell Interactions and Degradation in Parallel Strings: Implications for the Battery Management System”. In: *Journal of Power Sources* 329 (2016), pp. 574–585. DOI: https://doi.org/10.1016/j.jpowsour.2016.07.121.

[8] Cheng Zhang et al. “Battery Modelling Methods for Electric Vehicles - A Review”. In: *2014 European Control Conference (ECC)*. IEEE, 2014, pp. 2673–2678. DOI: https://doi.org/10.1109/ECC.2014.6862541.

[9] V. J. Ovejas et al. “Effects of cycling on lithium-ion battery hysteresis and overvoltage”. In: *"Scientific Reports"* 9, 14875 (2019). DOI: https://doi.org/10.1038/s41598-019-51474-5.

[10] Edis Osmanbasic. *Battery Management Systems–Part 3: Battery Charging Methods*. 2020. URL: https://www.engineering.com/story/battery-management-systemspart-3-battery-charging-methods.

[11] *Simcenter Amesim - Optimize system performance from early design stages*. Siemens Digital Industries Software. URL: https://www.plm.automation.siemens.com/global/en/products/simcenter/simcenter-amesim.html.

[12] *Battery Definitions, Terms & Terminology*. Electronics-Notes. URL: https://www.electronics-notes.com/articles/electronic_components/battery-technology/terms-terminology-definitions.php.

[13] Frans Edison et al. “State of Energy (SOE) Estimation of LiNiCoAlO2 Battery Module Considering Cells Unbalance and Energy Efficiency”. In: *2017 4th International Conference on Electric Vehicular Technology (ICEVT)*. IEEE, 2017, pp. 100–106. DOI: 10.1109/ICEVT.2017.8323542.

[14] Alexander Farmann and Dirk Uwe Sauer. “Comparative study of reduced order equivalent circuit models for on-board state-of-available-power prediction of lithium-ion batteries in electric vehicles”. In: *"Applied Energy"* 225 (2018), pp. 1102–1122. DOI: https://doi.org/10.1016/j.apenergy.2018.05.066.

[15] *Electromotive Force: Terminal Voltage*. Lumen Learning. URL: https://courses.lumenlearning.com/physics/chapter/21-2-electromotive-force-terminal-voltage/.

[16] European Parliament. *CO2 emissions from cars: facts and figures*. 2019. URL: https://www.europarl.europa.eu/news/en/headlines/society/20190313STO31218/co2-emissions-from-cars-facts-and-figures-infographics.

[17] European Commission. *2030 climate & energy framework*. 2020. URL: https://ec.europa.eu/clima/policies/strategies/2030_en.

[18] Transport & Environment. *How clean are electric cars? - T&E's analysis of electric car lifecycle CO2 emissions*. 2020. URL: https://www.transportenvironment.org/sites/te/files/downloads/T%26E%E2%80%99s%20EV%20life%20cycle%20analysis%20LCA.pdf.

[19] Felix Kuhnert et al. *E-Mobility Sales Review Q1*. Strategy&, PwC, 2021. URL: https://www.strategyand.pwc.com/de/en/insights/2021/e-mobility-sales-review-q1.html.

[20] Colin McKerracher et al. *Electric Vehicle Outlook 2020*. Bloomberg, 2020. URL: https://about.bnef.com/electric-vehicle-outlook/.

[21] IEA. *Global EV Outlook 2020*. IEA, Paris, 2020. URL: https://www.iea.org/reports/global-ev-outlook-2020.

[22] Dale Hall and Nic Lutsey. *Effects of battery manufacturing on electric vehicle life-cycle greenhouse gas emissions*. International Council on Clean Transportation, 2018. URL: https://theicct.org/publications/EV-battery-manufacturing-emissions.

[23] Xian-Zhi Gong et al. “Study of the Characteristics of Battery Packs in Electric Vehicles With Parallel-Connected Lithium-Ion Battery Cells”. In: *2014 IEEE Applied Power Electronics Conference and Exposition - APEC 2014*. IEEE, 2014, pp. 3218–3224. DOI: https://doi.org/10.1109/APEC.2014.6803766.

[24] Félix-Antoine LeBel et al. “A Lithium-Ion Battery Electro-Thermal Model of Parallellized Cells”. In: *2016 IEEE 84th Vehicular Technology Conference (VTC-Fall)*. IEEE, 2016, pp. 1–6. DOI: https://doi.org/10.1109/VTCFall.2016.7880858.

[25] Alexander Farmann and Dirk Uwe Sauer. “A comprehensive review of on-board State-of-Available-Power prediction techniques for lithium-ion batteries in electric vehicles”. In: *Journal of Power Sources* 329 (2016), pp. 123–137. DOI: https://doi.org/10.1016/j.jpowsour.2016.08.031.

[26] Rui Xiong et al. “Online Estimation of Peak Power Capability of Li-Ion Batteries in Electric Vehicles by a Hardware-in-Loop Approach”. In: *Energies* 5.5 (2012), pp. 1455–1469. DOI: https://doi.org/10.3390/en5051455.

[27] Xiao-Song Hu et al. “Model-Based Dynamic Power Assessment of Lithium-Ion Batteries Considering Different Operating Conditions”. In: *IEEE Transactions on Industrial Informatics* 10.3 (2014), pp. 1948–1959. DOI: https://doi.org/10.1109/TII.2013.2284713.

[28] Chang-Fu Zou et al. “Power capability prediction for lithium-ion batteries using economic nonlinear model predictive control”. In: *"Journal of Power Sources"* 396 (2018), pp. 580–589. DOI: https://doi.org/10.1016/j.jpowsour.2018.06.034.

[29] F. Altaf and A. Klintberg. *Improved Method for Controlling an Energy Storage System - Part 1*. WO Patent App. PCT/EP2019/086833, Publication No. WO/2020/128066, Jun. 25, 2020.

[30] F. Altaf and A. Klintberg. *Improved Method for Controlling an Energy Storage System - Part 2*. WO Patent App. PCT/EP2019/086835, Publication No. WO/2020/128068, Jun. 25, 2020.

[31] F. Altaf and B. Farag A. Josefsson J. Enerbäck. *A Method for Controlling Electrical Connection of Battery Packs*. WO Patent App. PCT/EP2019/068021, Publication No.
WO/2021/001046, Jan. 07, 2021.

[32] Lan-Guang Lu et al. “A review on the key issues for lithium-ion battery management in electric vehicles”. In: *Journal of Power Sources* 226 (2013), pp. 272–288. DOI: https://doi.org/10.1016/j.jpowsour.2012.10.060.

[33] Melissa Morris and Sabri Tosunoglu. “Comparison of rechargeable battery technologies”. In: *Early Career Technical Journal* 11 (2012), pp. 148–155. URL: https://www.researchgate.net/publication/281931837_COMPARISON_OF_RECHARGEABLE_BATTERY_TECHNOLOGIES.

[34] Jakub Lach et al. “Applications of carbon in lead-acid batteries: a review”. In: *Journal of Solid State Electrochemistry* 23 (2019), pp. 693–705. DOI: https://doi.org/10.1007/s10008-018-04174-5.

[35] Yasin Emre Durmus et al. “Side by Side Battery Technologies with Lithium-Ion Based Batteries”. In: *Advanced Energy Materials* 10.24, 2000089 (2020). DOI: https://doi.org/10.1002/aenm.202000089.

[36] Resmi Suresh et al. “Modeling of rechargeable batteries”. In: *Current Opinion in Chemical Engineering* 13 (2016). Energy and Environmental Engineering / Reaction engineering and catalysis, pp. 63–74. DOI: https://doi.org/10.1016/j.coche.2016.08.005.

[37] Xin-Fan Lin et al. “A lumped-parameter electro-thermal model for cylindrical batteries”. In: *Journal of Power Sources* 257 (2014), pp. 1–11. DOI: https://doi.org/10.1016/j.jpowsour.2014.01.097.

[38] Xiao-Song Hu et al. “A comparative study of equivalent circuit models for Li-ion batteries”. In: *Journal of Power Sources* 198 (2012), pp. 359–367. DOI: https://doi.org/10.1016/j.jpowsour.2011.10.013.

[39] Thomas Bruen and James Marco. “Modelling and experimental evaluation of parallel connected lithium ion cells for an electric vehicle battery system”. In: *Journal of Power Sources* 310 (2016), pp. 91–101. DOI: https://doi.org/10.1016/j.jpowsour.2016.01.001.

[40] Rui-Feng Zhang et al. “A Study on the Open Circuit Voltage and State of Charge Characterization of High Capacity Lithium-Ion Battery Under Different Temperature”. In: *Energies* 11.9, 2408 (2018). DOI: https://doi.org/10.3390/en11092408.

[41] Gregory L.Plett. “Extended Kalman filtering for battery management systems of LiPB-based HEV battery packs: Part 2. Modeling and identification”. In: *Journal of Power Sources* 134.2 (2004), pp. 262–276. DOI: https://doi.org/10.1016/j.jpowsour.2004.02.032.

[42] Simon Elvmarker. “Visualization and simulation of idle truck energy usage: Prediction of battery discharge in a Volvo truck cab”. Uppsala University, 2018. URL: http://uu.diva-portal.org/smash/record.jsf?pid=diva2:1257830.

[43] Andrzej Lebkowski. “Temperature, Overcharge and Short-Circuit Studies of Batteries used in Electric Vehicles”. In: *Przeglad Elektrotechniczny* 5 (2017). DOI: http://dx.doi.org/10.15199/48.2017.05.13.

[44] Dian Wang et al. “Online Lithium-Ion Battery Internal Resistance Measurement Application in State-of-Charge Estimation Using the Extended Kalman Filter”. In: *Energies* 10.9, 1284 (2017). DOI: https://doi.org/10.3390/en10091284.

[45] Evelina Wikner. “Lithium ion Battery Aging: Battery Lifetime Testing and Physics-based Modeling for Electric Vehicle Applications”. PhD thesis. Chalmers University of Technology, 2017. URL: https://research.chalmers.se/en/publication/249356.

[46] Nick Robinson. *What Is Thermodynamics?* Sciencing, 2017. URL: https://sciencing.com/efficiency-physics-definition-formula-examples-13722775.html.

[47] Huw Fox and William Bolton. *Mathematics for Engineers and Technologists*. Elsevier Ltd., 2002. ISBN: 978-0-7506-5544-6. DOI: https://doi.org/10.1016/B978-0-7506-5544-6.X5000-0.

[48] Ching-Chuen Chan and Y.S Wong. “Electric Vehicles Charge Forward”. In: *"IEEE Power and Energy Magazine"* 2.6 (2004), pp. 24–33. DOI: https://doi.org/10.1109/MPAE.2004.1359010.

[49] Upender Rao Koleti et al. “The development of optimal charging strategies for lithium-ion batteries to prevent the onset of lithium plating at low ambient temperatures”. In: *"Journal of Energy Storage"* 24, 100798 (2019). DOI: https://doi.org/10.1016/j.est.2019.100798.

[50] V.Svoboda. *Encyclopedia of Electrochemical Power Sources*. Elsevier B.V, 2009, pp. 424–442. ISBN: 978-0-444-52745-5.

[51] Mohamad Syazarudin Md Said and Mohd Zahirasri Mohd Tohir. “Prediction of Lithium-ion Battery Thermal Runaway Propagation for Large Scale Applications Fire Hazard Quantification”. In: *Processes* 7.10, 703 (2019). DOI: https://doi.org/10.3390/pr7100703.

[52] Rim Saada et al. “Causes and consequences of thermal runaway incidents—Will they ever be avoided?” In: *Process Safety and Environmental Protection* 97 (2015). Bhopal 30th Anniversary, pp. 109–115. DOI: https://doi.org/10.1016/j.psep.2015.02.005.

[53] Ying Bai et al. “Reversible and irreversible heat generation of NCA/Si–C pouch cell during electrochemical energy-storage process”. In: *"Journal of Energy Chemistry"* 29 (2019), pp. 95–102. DOI: https://doi.org/10.1016/j.jechem.2018.02.016.

[54] Vilayanur V. Viswanathan et al. “Effect of entropy change of lithium intercalation in cathodes and anodes on Li-ion battery thermal management”. In: *"Journal of Power Sources"* 195.11 (2010), pp. 3720–3729. DOI: https://doi.org/10.1016/j.jpowsour.2009.11.103.

[55] Todd M.Bandhauer et al. “Temperature-dependent electrochemical heat generation in a commercial lithium-ion battery”. In: *"Journal of Power Sources"* 247 (2014), pp. 618–628. DOI: https://doi.org/10.1016/j.jpowsour.2013.08.015.

[56] Kandler Smith and Chao-Yang Wang. “Power and thermal characterization of a lithium-ion battery pack for hybrid-electric vehicles”. In: *"Journal of Power Sources"* 160.1 (2006), pp. 662–673. DOI: https://doi.org/10.1016/j.jpowsour.2006.01.038.

[57] Martin J. Brand et al. “Current distribution within parallel-connected battery cells”. In: *Journal of Power Sources* 334 (2016), pp. 202–212. DOI: https://doi.org/10.1016/j.jpowsour.2016.10.010.

[58] Dong Zhang et al. “Interval Observer for SOC Estimation in Parallel-Connected Lithium-ion Batteries”. In: *2020 American Control Conference (ACC)*. IEEE, 2020, pp. 1149–1154. DOI: https://doi.org/10.23919/ACC45564.2020.9147468.

[59] Dong Zhang et al. “State of Charge Estimation of Parallel Connected Battery Cells via Descriptor System Theory”. In: *2020 American Control Conference (ACC)*. IEEE, 2020, pp. 2207–2212. DOI: https://doi.org/10.23919/ACC45564.2020.9147284.

[60] Gregory Plett. “Extended Kalman filtering for battery management systems of LiPB-based HEV battery packs: Part 3. State and parameter estimation”. In: *"Journal of Power Sources"* 134.2 (2004), pp. 277–292. DOI: https://doi.org/10.1016/j.jpowsour.2004.02.033.

[61] Gregory Plett. “Sigma-point Kalman filtering for battery management systems of LiPB-based HEV battery packs: Part 2: Simultaneous state and parameter estimation”. In: *"Journal of Power Sources"* 161.2 (2006), pp. 1369–1384. DOI: https://doi.org/10.1016/j.jpowsour.2006.06.004.

[62] Torsten Wik et al. “Implementation and robustness of an analytically based battery state of power”. In: *Journal of Power Sources* 287 (2015), pp. 448–457. DOI: https://doi.org/10.1016/j.jpowsour.2015.03.165.

[63] R. Dyche Anderson et al. “Real Time Battery Power Capability Estimation”. In: *2012 American Control Conference (ACC)*. IEEE, 2012, pp. 592–597. DOI: https://doi.org/10.1109/ACC.2012.6314892.

[64] Narissara Chatrattanawet et al. “Robust Model Predictive Control Strategy for LTV and LPV Systems of the Internal Reforming Solid Oxide Fuel Cell”. In: *12th International Symposium on Process Systems Engineering and 25th European Symposium on Computer Aided Process Engineering*. Vol. 37. Elsevier Ltd, 2015, pp. 1733–1738. DOI: https://doi.org/10.1016/B978-0-444-63577-8.50134-0.

[65] Solomon Sunday Oyelere. "The Application of Model Predictive Control (MPC) to Fast Systems such as Autonomous Ground Vehicles (AGV)". In: *IOSR Journal of Computer Engineering (IOSR-JCE)* 16.3 (2014), pp. 27–37. DOI: http://dx.doi.org/10.9790/0661-16342737.

[66] Joel A.Paulson et al. "Chapter 14 - Fast stochastic model predictive control of end-to-end continuous pharmaceutical manufacturing". In: *Process Systems Engineering for Pharmaceutical Manufacturing*. Vol. 41. Computer Aided Chemical Engineering. Elsevier Ltd, 2018, pp. 353–378. ISBN: 978-0-444-63963-9. DOI: https://doi.org/10.1016/B978-0-444-63963-9.00014-2.

[67] Jan Dentler. "Real-time Model Predictive Control of Cooperative Aerial Manipulation". PhD thesis. University of Luxembourg, 2018. DOI: http://dx.doi.org/10.13140/RG.2.2.20234.31687/1.

[68] Lemma Dendena Tufa and Chong-Zhi Ka. "Effect of Model Plant Mismatch on MPC Performance and Mismatch Threshold Determination". In: *4th International Conference on Process Engineering and Advanced Materials*. Vol. 148. Elsevier Ltd, 2016, pp. 1008–1014. DOI: https://doi.org/10.1016/j.proeng.2016.06.518.

[69] Jacob Mattingley et al. "Code Generation for Receding Horizon Control". In: *2010 IEEE International Symposium on Computer-Aided Control System Design*. IEEE, 2010, pp. 985–992. DOI: https://doi.org/10.1109/CACSD.2010.5612665.

[70] Rolf Findeisen and Frank Allgöwer. "An introduction to nonlinear model predictive control". In: *21st Benelux Meeting on Systems and Control*. 2002. URL: https://www.researchgate.net/publication/288262596_An_introduction_to_nonlinear_model_predictive_control.

[71] Stephen J. Wright. "Efficient Convex Optimization for Linear MPC". In: *Handbook of Model Predictive Control*. Control Engineering. Birkhäuser Basel, 2019, pp. 287–303. ISBN: 978-3-319-77489-3. DOI: https://doi.org/10.1007/978-3-319-77489-3_13.

[72] Moritz Diehl et al. "Efficient Numerical Methods for Nonlinear MPC and Moving Horizon Estimation". In: *Nonlinear Model Predictive Control*. Lecture Notes in Control and Information Sciences. Springer, 2008, pp. 391–417. ISBN: 978-3-642-01094-1. DOI: https://doi.org/10.1007/978-3-642-01094-1_32.

[73] Abhishek Dhar and Shubhendu Bhasin. "Adaptive MPC for Uncertain Discrete-Time LTI MIMO Systems with Incremental Input Constraints". In: *IFAC-PapersOnLine* 51.1 (2018). 5th IFAC Conference on Advances in Control and Optimization of Dynamical Systems ACODS 2018, pp. 329–334. DOI: https://doi.org/10.1016/j.ifacol.2018.05.040.

[74] Saša V. Raković. "Robust Model Predictive Control". In: *Encyclopedia of Systems and Control*. Springer, London, 2020. ISBN: 978-1-4471-5102-9. DOI: https://doi.org/10.1007/978-1-4471-5102-9_2-3.

[75] Matthew Ellis et al. "A tutorial review of economic model predictive control methods". In: *"Journal of Process Control"* 24.8 (2014), pp. 1156–1178. DOI: https://doi.org/10.1016/j.jprocont.2014.03.010.

[76] Tri Tran et al. “Economic Model Predictive Control - A Review”. In: *The 31st International Symposium on Automation and Robotics in Construction and Mining (ISARC 2014)*. 2014, pp. 35–42. DOI: https://doi.org/10.22260/ISARC2014/0006.

[77] Chang-Fu Zou et al. “Electrochemical Estimation and Control for Lithium-Ion Battery Health-Aware Fast Charging”. In: *IEEE Transactions on Industrial Electronics* 65.8 (2018), pp. 6635–6645. DOI: https://doi.org/10.1109/TIE.2017.2772154.

[78] Marcelo A. Xavier and M. Scott Trimboli. “Lithium-ion battery cell-level control using constrained model predictive control and equivalent circuit models”. In: *"Journal of Power Sources"* 285 (2015), pp. 374–384. DOI: https://doi.org/10.1016/j.jpowsour.2015.03.074.

[79] Zhen-Yu She et al. “What are the barriers to widespread adoption of battery electric vehicles? A survey of public perception in Tianjin, China”. In: *"Transport Policy"* 56 (2017), pp. 29–40. DOI: https://doi.org/10.1016/j.tranpol.2017.03.001.

Appendix A

Appendix A presents the results from the sensitivity analysis performed in the MATLAB/Simulink framework. The relevant chapter to this appendix is Chapter 4. Every test includes difference from nominal charge/discharge SOP for the three time-horizons.

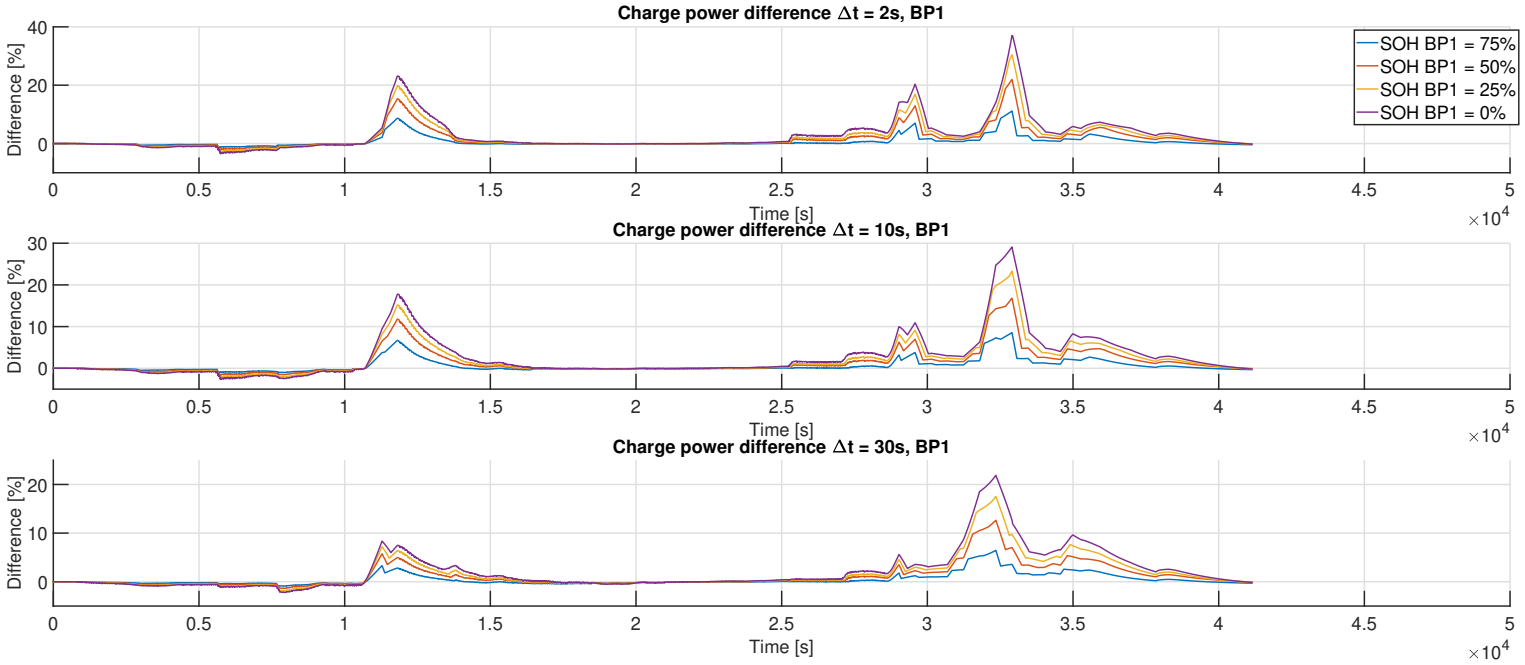

Figure 44: Difference from nominal SOP for 0, 25, 50 and 75% SOH and time-horizons 2, 10 and 30 seconds, during charging; MATLAB/Simulink framework.

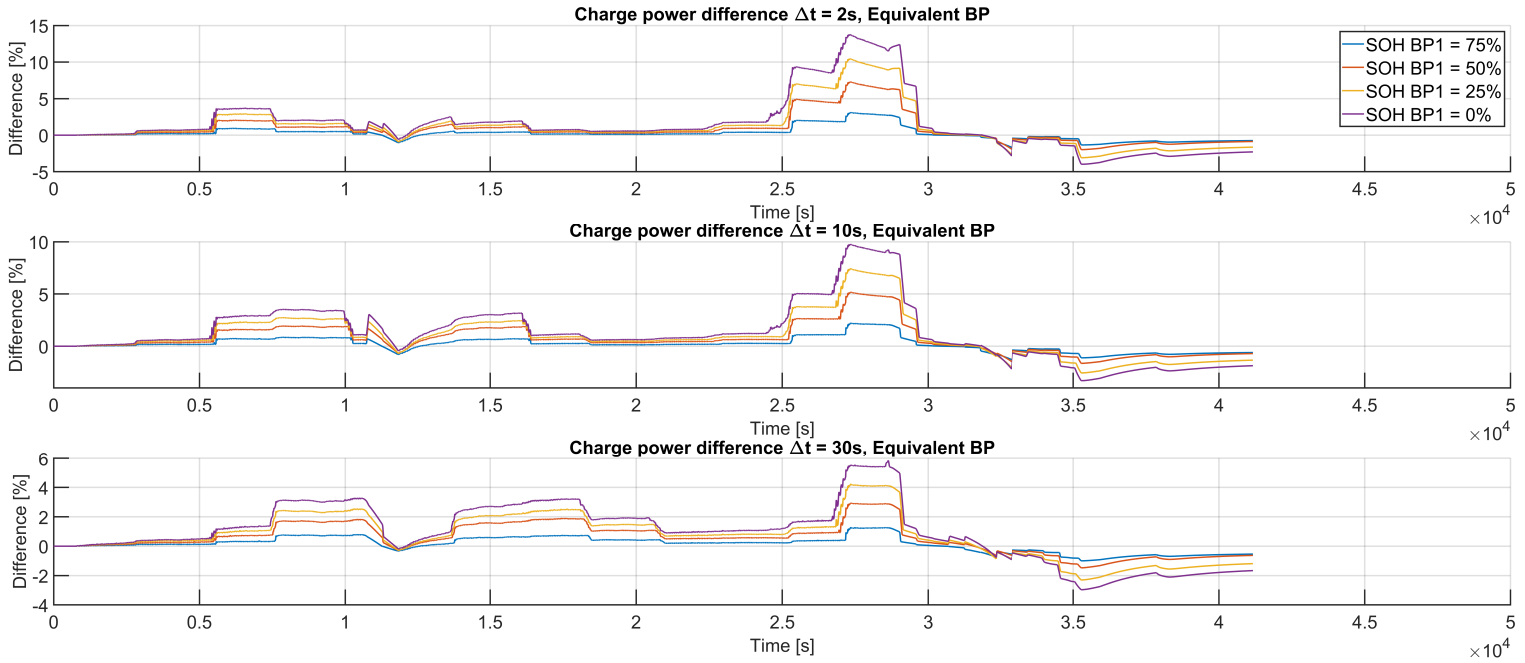

Figure 45: Representative pack SOP for 0, 25, 50 and 75% SOH and time-horizons 2, 10 and 30 seconds, during charging; MATLAB/Simulink framework.

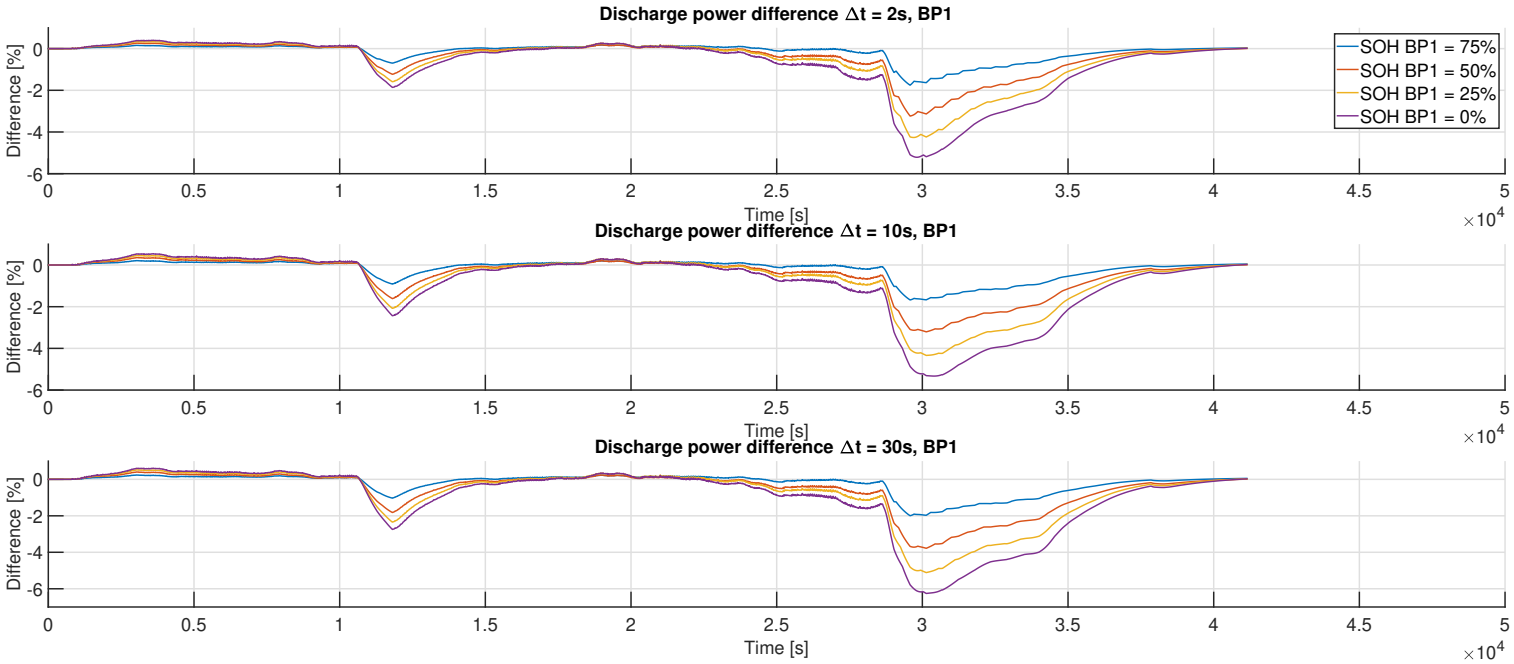

Figure 46: Difference from nominal SOP for 0, 25, 50 and 75% SOH and time-horizons 2, 10 and 30 seconds, during discharge; MATLAB/Simulink framework.

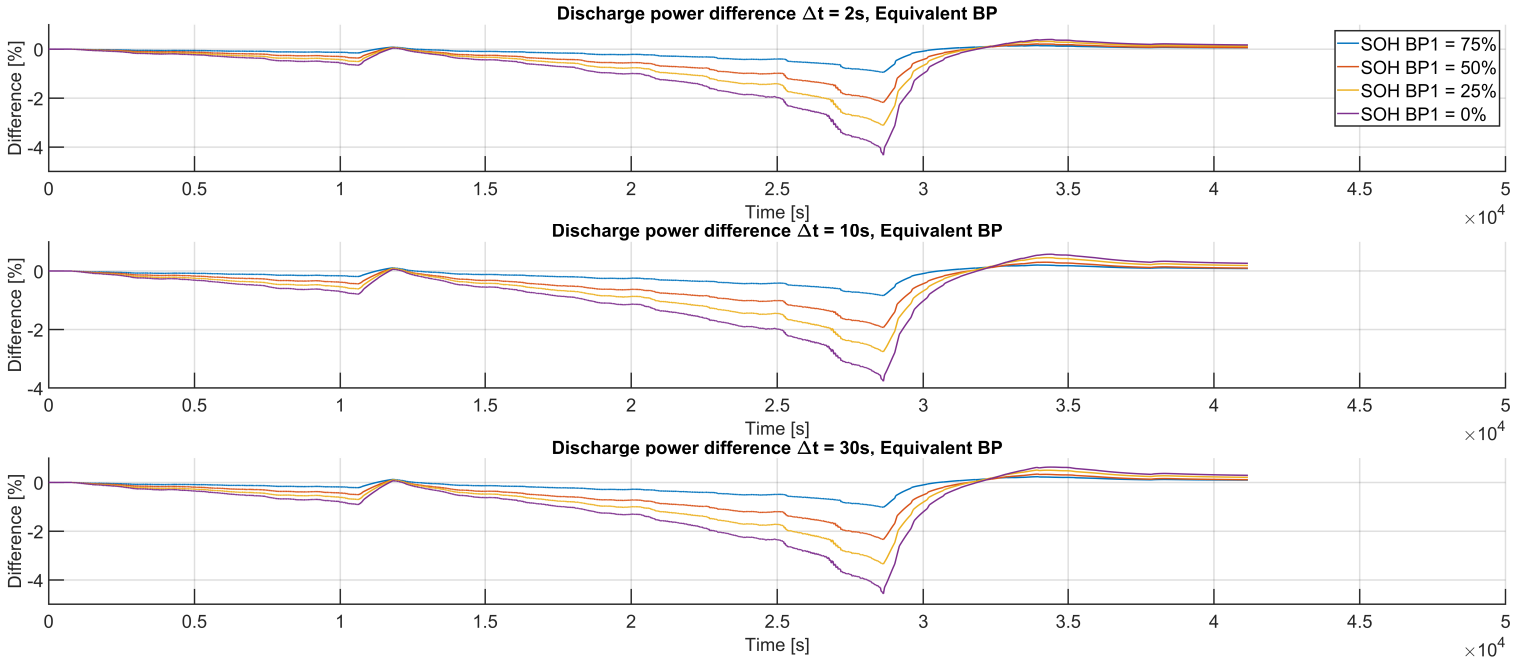

Figure 47: Representative pack SOP for 0, 25, 50 and 75% SOH and time-horizons 2, 10 and 30 seconds, during discharge; MATLAB/Simulink framework.

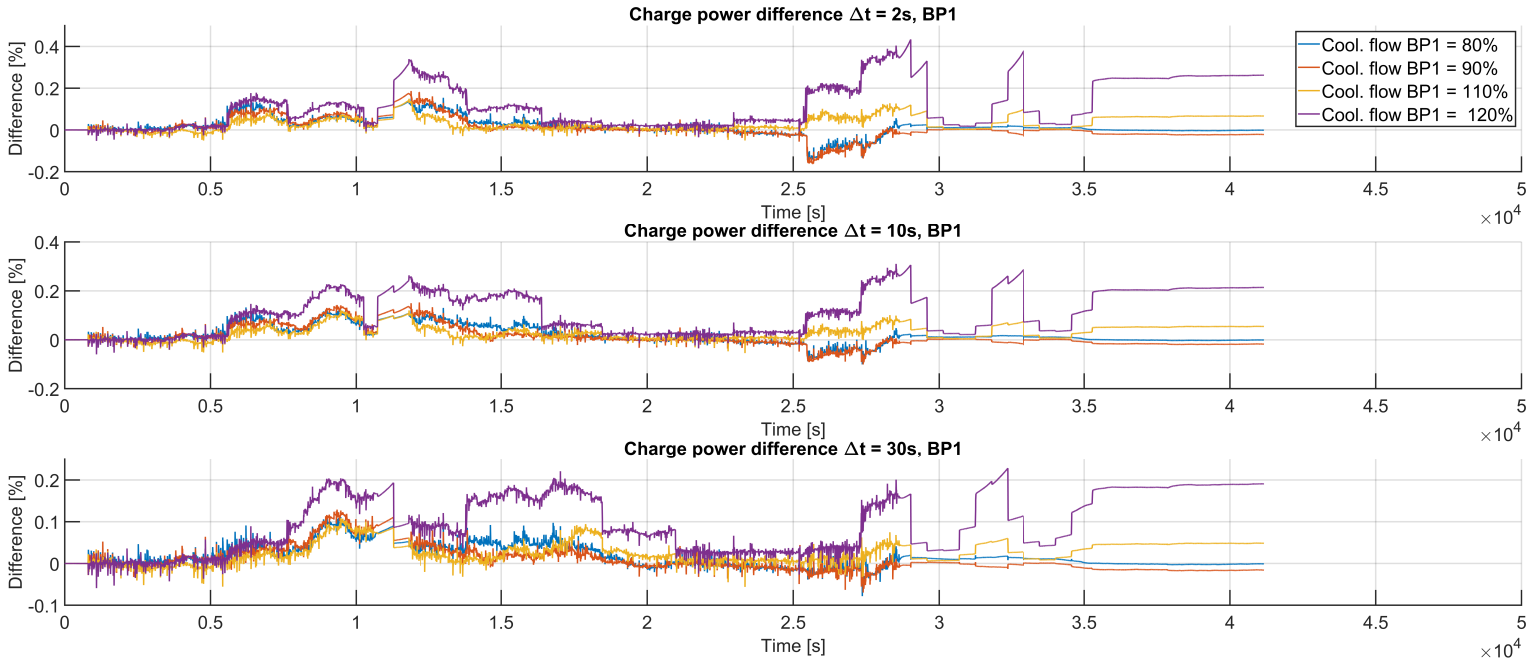

Figure 48: Difference from nominal SOP for 80, 90, 110 and 120% coolant flow-rate and time-horizons 2, 10 and 30 seconds, during charging; MATLAB/Simulink framework.

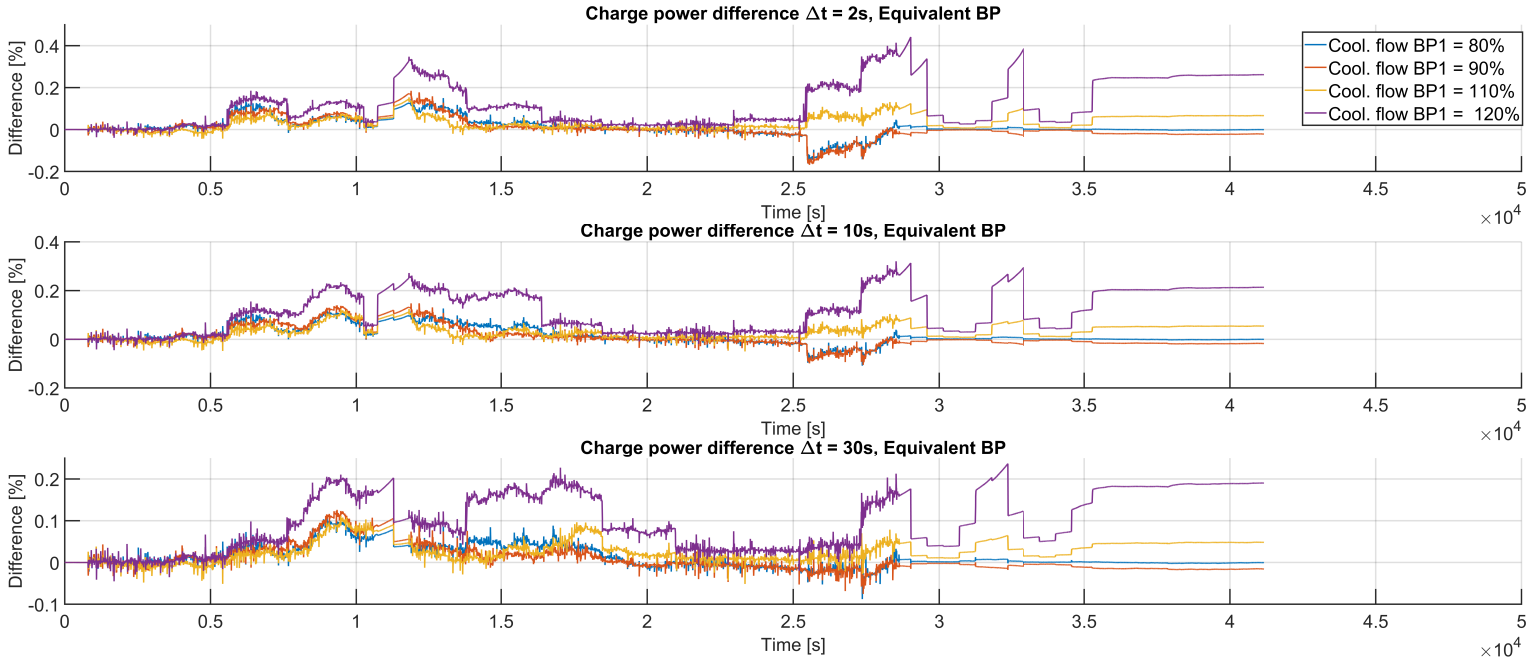

Figure 49: Representative pack SOP for 80, 90, 110 and 120% coolant flow-rate and time-horizons 2, 10 and 30 seconds, during charging; MATLAB/Simulink framework.

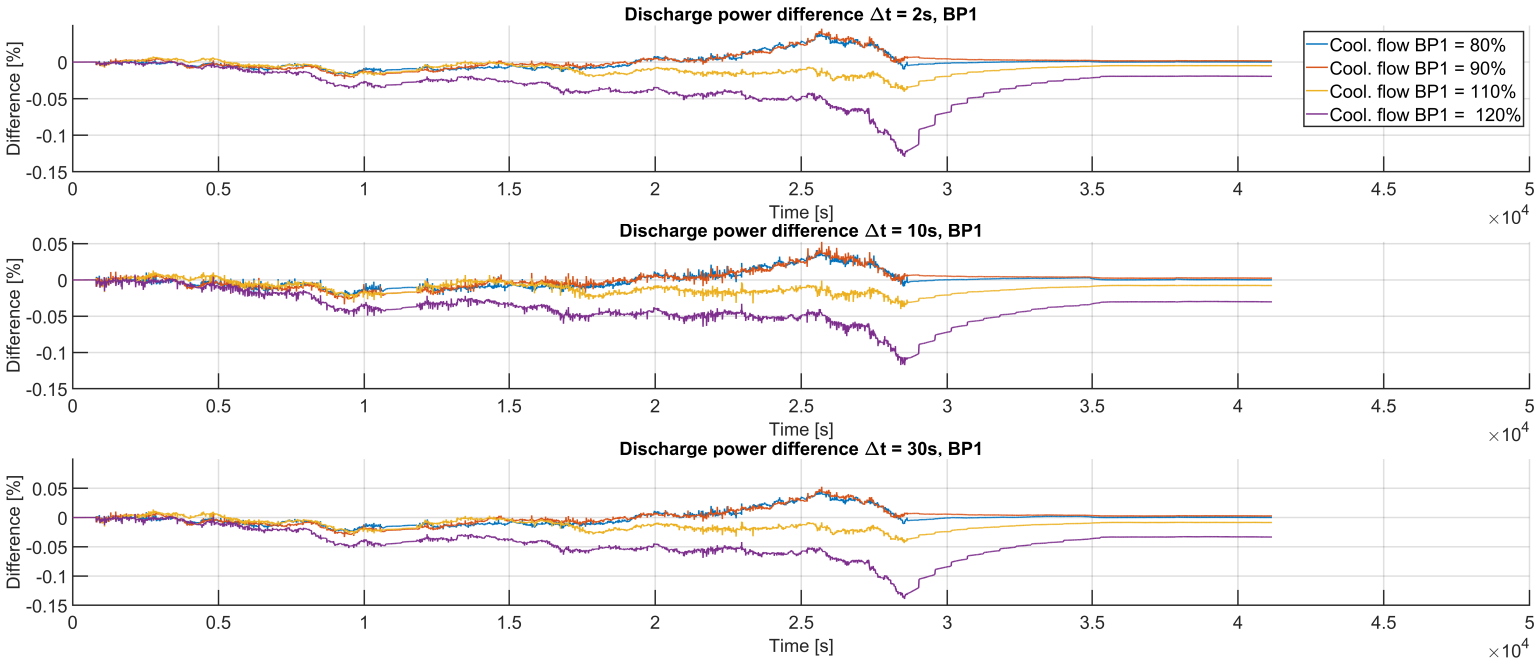

Figure 50: Difference from nominal SOP for 80, 90, 110 and 120% coolant flow-rate and time-horizons 2, 10 and 30 seconds, during discharge; MATLAB/Simulink framework.

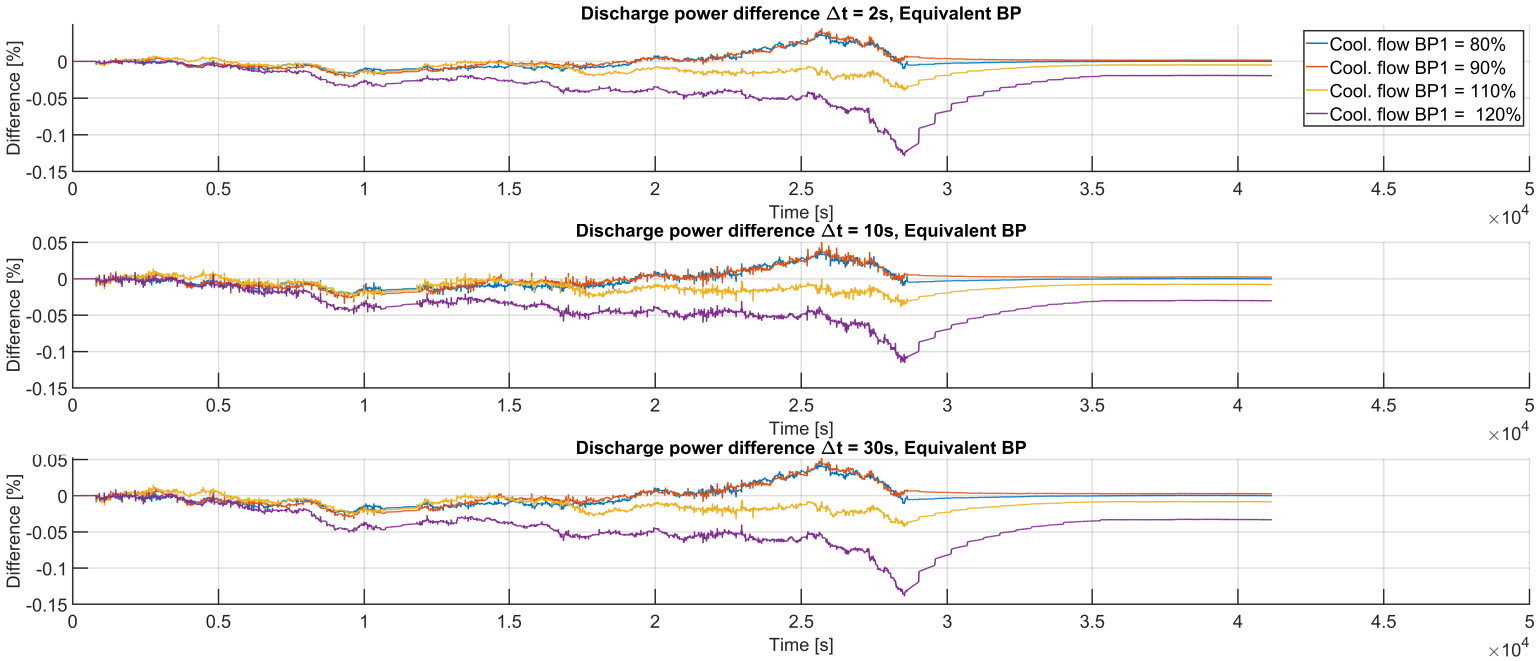

Figure 51: Representative pack SOP for 80, 90, 110 and 120% coolant flow-rate and time-horizons 2, 10 and 30 seconds, during discharge; MATLAB/Simulink framework.

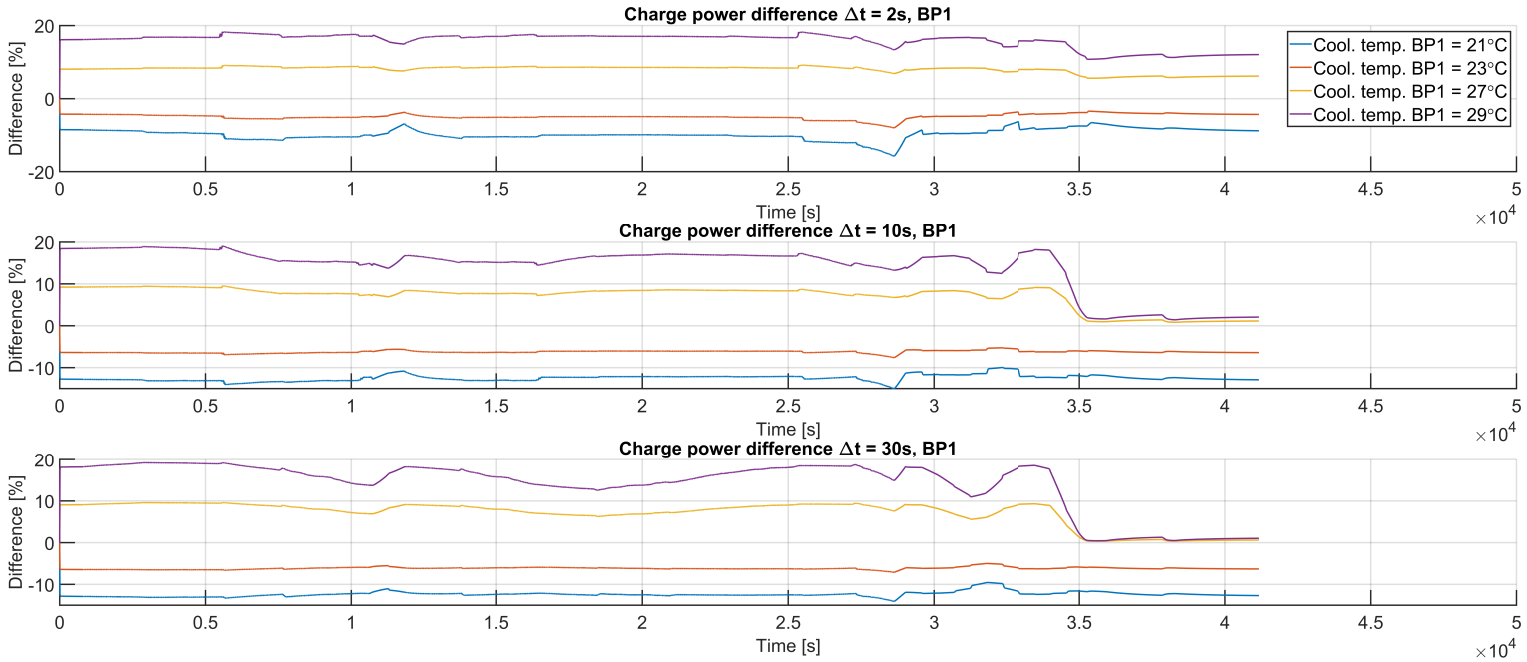

Figure 52: Difference from nominal SOP for 21, 23, 27 and 29 °C coolant temperature and time-horizons 2, 10 and 30 seconds, during charging. Nominal packs at nominal coolant temperature 25°C; MATLAB/Simulink framework.

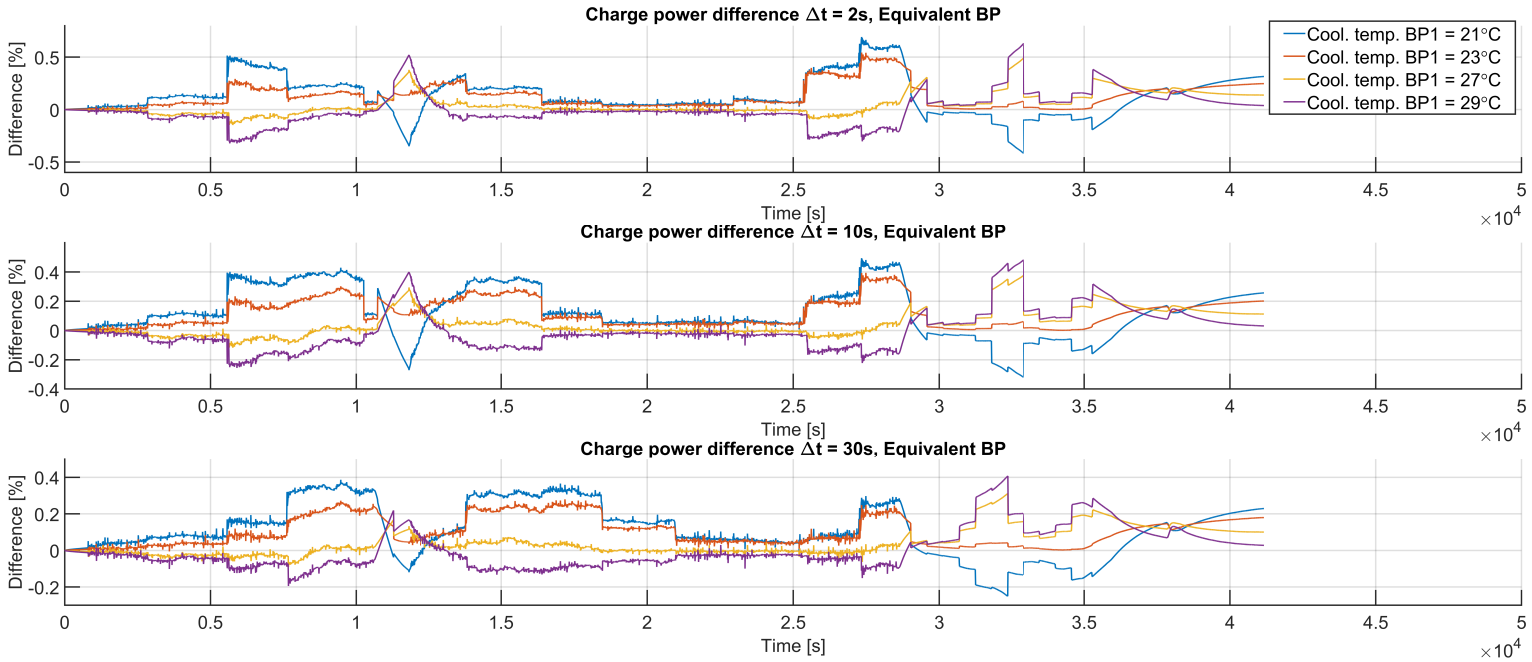

Figure 53: Representative pack SOP for 21, 23, 27 and 29 °C coolant temperature and time-horizons 2, 10 and 30 seconds, during charging. Nominal packs at nominal coolant temperature 25°C; MATLAB/Simulink framework.

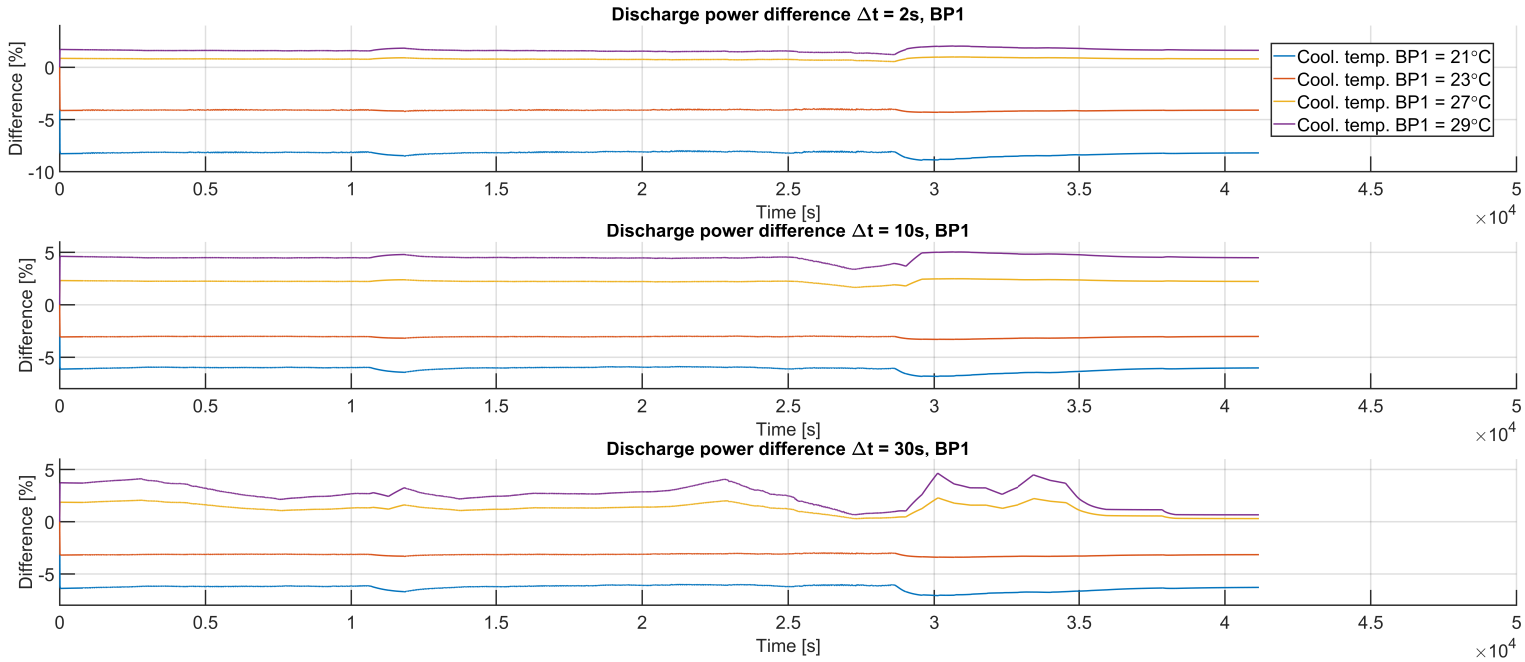

Figure 54: Difference from nominal SOP for 21, 23, 27 and 29 °C coolant temperature and time-horizons 2, 10 and 30 seconds, during discharge. Nominal packs at nominal coolant temperature 25°C; MATLAB/Simulink framework.

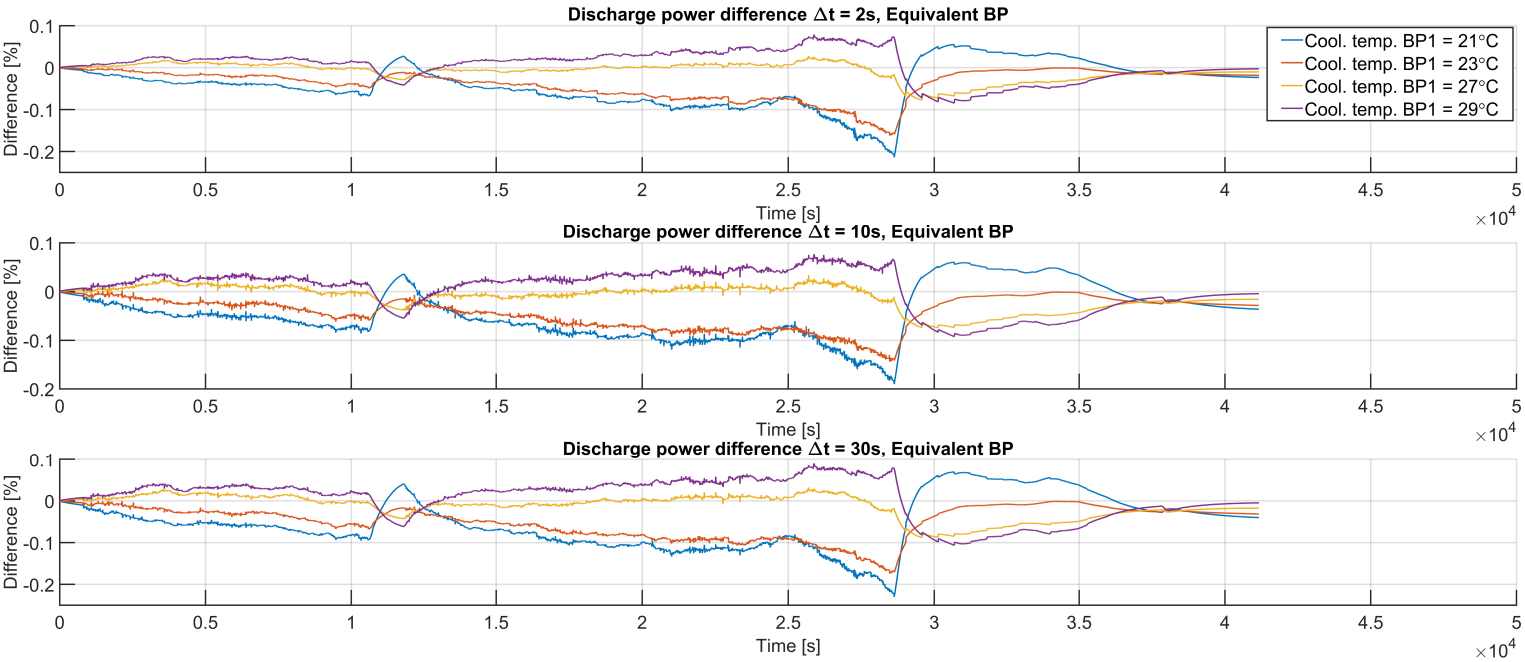

Figure 55: Representative pack SOP for 21, 23, 27 and 29 °C coolant temperature and time-horizons 2, 10 and 30 seconds, during discharge. Nominal packs at nominal coolant temperature 25°C; MATLAB/Simulink framework.

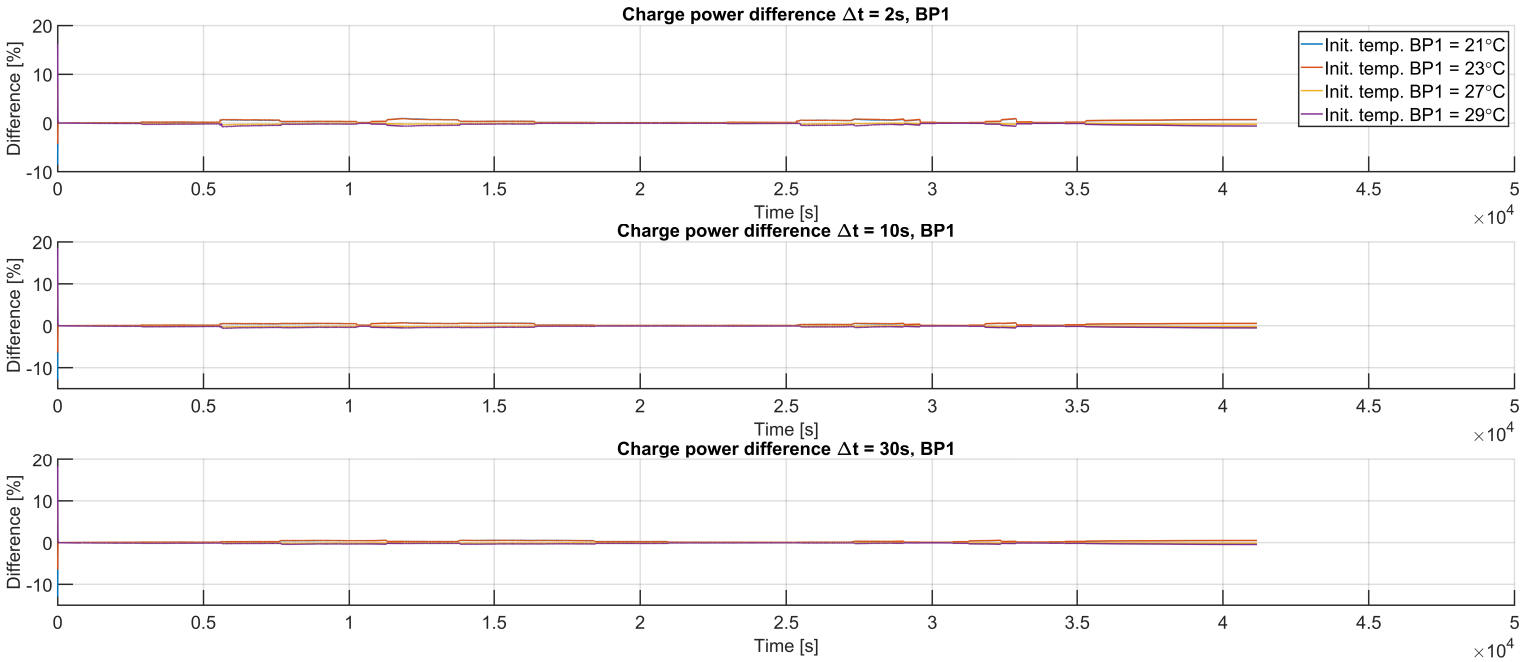

Figure 56: Difference from nominal SOP for 21, 23, 27 and 29 °C initial temperature and time-horizons 2, 10 and 30 seconds, during charging. Nominal packs at nominal initial temperature 25°C; MATLAB/Simulink framework.

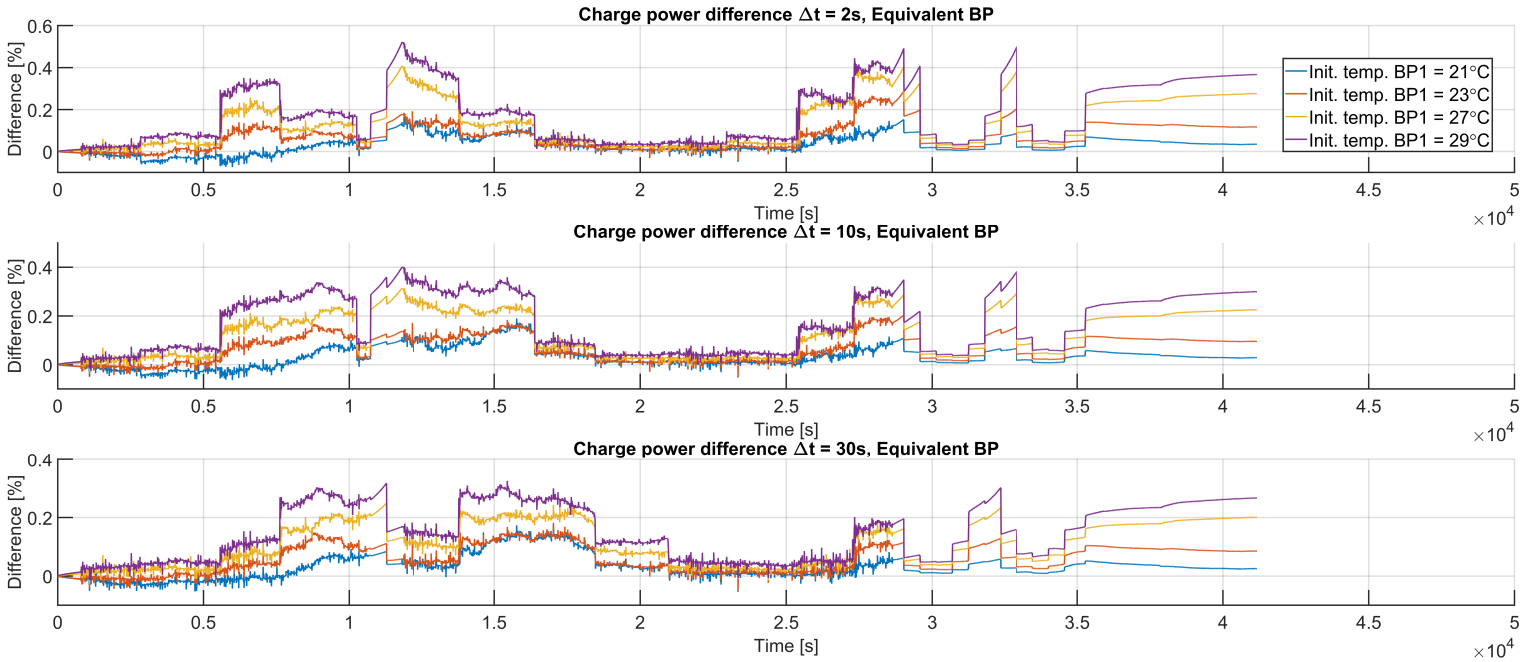

Figure 57: Representative pack SOP for 21, 23, 27 and 29 °C initial temperature and time-horizons 2, 10 and 30 seconds, during charging. Nominal packs at nominal initial temperature 25°C; MATLAB/Simulink framework.

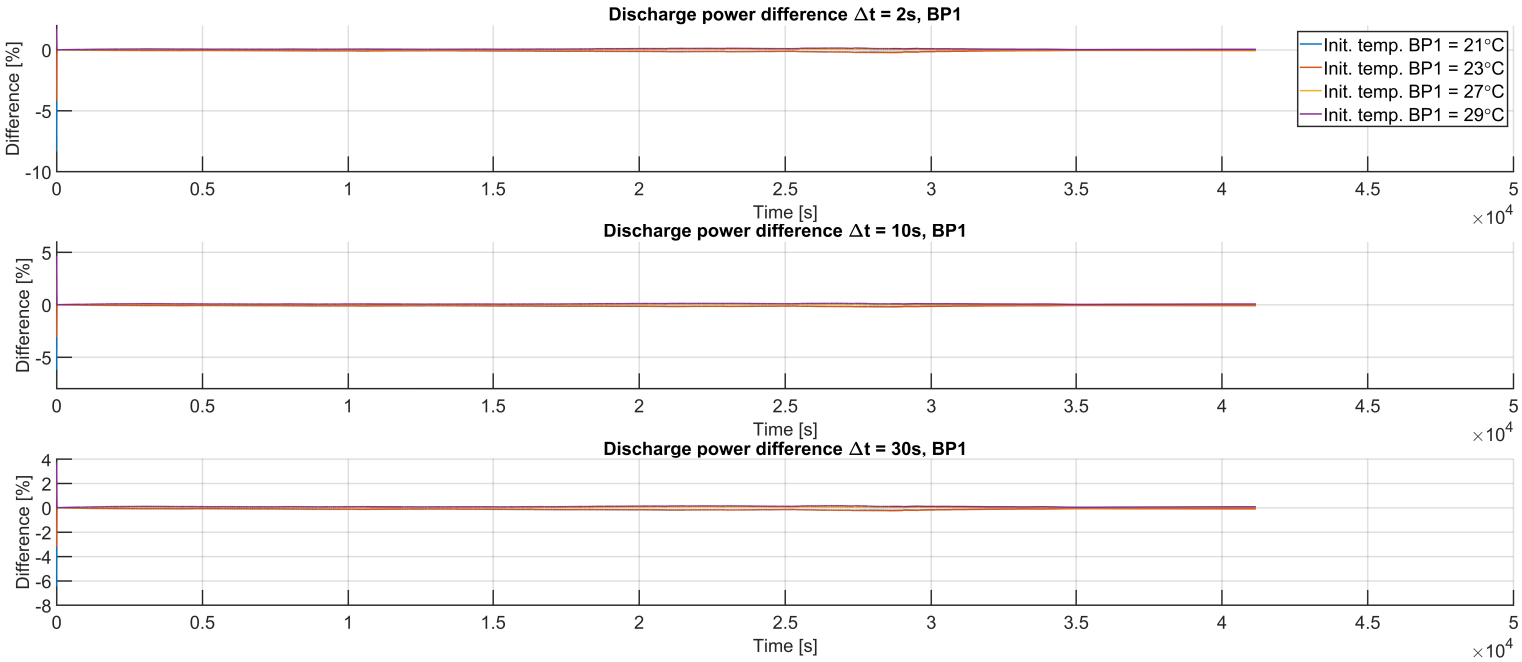

Figure 58: Difference from nominal SOP for 21, 23, 27 and 29 °C initial temperature and time-horizons 2, 10 and 30 seconds, during discharge. Nominal packs at nominal initial temperature 25°C; MATLAB/Simulink framework.

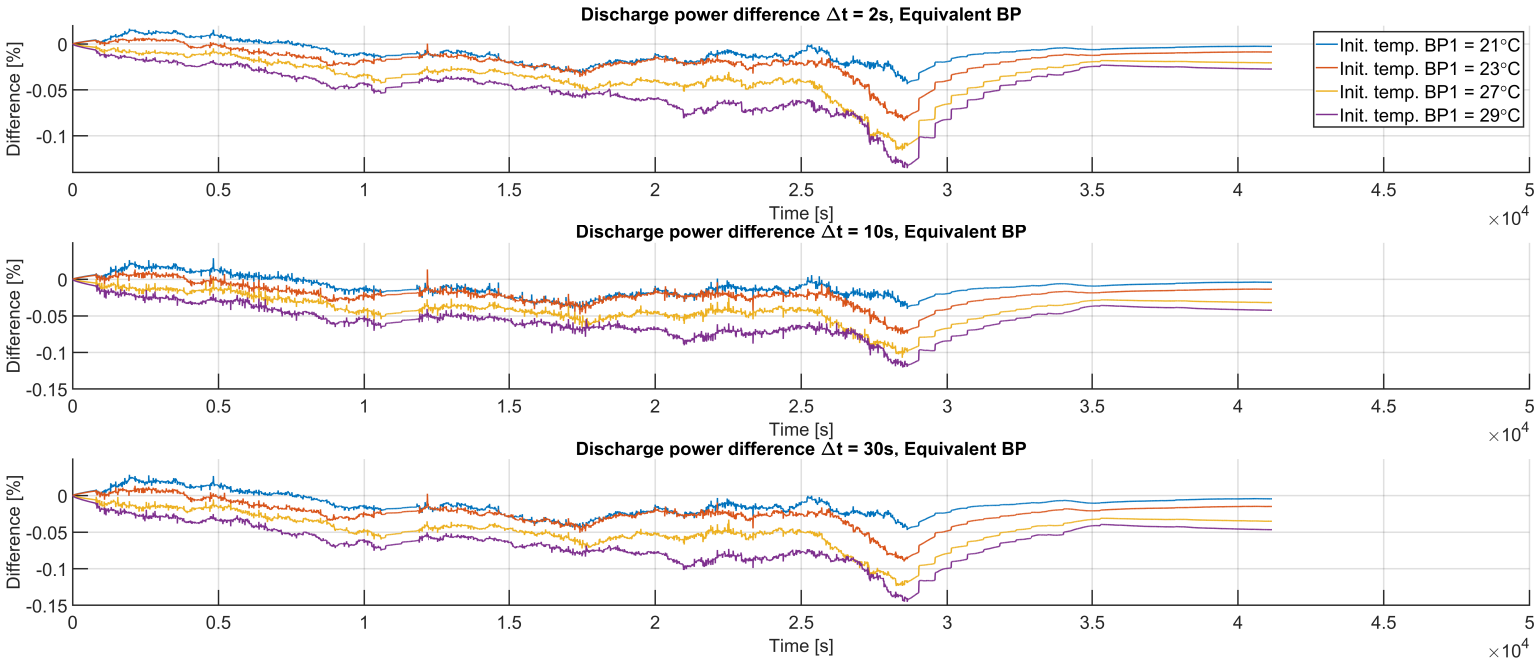

Figure 59: Representative pack SOP for 21, 23, 27 and 29 °C initial temperature and time-horizons 2, 10 and 30 seconds, during discharge. Nominal packs at nominal initial temperature 25°C; MATLAB/Simulink framework.

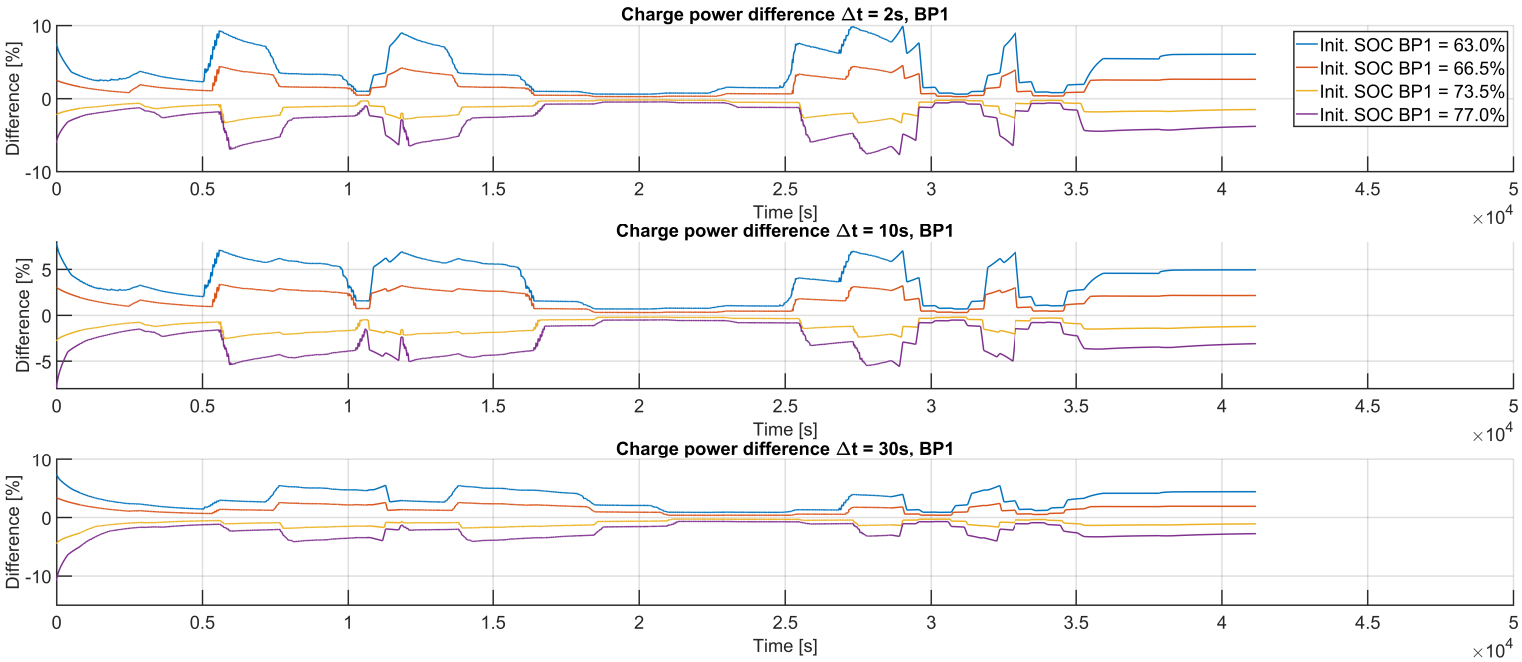

Figure 60: Difference from nominal SOP for 63.0, 66.5, 73.5 and 77% initial SOC and time-horizons 2, 10 and 30 seconds, during charging. Nominal packs at nominal initial SOC 70%; MATLAB/Simulink framework.

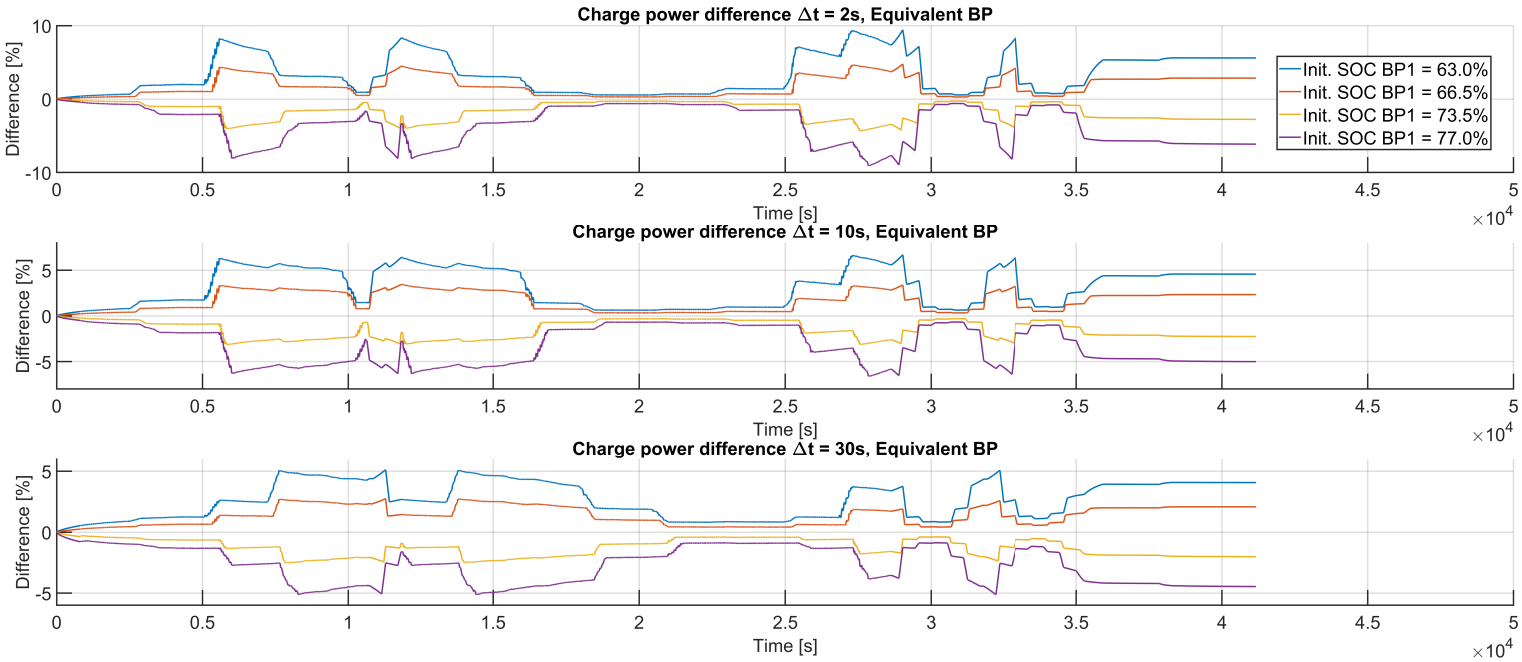

Figure 61: Representative pack SOP for 63.0, 66.5, 73.5 and 77% initial SOC and time-horizons 2, 10 and 30 seconds, during charging. Nominal packs at nominal initial SOC 70%; MATLAB/Simulink framework.

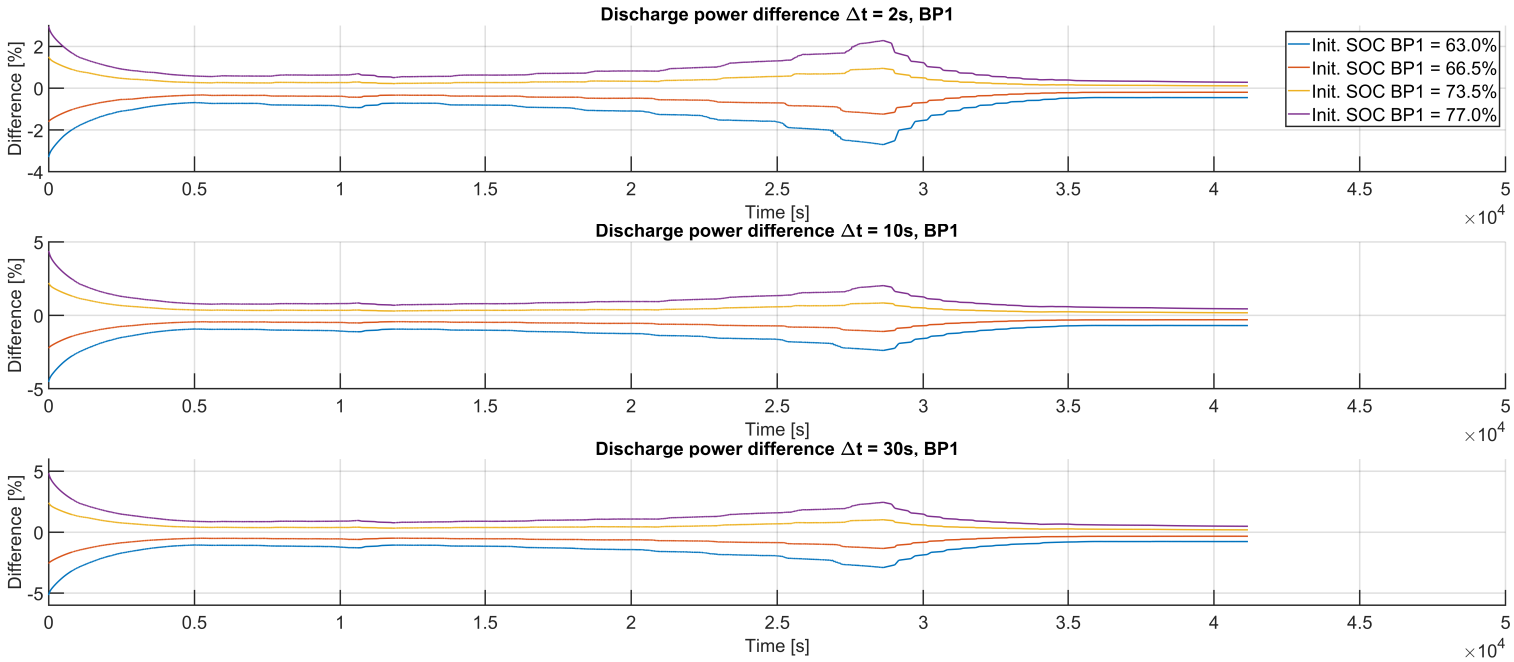

Figure 62: Difference from nominal SOP for 63.0, 66.5, 73.5 and 77% initial SOC and time-horizons 2, 10 and 30 seconds, during discharge. Nominal packs at nominal initial SOC 70%; MATLAB/Simulink framework.

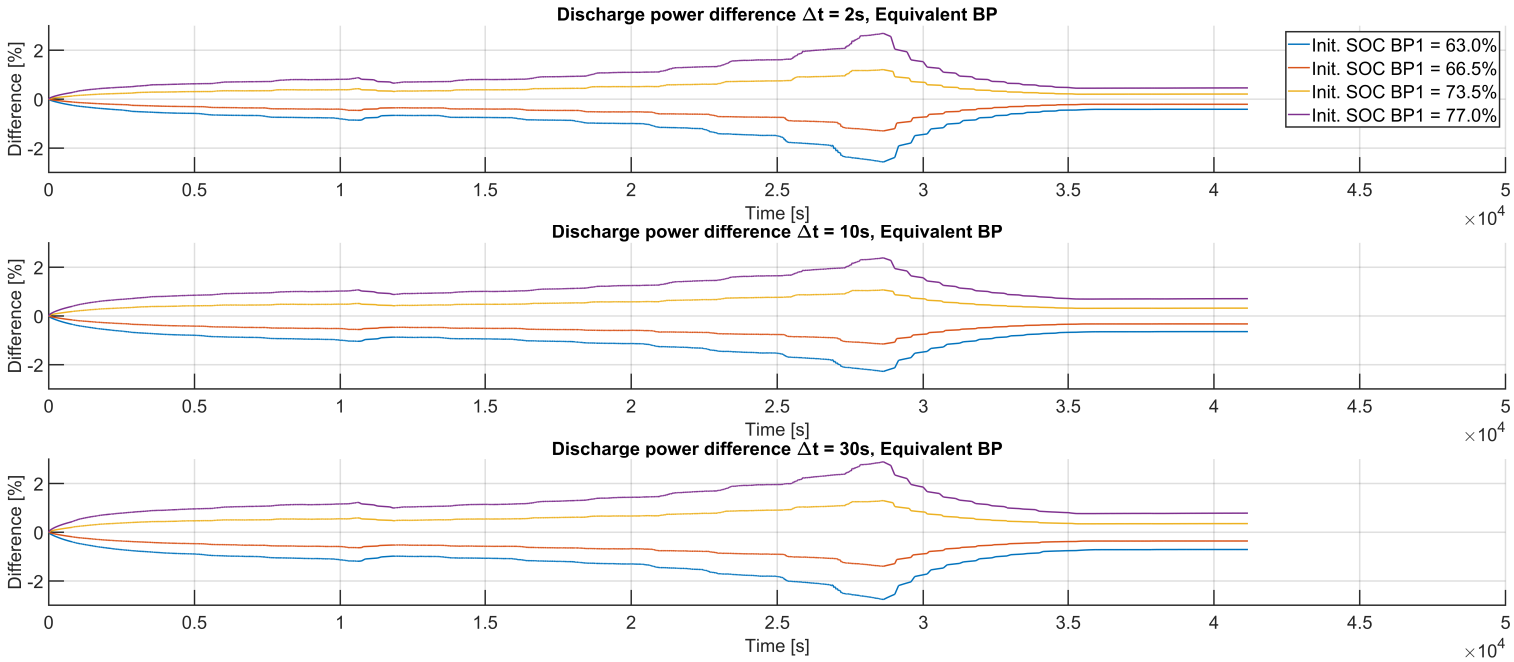

Figure 63: Representative pack SOP for 63.0, 66.5, 73.5 and 77% initial SOC and time-horizons 2, 10 and 30 seconds, during discharge. Nominal packs at nominal initial SOC 70%; MATLAB/Simulink framework.

Appendix B

Appendix B presents the results from the sensitivity analysis performed in the Simcenter Amesim framework. The relevant chapter to this appendix is Chapter 4. Every test includes difference from nominal charge/discharge SOP for the three time-horizons.

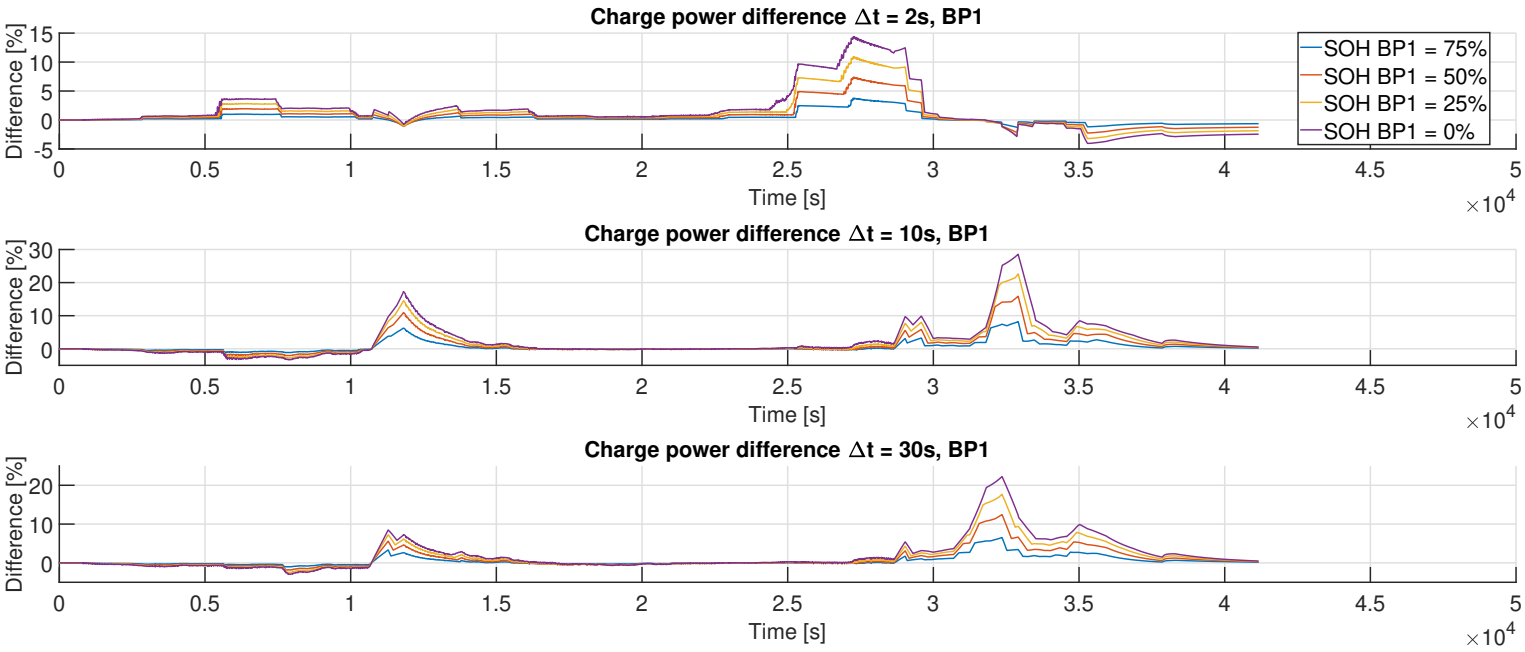

Figure 64: Difference from nominal SOP for 0, 25, 50 and 75% SOH and time-horizons 2, 10 and 30 seconds, during charging; Simcenter Amesim framework.

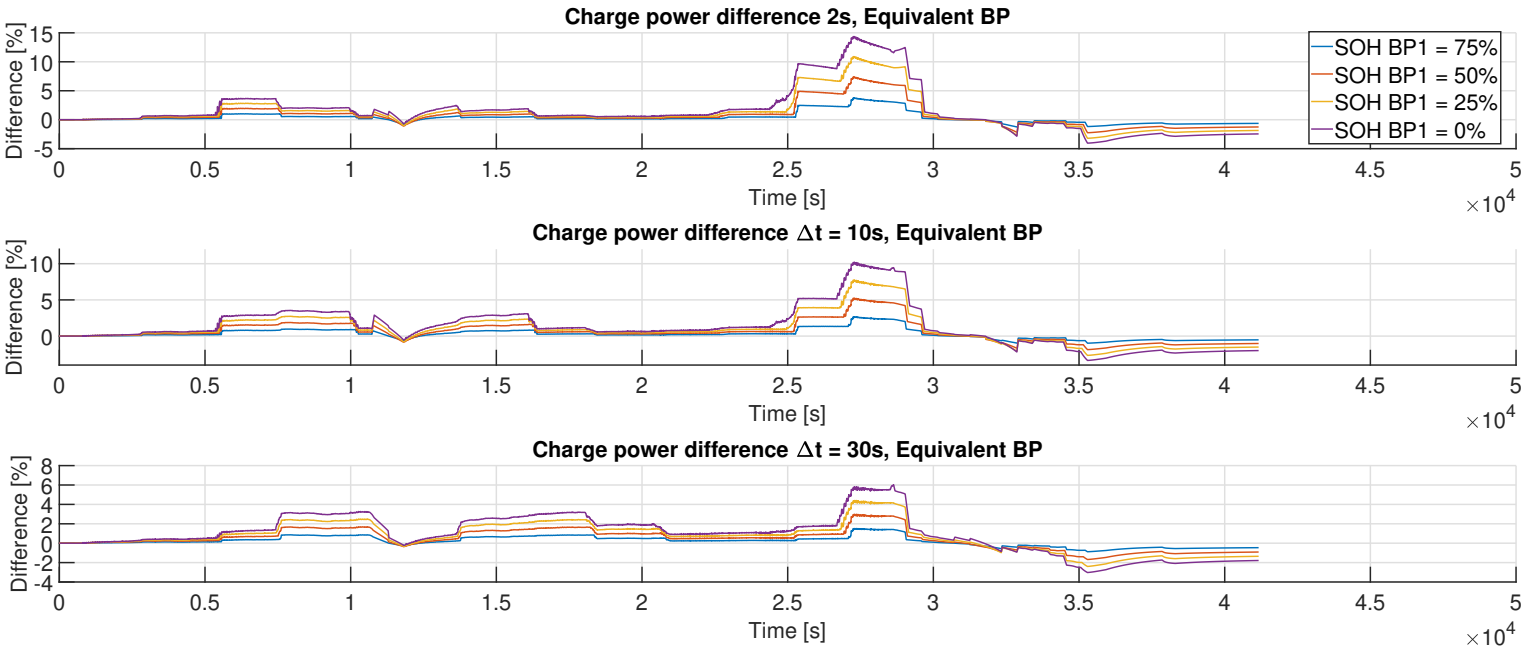

Figure 65: Representative pack SOP for 0, 25, 50 and 75% SOH and time-horizons 2, 10 and 30 seconds, during charging; Simcenter Amesim framework.

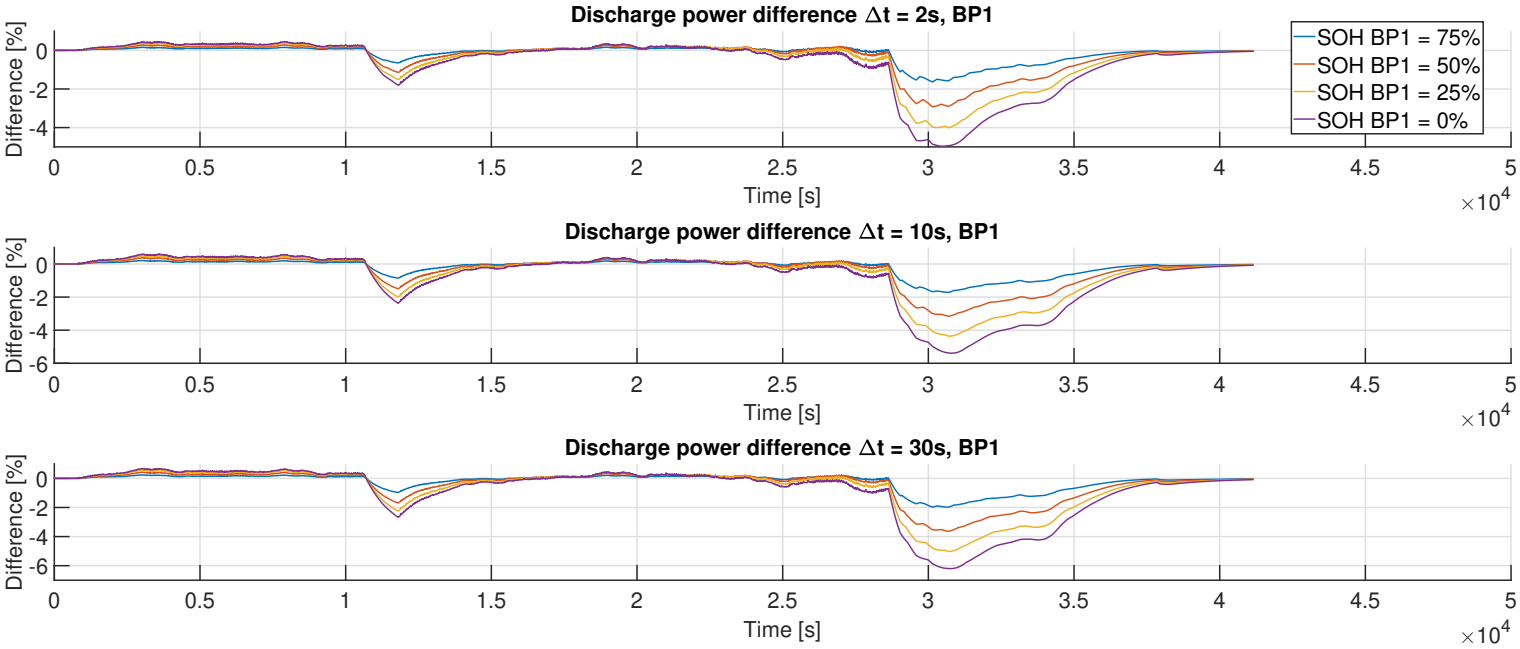

Figure 66: Difference from nominal SOP for 0, 25, 50 and 75% SOH and time-horizons 2, 10 and 30 seconds, during discharge; Simcenter Amesim framework.

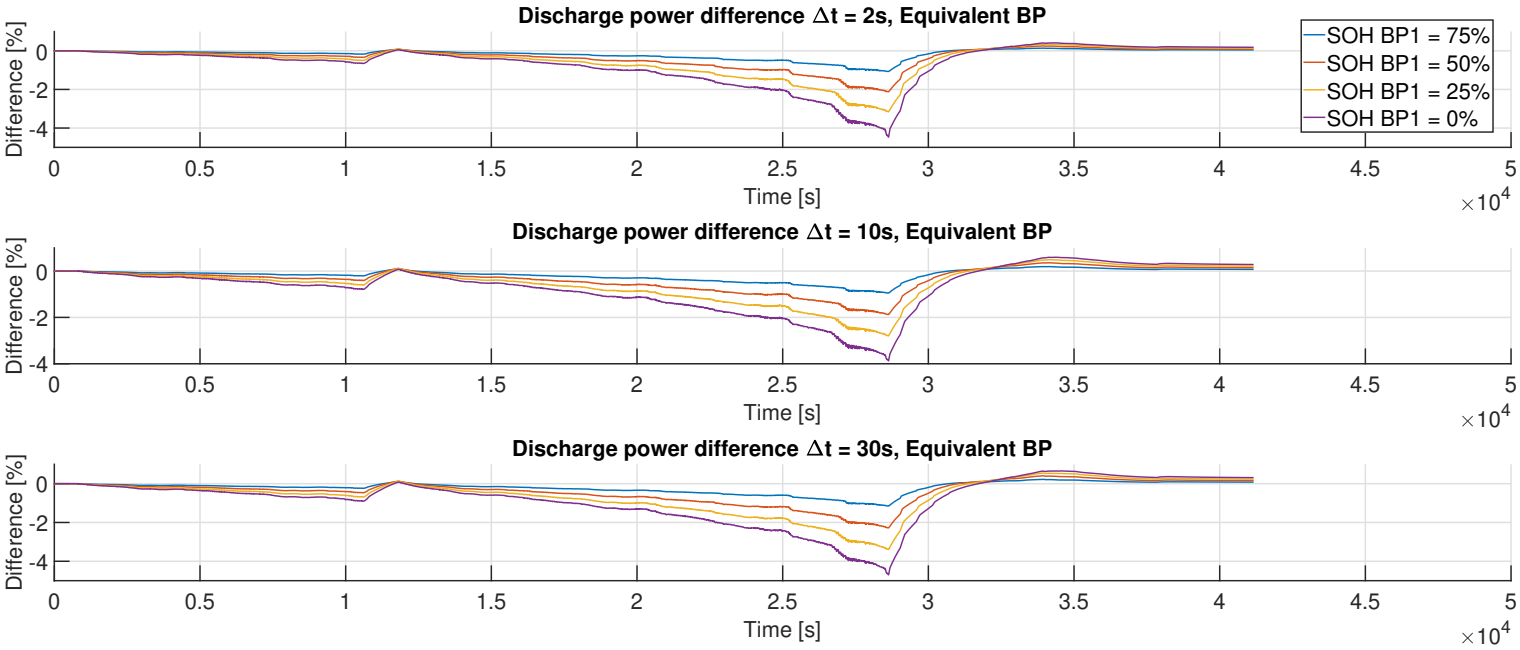

Figure 67: Representative pack SOP for 0, 25, 50 and 75% SOH and time-horizons 2, 10 and 30 seconds, during discharge; Simcenter Amesim framework.

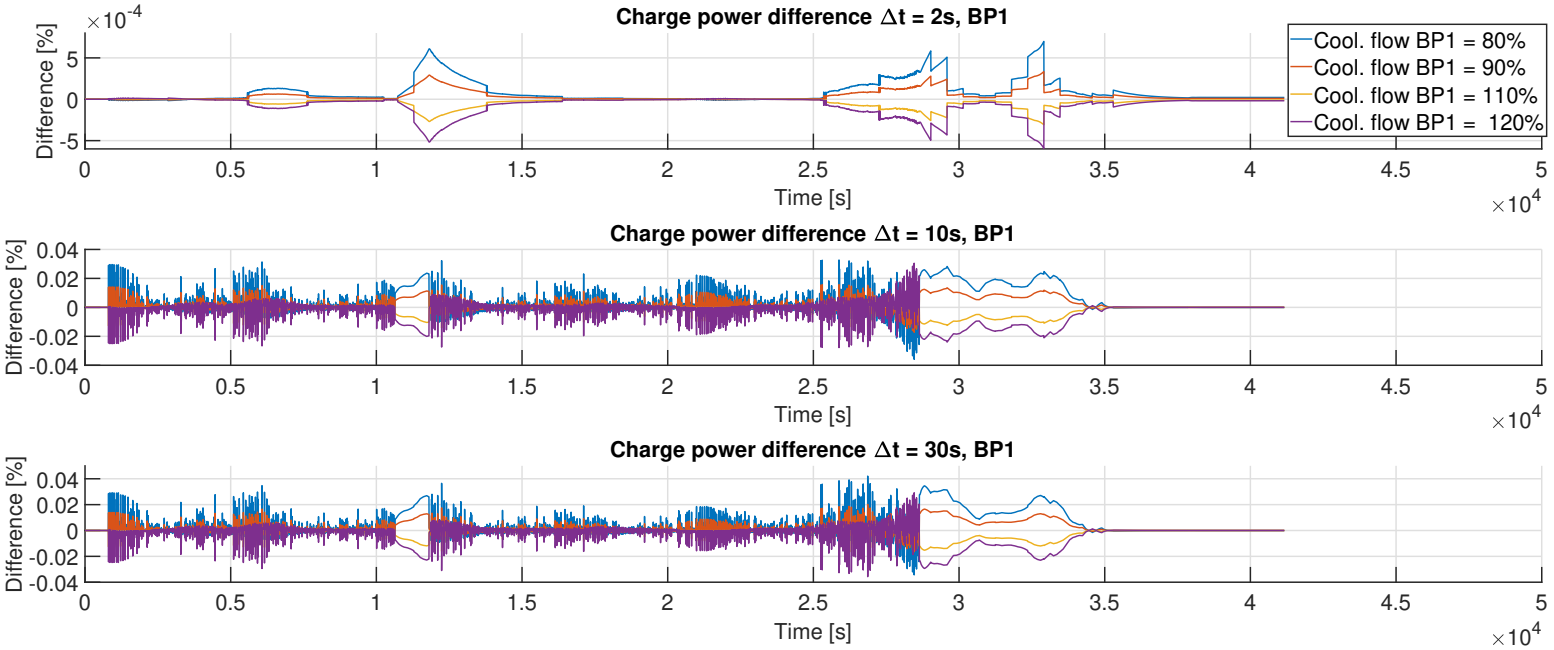

Figure 68: Difference from nominal SOP for 80, 90, 110 and 120% coolant flow-rate and time-horizons 2, 10 and 30 seconds, during charging; Simcenter Amesim framework.

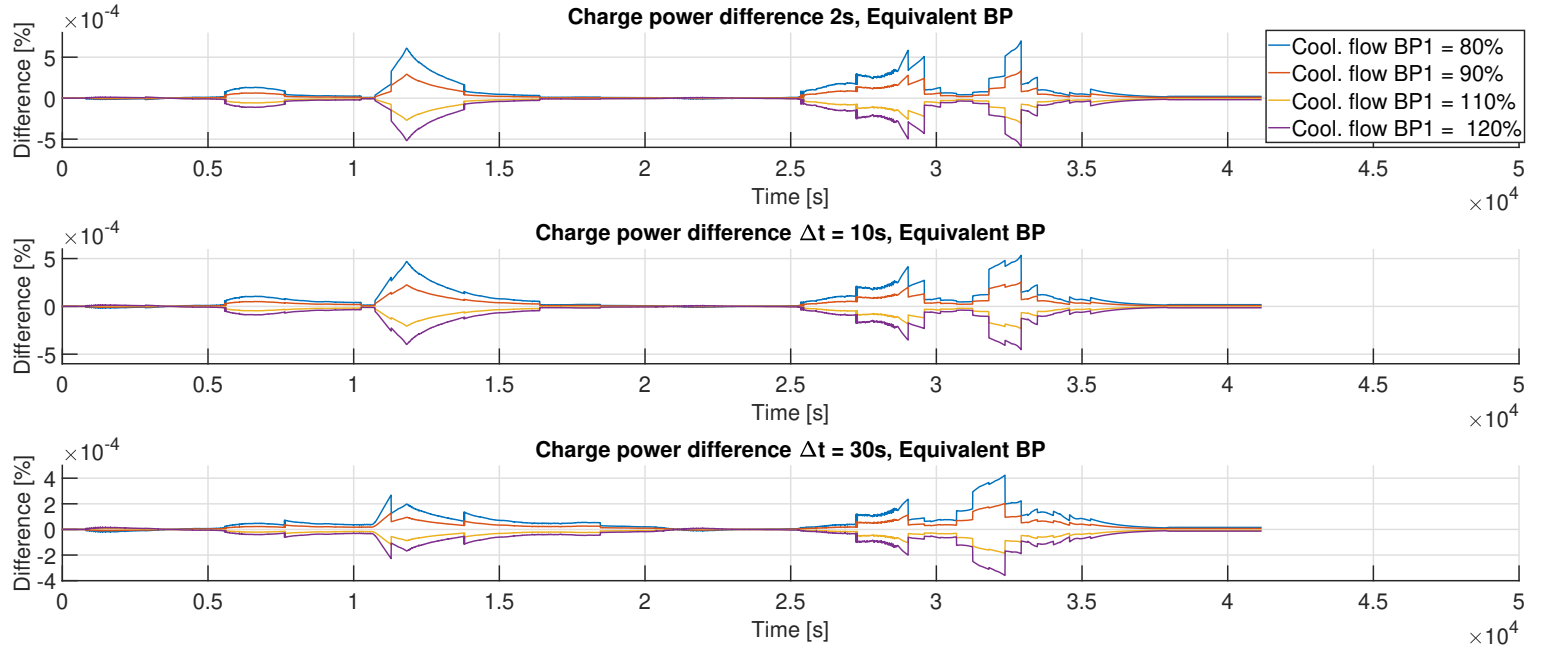

Figure 69: Representative pack SOP for 80, 90, 110 and 120% coolant flow-rate and time-horizons 2, 10 and 30 seconds, during charging; Simcenter Amesim framework.

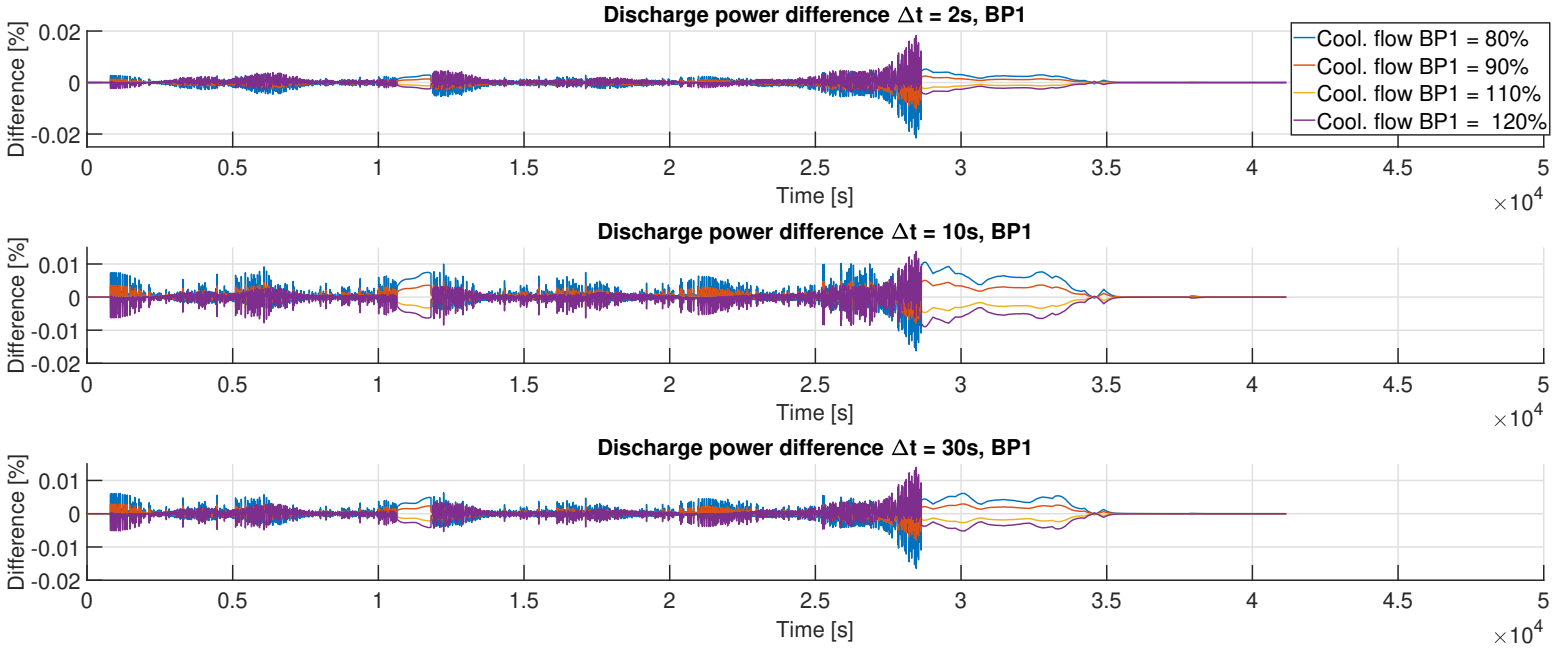

Figure 70: Difference from nominal SOP for 80, 90, 110 and 120% coolant flow-rate and time-horizons 2, 10 and 30 seconds, during discharge; Simcenter Amesim framework.

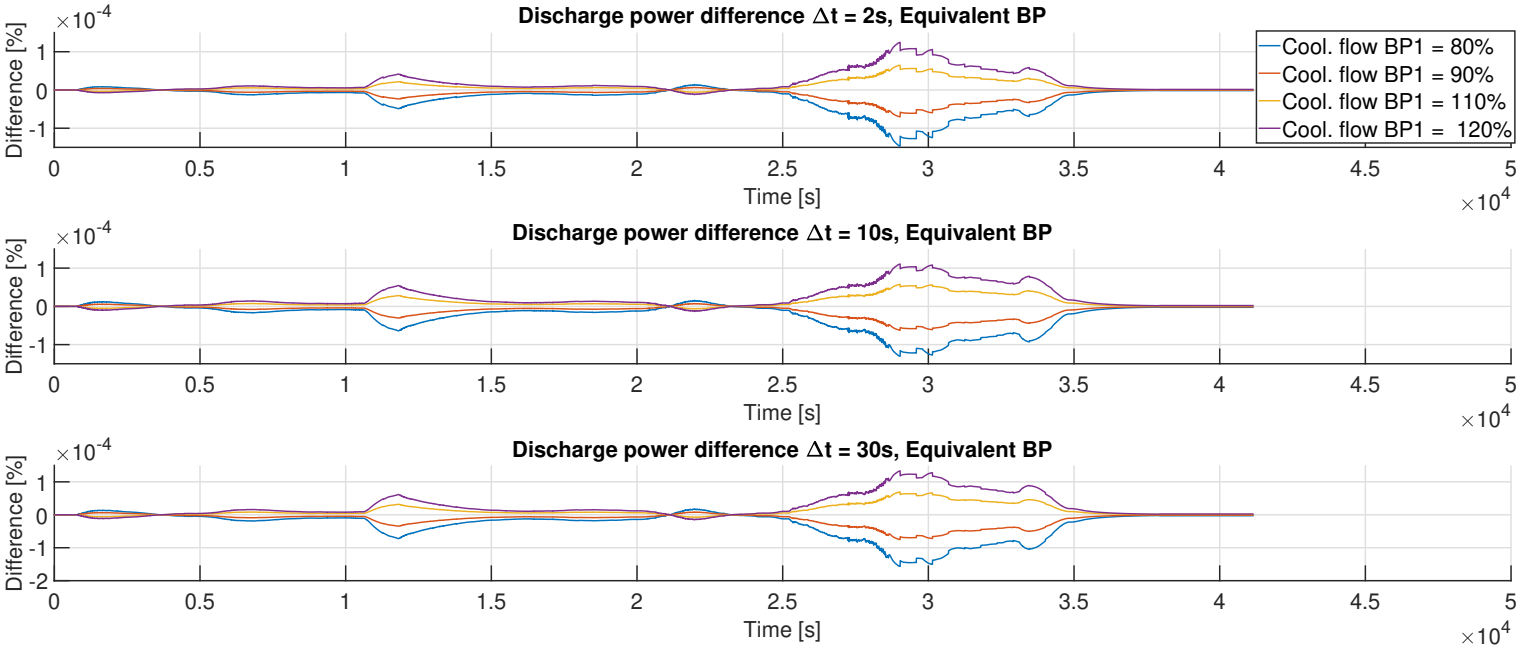

Figure 71: Representative pack SOP for 80, 90, 110 and 120% coolant flow-rate and time-horizons 2, 10 and 30 seconds, during discharge; Simcenter Amesim framework.

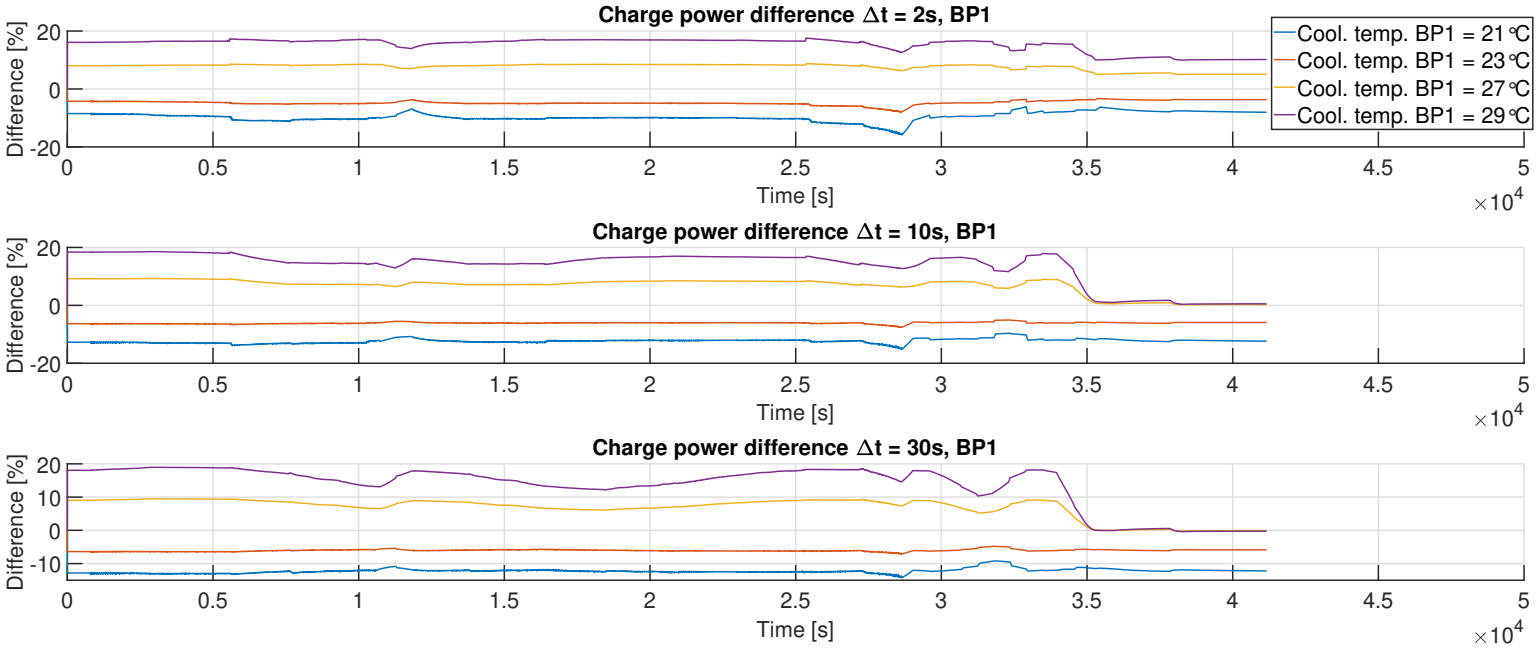

Figure 72: Difference from nominal SOP for 21, 23, 27 and 29 °C coolant temperature and time-horizons 2, 10 and 30 seconds, during charging. Nominal packs at nominal coolant temperature 25°C; Simcenter Amesim framework.

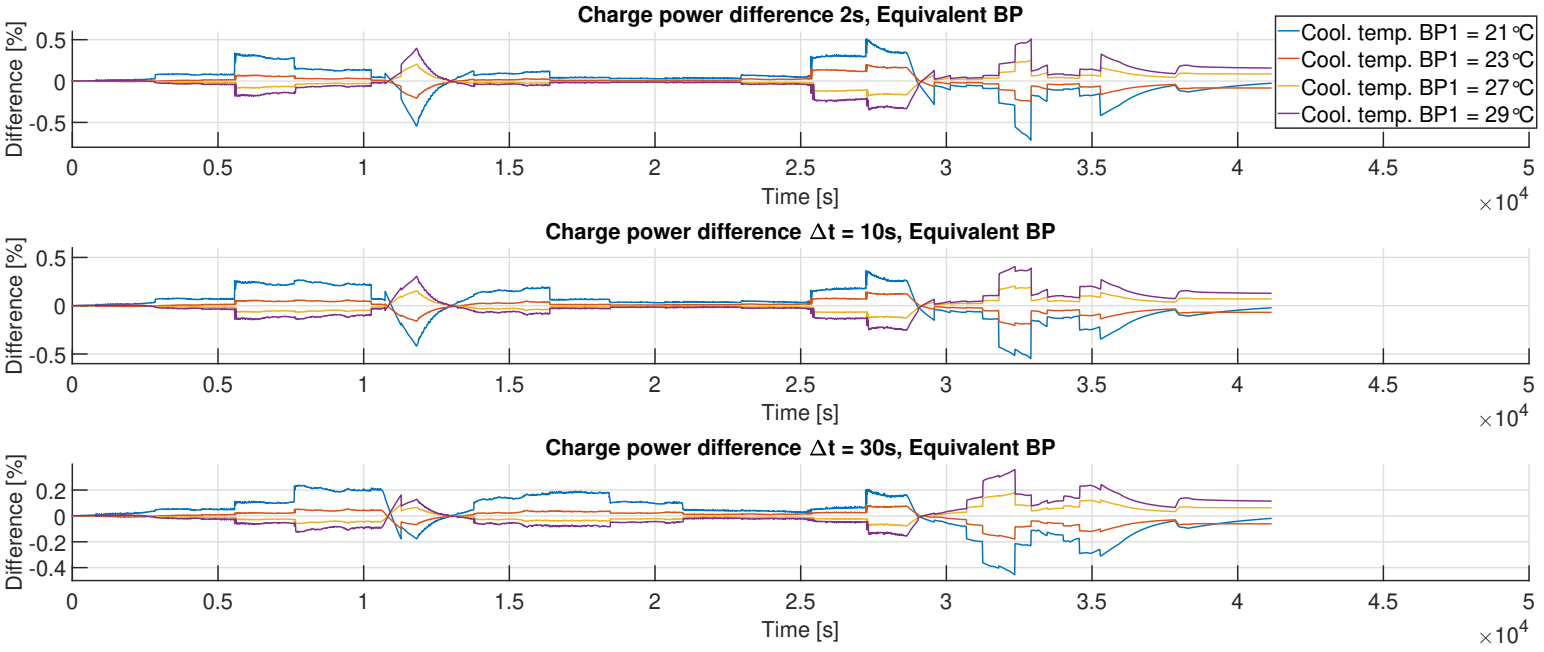

Figure 73: Representative pack SOP for 21, 23, 27 and 29 °C coolant temperature and time-horizons 2, 10 and 30 seconds, during charging. Nominal packs at nominal coolant temperature 25°C; Simcenter Amesim framework.

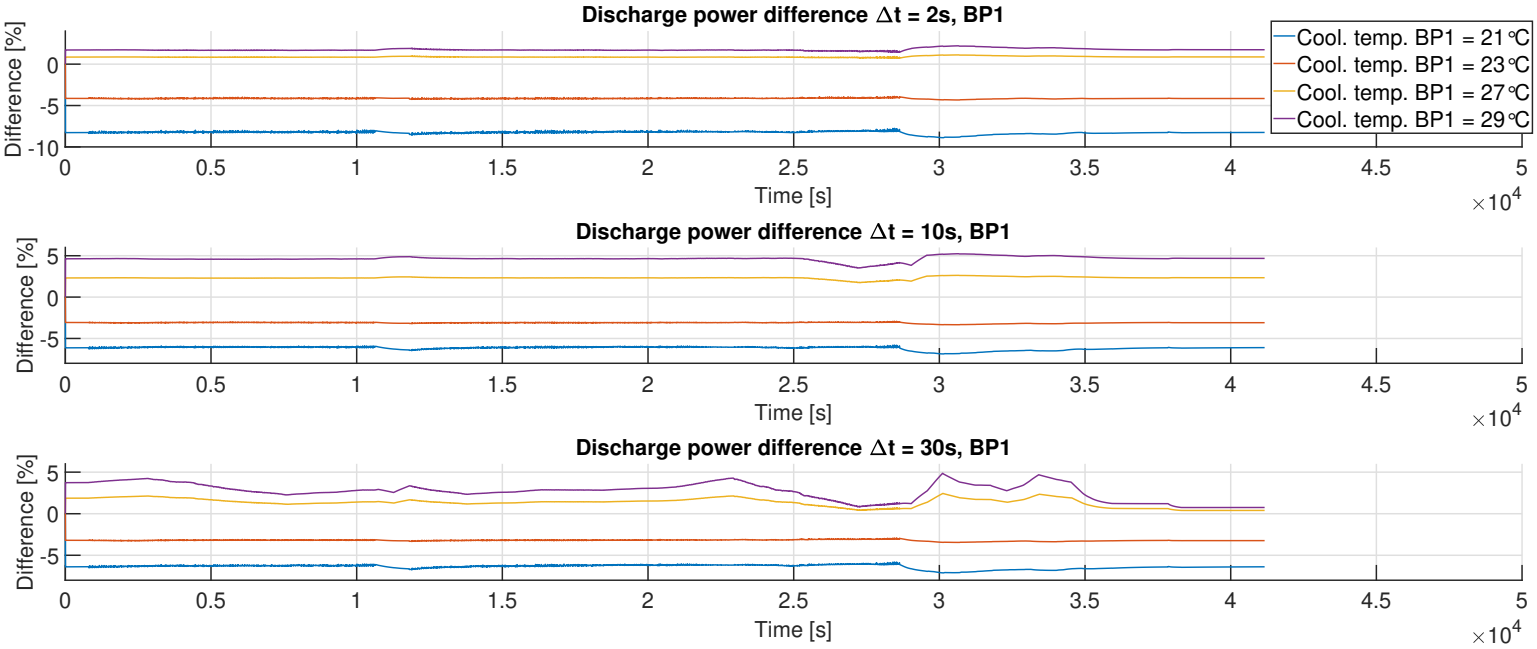

Figure 74: Difference from nominal SOP for 21, 23, 27 and 29 °C coolant temperature and time-horizons 2, 10 and 30 seconds, during discharge. Nominal packs at nominal coolant temperature 25°C; Simcenter Amesim framework.

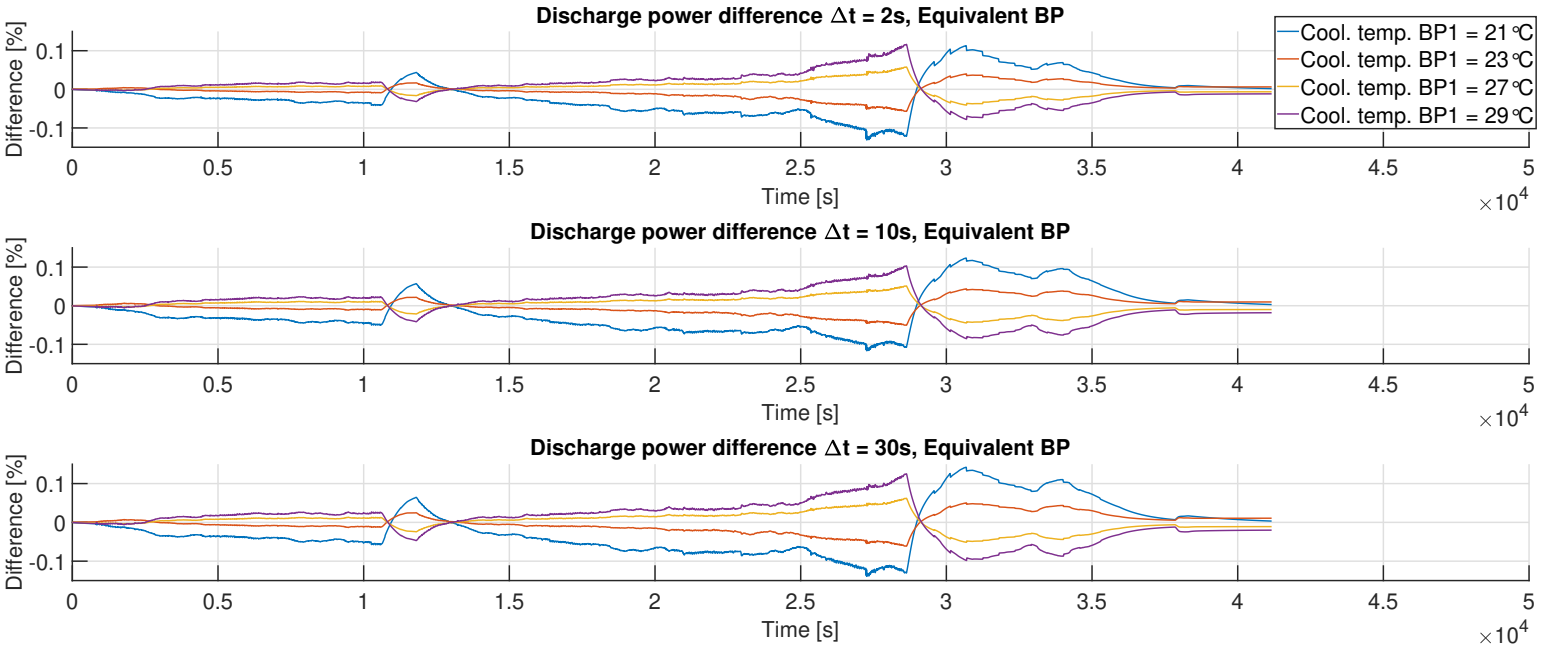

Figure 75: Representative pack SOP for 21, 23, 27 and 29 °C coolant temperature and time-horizons 2, 10 and 30 seconds, during discharge. Nominal packs at nominal coolant temperature 25°C; Simcenter Amesim framework.

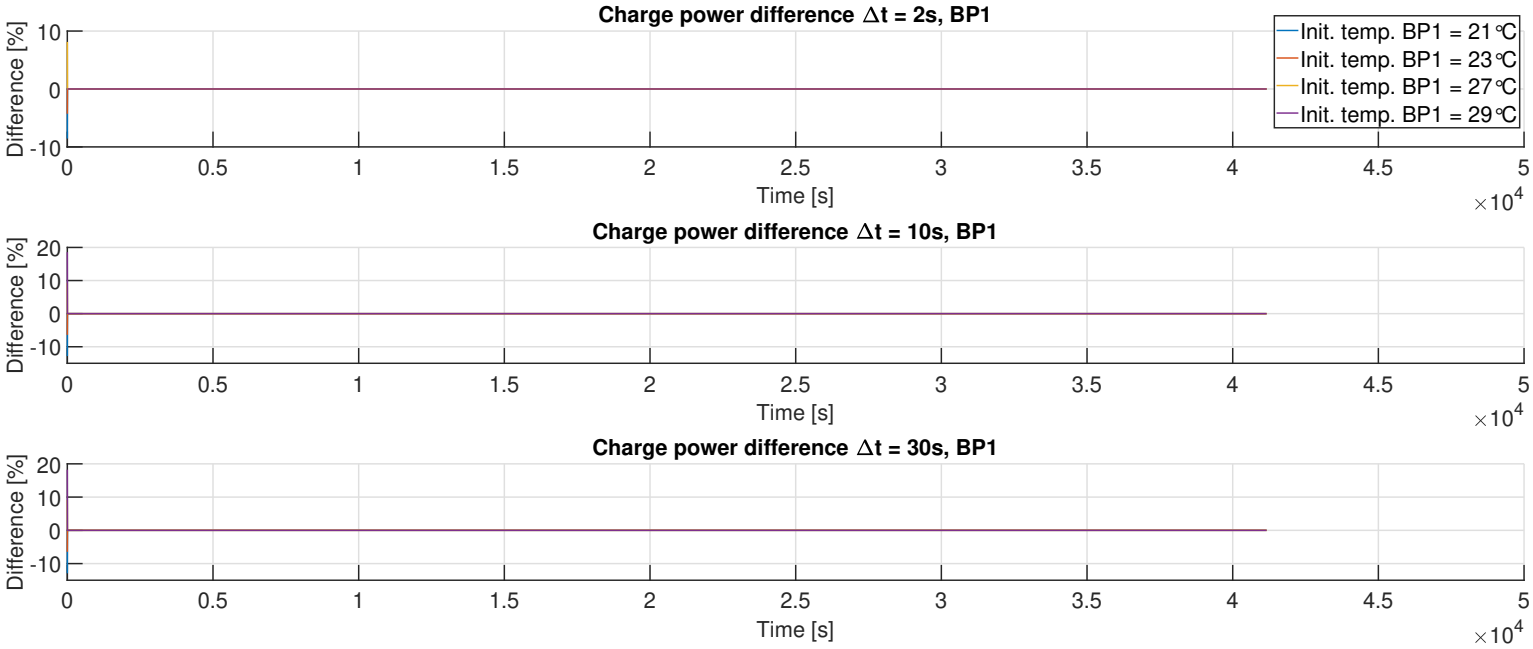

Figure 76: Difference from nominal SOP for 21, 23, 27 and 29 °C initial temperature and time-horizons 2, 10 and 30 seconds, during charging. Nominal packs at nominal initial temperature 25°C; Simcenter Amesim framework.

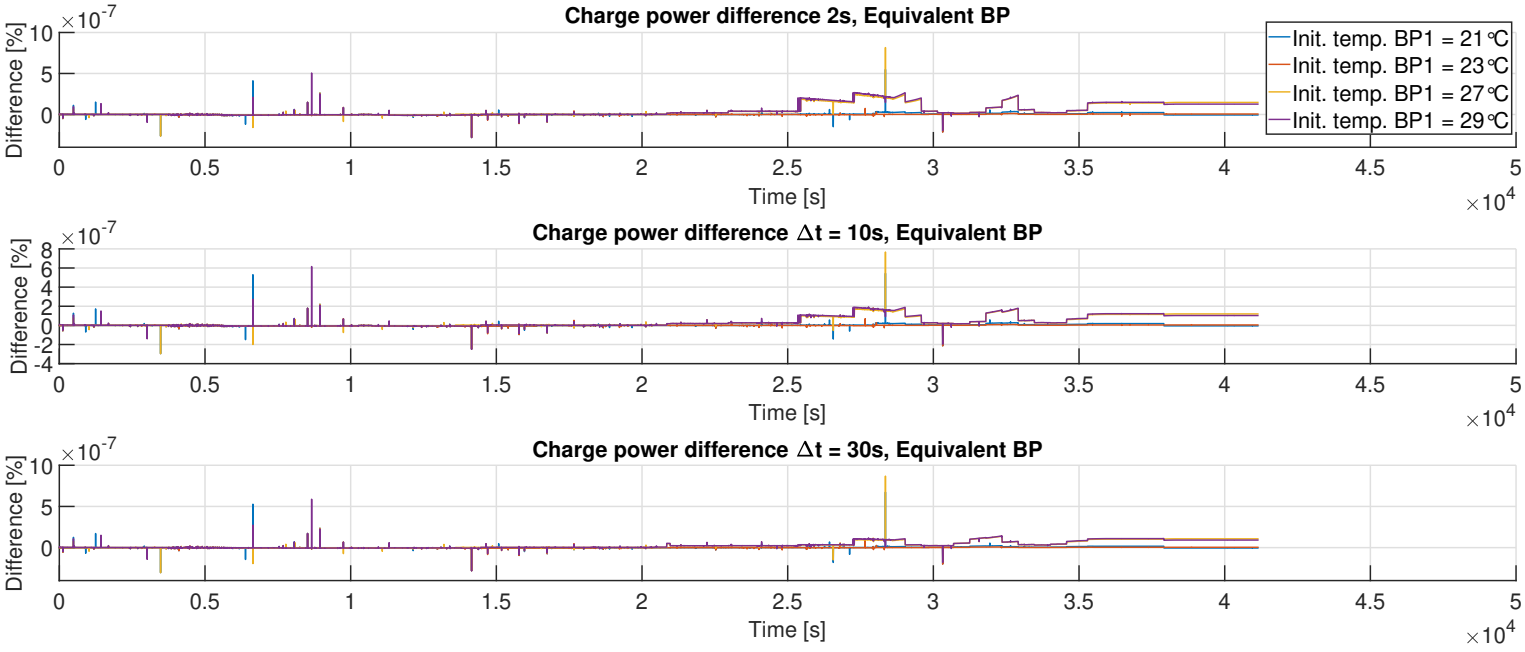

Figure 77: Representative pack SOP for 21, 23, 27 and 29 °C initial temperature and time-horizons 2, 10 and 30 seconds, during charging. Nominal packs at nominal initial temperature 25°C; Simcenter Amesim framework.

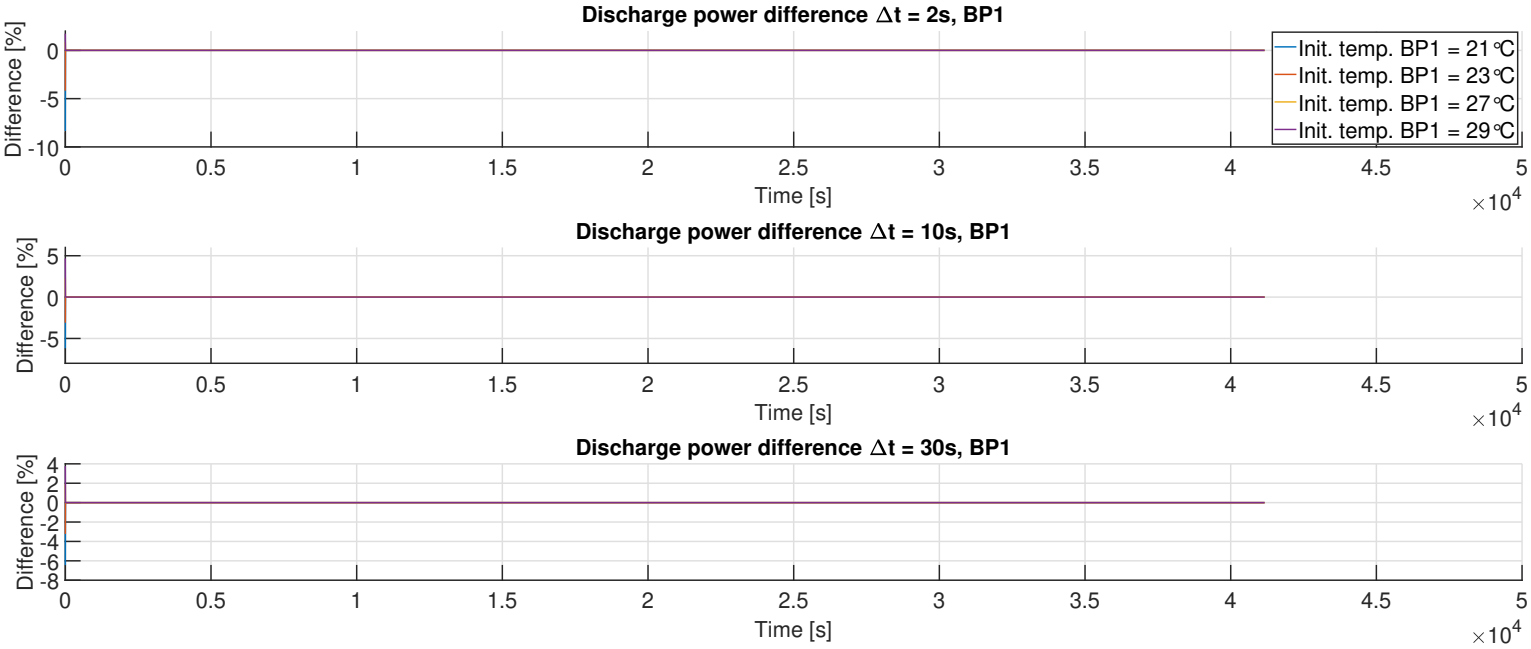

Figure 78: Difference from nominal SOP for 21, 23, 27 and 29 °C initial temperature and time-horizons 2, 10 and 30 seconds, during discharge. Nominal packs at nominal initial temperature 25°C; Simcenter Amesim framework.

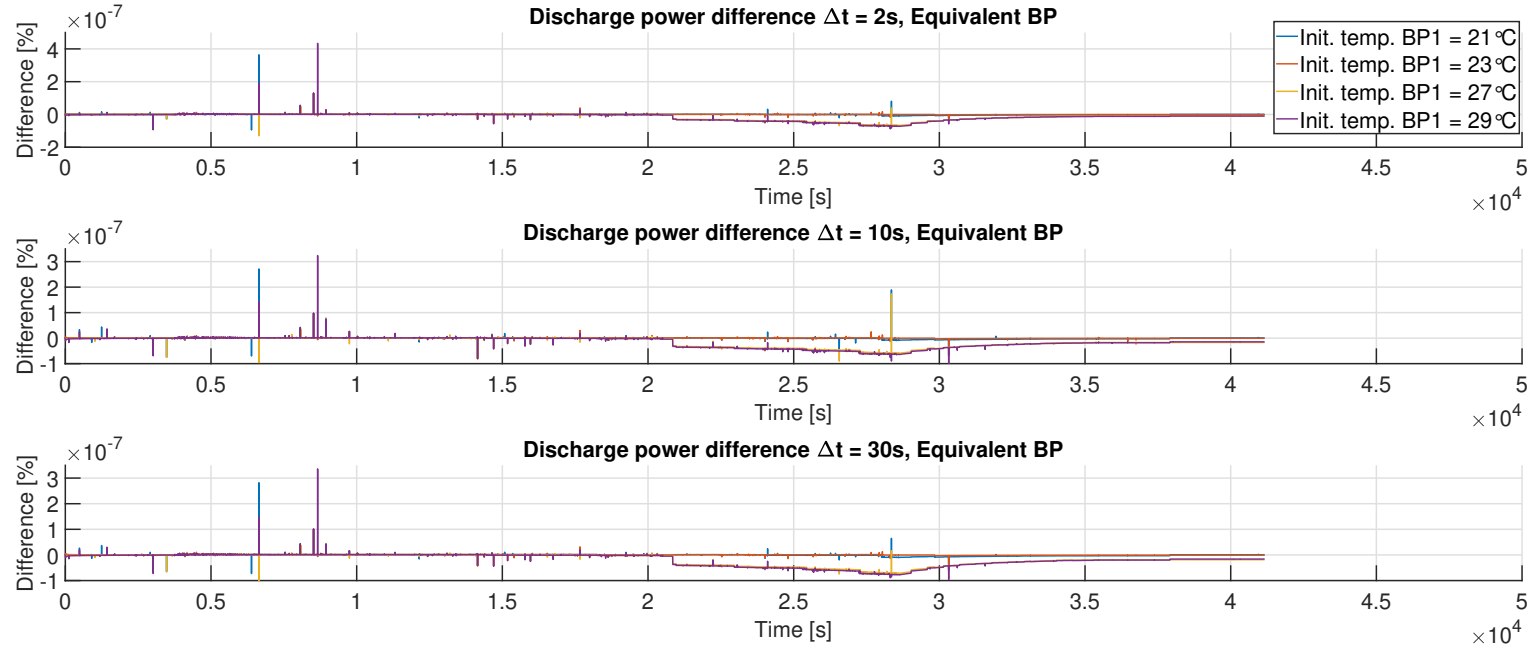

Figure 79: Representative pack SOP for 21, 23, 27 and 29 °C initial temperature and time-horizons 2, 10 and 30 seconds, during discharge. Nominal packs at nominal initial temperature 25°C; Simcenter Amesim framework.

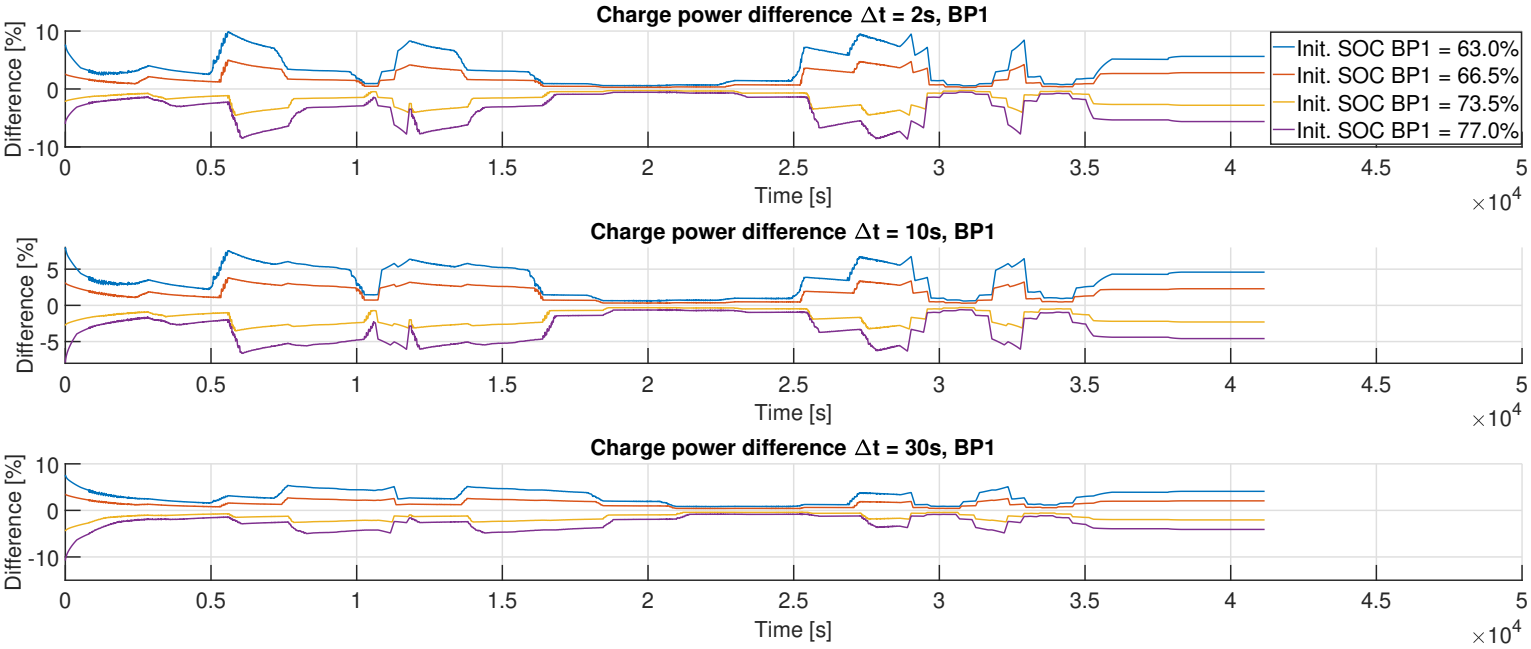

Figure 80: Difference from nominal SOP for 63.0, 66.5, 73.5 and 77% initial SOC and time-horizons 2, 10 and 30 seconds, during charging. Nominal packs at nominal initial SOC 70%; Simcenter Amesim framework.

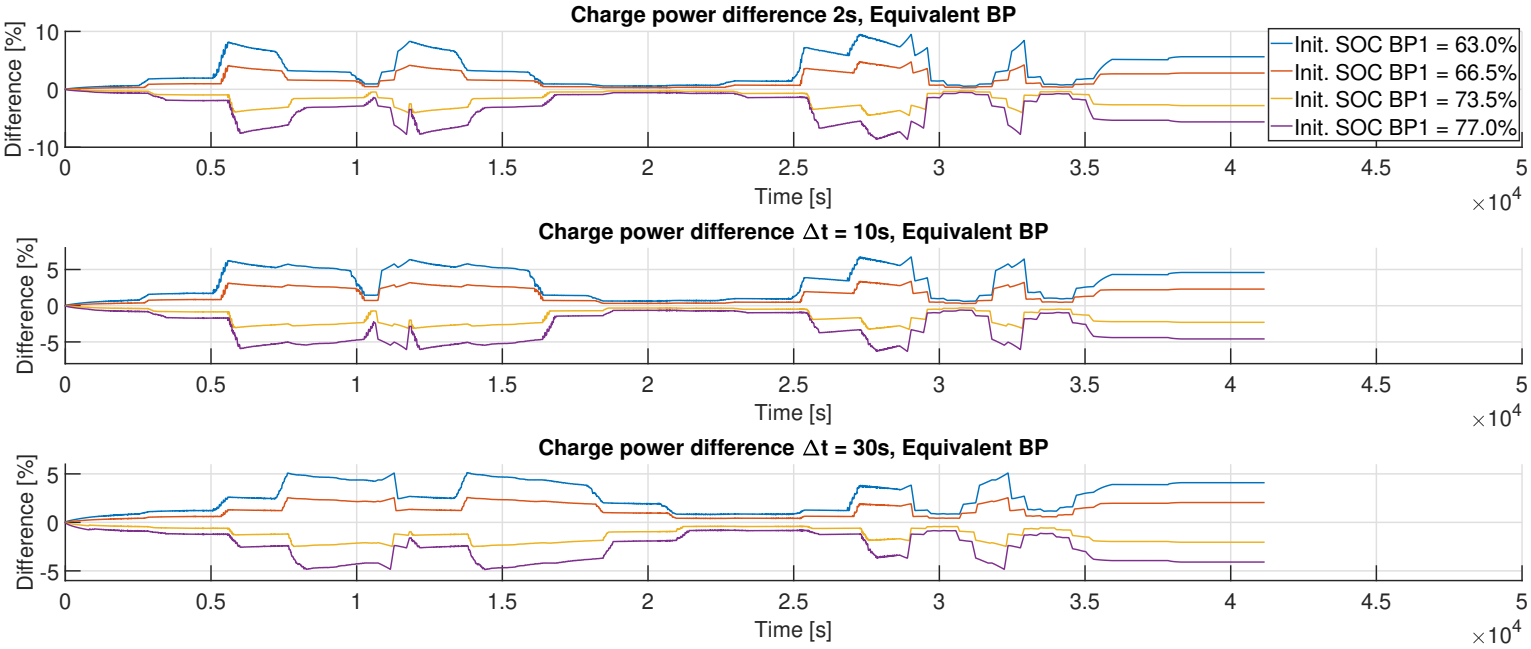

Figure 81: Representative pack SOP for 63.0, 66.5, 73.5 and 77% initial SOC and time-horizons 2, 10 and 30 seconds, during charging. Nominal packs at nominal initial SOC 70%; Simcenter Amesim framework.

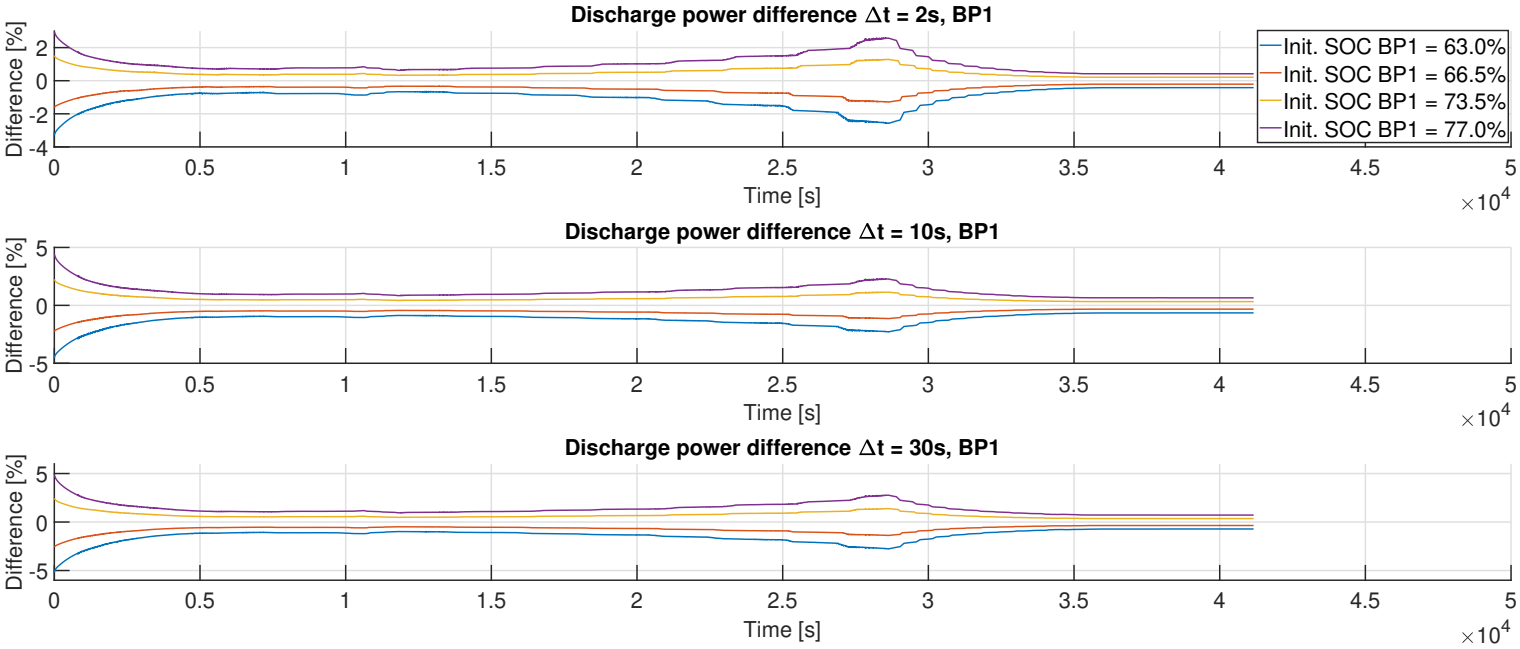

Figure 82: Difference from nominal SOP for 63.0, 66.5, 73.5 and 77% initial SOC and time-horizons 2, 10 and 30 seconds, during discharge. Nominal packs at nominal initial SOC 70%; Simcenter Amesim framework.

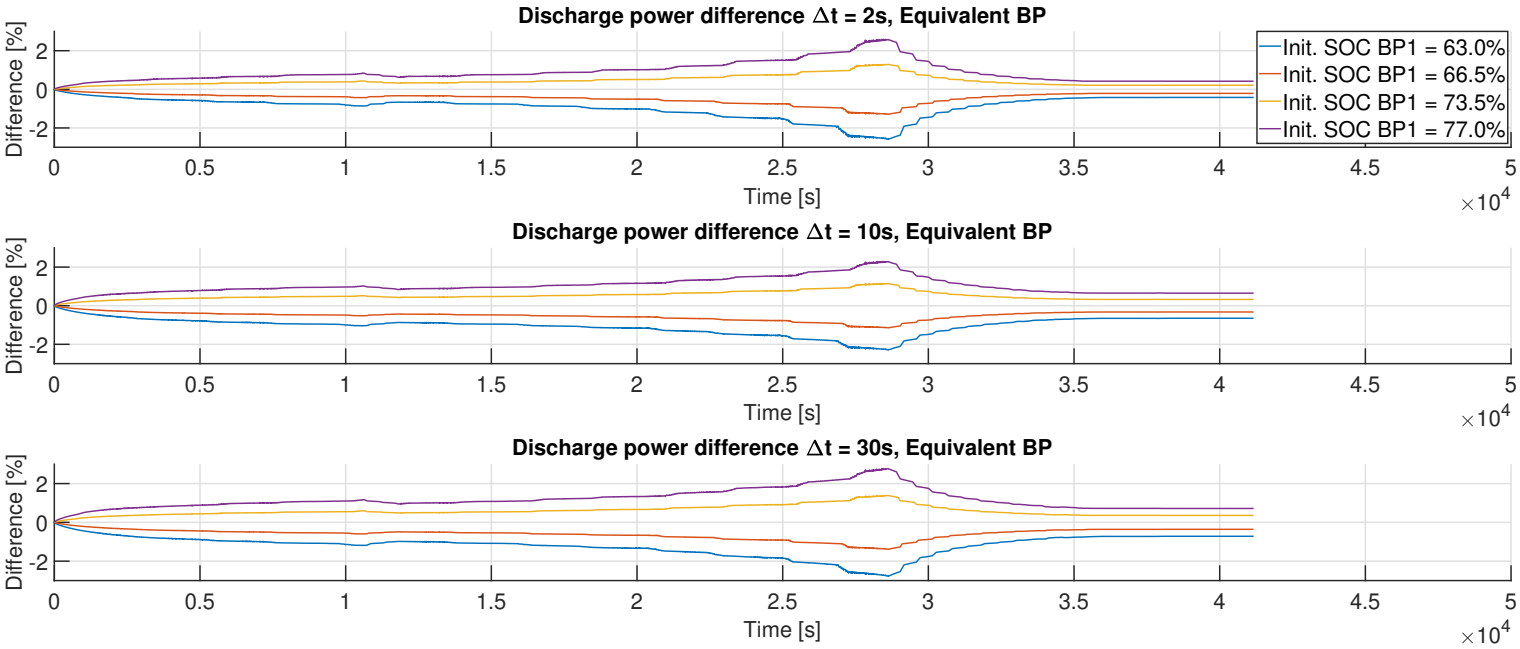

Figure 83: Representative pack SOP for 63.0, 66.5, 73.5 and 77% initial SOC and time-horizons 2, 10 and 30 seconds, during discharge. Nominal packs at nominal initial SOC 70%; Simcenter Amesim framework.

Appendix C

Appendix C provides a more in-depth description of the Simcenter Amesim model presented in Chapter 3. This section can be especially beneficial for readers that are not familiar with this framework. For more information, the reader is referred to the Simcenter Amesim documentation.

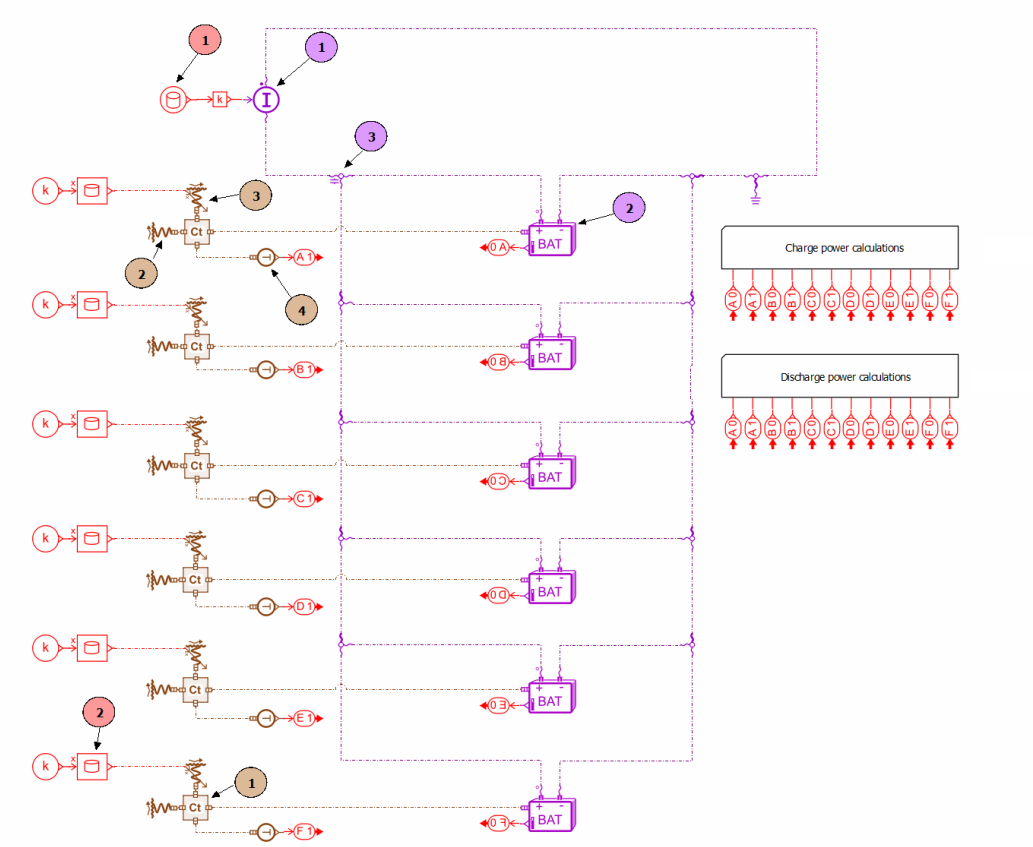

Figure 84: Representative Simcenter Amesim figure with notations.

The components can be divided into three libraries: electrical (purple), thermal (brown) and signal (red). Below is a short explanation of the marked components' function in the system.

Electrical components:

1. The *current source* supplies current to the electrical circuit.
2. In the *battery pack model* one can select different specifications for the cell model, such as: number of RC-networks, heat-generation model and hysteresis modelling.
3. The system needs a *capacitor junction* to break an algebraic loop.

Thermal components:

1. The *thermal mass* specifies the material and mass of the object (battery pack).
2. This models the *heat-exchange through free convection* (ambient temperature).

3. This models the *heat-exchange through forced convection* (coolant).

4. The *temperature sensor* converts the temperature to a signal.

Signal components:

1. This component performs table look-up to provide the *current load-profile*.

2. This table look-up converts a *coolant flow-rate* (k) to a heat-exchange coefficient.

The battery-pack and the thermal-convection components allow for more complex/detailed modelling depending on the data at hand. The thermal components assume a generic geometry, while the battery-pack model is configured to use:

- Second order RC network.
- Hysteresis modelling.
- Heat generation in the battery is calculated as RI^2
- Reversible heat generation (entropic heat).

The internal resistance, RC-pairs and OCV-source all use data-tables and interpolation to obtain their values during run-time.

The charge and discharge powers are calculated through table look-up (giving the maximum current applicable for a certain time-horizon), and then scaled appropriately.

Appendix D

Appendix D presents a more detailed description of the simplified models used in the model predictive SOP estimation. The relevant chapter for this appendix includes Chapter 5.

Recall the general formula for determining the current split between N battery packs:

$$I_k = \frac{1}{\phi}\prod_{i\neq k}^{N} R_{0i}\cdot I_{\text{dem}} + \frac{1}{\phi}\sum_{k\neq i}^{N}\left((V_{\text{OCV}_k} - V_{\text{OCV}_i})\cdot\prod_{\substack{j\neq k\\ j\neq i}}^{N} R_{oj}\right), \quad \phi = \sum_{i=1}^{N}\left(\prod_{k\neq i}^{N} R_{0k}\right)$$

Furthermore, the Open-Circuit-Voltage dynamics for cell k [39]:

$$\dot{V}_{\text{OCV}_k} = \frac{I_k}{C_{0,k}}, \quad C_{0,k} = 3600 Q_k \frac{d\text{SOC}(V_{\text{OCV}_k})}{dV_{\text{OCV}_k}}$$

Then for the case of this study, which includes six packs, with the states $x_k = V_{\text{OCV}_k}$, outputs $y_k = I_k$ and input $u = I_{\text{dem}}$, the state-space description becomes:

$$\dot{x}(t) = Ax(t) + Bu(t)$$
$$y(t) = Cx(t) + Du(t)$$

$$A = \frac{1}{\phi}\begin{bmatrix}
K_1 & \frac{R_{03}\,R_{04}\,R_{05}\,R_{06}}{C_{01}} & \frac{R_{02}\,R_{04}\,R_{05}\,R_{06}}{C_{01}} & \frac{R_{02}\,R_{03}\,R_{05}\,R_{06}}{C_{01}} & \frac{R_{02}\,R_{03}\,R_{04}\,R_{06}}{C_{01}} & \frac{R_{02}\,R_{03}\,R_{04}\,R_{05}}{C_{01}} \\
\frac{R_{03}\,R_{04}\,R_{05}\,R_{06}}{C_{02}} & K_2 & \frac{R_{01}\,R_{04}\,R_{05}\,R_{06}}{C_{02}} & \frac{R_{01}\,R_{03}\,R_{05}\,R_{06}}{C_{02}} & \frac{R_{01}\,R_{03}\,R_{04}\,R_{06}}{C_{02}} & \frac{R_{01}\,R_{03}\,R_{04}\,R_{05}}{C_{02}} \\
\frac{R_{02}\,R_{04}\,R_{05}\,R_{06}}{C_{03}} & \frac{R_{01}\,R_{04}\,R_{05}\,R_{06}}{C_{03}} & K_3 & \frac{R_{01}\,R_{02}\,R_{05}\,R_{06}}{C_{03}} & \frac{R_{01}\,R_{02}\,R_{04}\,R_{06}}{C_{03}} & \frac{R_{01}\,R_{02}\,R_{04}\,R_{05}}{C_{03}} \\
\frac{R_{02}\,R_{03}\,R_{05}\,R_{06}}{C_{04}} & \frac{R_{01}\,R_{03}\,R_{05}\,R_{06}}{C_{04}} & \frac{R_{01}\,R_{02}\,R_{05}\,R_{06}}{C_{04}} & K_4 & \frac{R_{01}\,R_{02}\,R_{03}\,R_{06}}{C_{04}} & \frac{R_{01}\,R_{02}\,R_{03}\,R_{05}}{C_{04}} \\
\frac{R_{02}\,R_{03}\,R_{04}\,R_{06}}{C_{05}} & \frac{R_{01}\,R_{03}\,R_{04}\,R_{06}}{C_{05}} & \frac{R_{01}\,R_{02}\,R_{04}\,R_{06}}{C_{05}} & \frac{R_{01}\,R_{02}\,R_{03}\,R_{06}}{C_{05}} & K_5 & \frac{R_{01}\,R_{02}\,R_{03}\,R_{04}}{C_{05}} \\
\frac{R_{02}\,R_{03}\,R_{04}\,R_{05}}{C_{06}} & \frac{R_{01}\,R_{03}\,R_{04}\,R_{05}}{C_{06}} & \frac{R_{01}\,R_{02}\,R_{04}\,R_{05}}{C_{06}} & \frac{R_{01}\,R_{02}\,R_{03}\,R_{05}}{C_{06}} & \frac{R_{01}\,R_{02}\,R_{03}\,R_{04}}{C_{06}} & K_6
\end{bmatrix}$$

where

$$K_1 = -\frac{R_{02}\,R_{03}\,R_{04}\,R_{05} + R_{02}\,R_{03}\,R_{04}\,R_{06} + R_{02}\,R_{03}\,R_{05}\,R_{06} + R_{02}\,R_{04}\,R_{05}\,R_{06} + R_{03}\,R_{04}\,R_{05}\,R_{06}}{C_{01}}$$

$$K_2 = -\frac{R_{01}\,R_{03}\,R_{04}\,R_{05} + R_{01}\,R_{03}\,R_{04}\,R_{06} + R_{01}\,R_{03}\,R_{05}\,R_{06} + R_{01}\,R_{04}\,R_{05}\,R_{06} + R_{03}\,R_{04}\,R_{05}\,R_{06}}{C_{02}}$$

$$K_3 = -\frac{R_{01}\,R_{02}\,R_{04}\,R_{05} + R_{01}\,R_{02}\,R_{04}\,R_{06} + R_{01}\,R_{02}\,R_{05}\,R_{06} + R_{01}\,R_{04}\,R_{05}\,R_{06} + R_{02}\,R_{04}\,R_{05}\,R_{06}}{C_{03}}$$

$$K_4 = -\frac{R_{01}\,R_{02}\,R_{03}\,R_{05} + R_{01}\,R_{02}\,R_{03}\,R_{06} + R_{01}\,R_{02}\,R_{05}\,R_{06} + R_{01}\,R_{03}\,R_{05}\,R_{06} + R_{02}\,R_{03}\,R_{05}\,R_{06}}{C_{04}}$$

$$K_5 = -\frac{R_{01}\,R_{02}\,R_{03}\,R_{04} + R_{01}\,R_{02}\,R_{03}\,R_{06} + R_{01}\,R_{02}\,R_{04}\,R_{06} + R_{01}\,R_{03}\,R_{04}\,R_{06} + R_{02}\,R_{03}\,R_{04}\,R_{06}}{C_{05}}$$

$$K_6 = -\frac{R_{01}\,R_{02}\,R_{03}\,R_{04} + R_{01}\,R_{02}\,R_{03}\,R_{05} + R_{01}\,R_{02}\,R_{04}\,R_{05} + R_{01}\,R_{03}\,R_{04}\,R_{05} + R_{02}\,R_{03}\,R_{04}\,R_{05}}{C_{06}}$$

$$B = \frac{1}{\phi}\begin{bmatrix} \frac{R_{02}\,R_{03}\,R_{04}\,R_{05}\,R_{06}}{C_{01}} \\ \frac{R_{01}\,R_{03}\,R_{04}\,R_{05}\,R_{06}}{C_{02}} \\ \frac{R_{01}\,R_{02}\,R_{04}\,R_{05}\,R_{06}}{C_{03}} \\ \frac{R_{01}\,R_{02}\,R_{03}\,R_{05}\,R_{06}}{C_{04}} \\ \frac{R_{01}\,R_{02}\,R_{03}\,R_{04}\,R_{06}}{C_{05}} \\ \frac{R_{01}\,R_{02}\,R_{03}\,R_{04}\,R_{05}}{C_{06}} \end{bmatrix}$$

$$C = \frac{1}{\phi}\begin{bmatrix} P_1 & R_{03}\,R_{04}\,R_{05}\,R_{06} & R_{02}\,R_{04}\,R_{05}\,R_{06} & R_{02}\,R_{03}\,R_{05}\,R_{06} & R_{02}\,R_{03}\,R_{04}\,R_{06} & R_{02}\,R_{03}\,R_{04}\,R_{05} \\ R_{03}\,R_{04}\,R_{05}\,R_{06} & P_2 & R_{01}\,R_{04}\,R_{05}\,R_{06} & R_{01}\,R_{03}\,R_{05}\,R_{06} & R_{01}\,R_{03}\,R_{04}\,R_{06} & R_{01}\,R_{03}\,R_{04}\,R_{05} \\ R_{02}\,R_{04}\,R_{05}\,R_{06} & R_{01}\,R_{04}\,R_{05}\,R_{06} & P_3 & R_{01}\,R_{02}\,R_{05}\,R_{06} & R_{01}\,R_{02}\,R_{04}\,R_{06} & R_{01}\,R_{02}\,R_{04}\,R_{05} \\ R_{02}\,R_{03}\,R_{05}\,R_{06} & R_{01}\,R_{03}\,R_{05}\,R_{06} & R_{01}\,R_{02}\,R_{05}\,R_{06} & P_4 & R_{01}\,R_{02}\,R_{03}\,R_{06} & R_{01}\,R_{02}\,R_{03}\,R_{05} \\ R_{02}\,R_{03}\,R_{04}\,R_{06} & R_{01}\,R_{03}\,R_{04}\,R_{06} & R_{01}\,R_{02}\,R_{04}\,R_{06} & R_{01}\,R_{02}\,R_{03}\,R_{06} & P_5 & R_{01}\,R_{02}\,R_{03}\,R_{04} \\ R_{02}\,R_{03}\,R_{04}\,R_{05} & R_{01}\,R_{03}\,R_{04}\,R_{05} & R_{01}\,R_{02}\,R_{04}\,R_{05} & R_{01}\,R_{02}\,R_{03}\,R_{05} & R_{01}\,R_{02}\,R_{03}\,R_{04} & P_6 \end{bmatrix}$$

where

$$P_1 = -\left(R_{02}\,R_{03}\,R_{04}\,R_{05} + R_{02}\,R_{03}\,R_{04}\,R_{06} + R_{02}\,R_{03}\,R_{05}\,R_{06} + R_{02}\,R_{04}\,R_{05}\,R_{06} + R_{03}\,R_{04}\,R_{05}\,R_{06}\right)$$
$$P_2 = -\left(R_{01}\,R_{03}\,R_{04}\,R_{05} + R_{01}\,R_{03}\,R_{04}\,R_{06} + R_{01}\,R_{03}\,R_{05}\,R_{06} + R_{01}\,R_{04}\,R_{05}\,R_{06} + R_{03}\,R_{04}\,R_{05}\,R_{06}\right)$$
$$P_3 = -\left(R_{01}\,R_{02}\,R_{04}\,R_{05} + R_{01}\,R_{02}\,R_{04}\,R_{06} + R_{01}\,R_{02}\,R_{05}\,R_{06} + R_{01}\,R_{04}\,R_{05}\,R_{06} + R_{02}\,R_{04}\,R_{05}\,R_{06}\right)$$
$$P_4 = -\left(R_{01}\,R_{02}\,R_{03}\,R_{05} + R_{01}\,R_{02}\,R_{03}\,R_{06} + R_{01}\,R_{02}\,R_{05}\,R_{06} + R_{01}\,R_{03}\,R_{05}\,R_{06} + R_{02}\,R_{03}\,R_{05}\,R_{06}\right)$$
$$P_5 = -\left(R_{01}\,R_{02}\,R_{03}\,R_{04} + R_{01}\,R_{02}\,R_{03}\,R_{06} + R_{01}\,R_{02}\,R_{04}\,R_{06} + R_{01}\,R_{03}\,R_{04}\,R_{06} + R_{02}\,R_{03}\,R_{04}\,R_{06}\right)$$
$$P_6 = -\left(R_{01}\,R_{02}\,R_{03}\,R_{04} + R_{01}\,R_{02}\,R_{03}\,R_{05} + R_{01}\,R_{02}\,R_{04}\,R_{05} + R_{01}\,R_{03}\,R_{04}\,R_{05} + R_{02}\,R_{03}\,R_{04}\,R_{05}\right)$$

$$D = \frac{1}{\phi}\begin{bmatrix} R_{02}\,R_{03}\,R_{04}\,R_{05}\,R_{06} \\ R_{01}\,R_{03}\,R_{04}\,R_{05}\,R_{06} \\ R_{01}\,R_{02}\,R_{04}\,R_{05}\,R_{06} \\ R_{01}\,R_{02}\,R_{03}\,R_{05}\,R_{06} \\ R_{01}\,R_{02}\,R_{03}\,R_{04}\,R_{06} \\ R_{01}\,R_{02}\,R_{03}\,R_{04}\,R_{05} \end{bmatrix}$$

$$\phi = R_{01}\,R_{02}\,R_{03}\,R_{04}\,R_{05} + R_{01}\,R_{02}\,R_{03}\,R_{04}\,R_{06} + R_{01}\,R_{02}\,R_{03}\,R_{05}\,R_{06} + R_{01}\,R_{02}\,R_{04}\,R_{05}\,R_{06} + R_{01}\,R_{03}\,R_{04}\,R_{05}\,R_{06} + R_{02}\,R_{03}\,R_{04}\,R_{05}\,R_{06}$$

Simplified model including SOC:
The electrical model has not changed, hence the current distribution can be calculated as before. The SOC dynamics of pack k is given by:

$$\dot{\mathrm{SOC}}_k = \frac{1}{3600 Q_k} \cdot I_k$$

The state-space description is therefore given as:

$$\dot{x}(t) = Ax(t) + Bu(t)$$
$$y(t) = Cx(t) + Du(t)$$

$$A = \frac{1}{\phi} \begin{bmatrix}
K_{11} & 0 & \frac{R_{03}\,R_{04}\,R_{05}\,R_{06}}{C_{01}} & 0 & \frac{R_{02}\,R_{04}\,R_{05}\,R_{06}}{C_{01}} & 0 & \frac{R_{02}\,R_{03}\,R_{05}\,R_{06}}{C_{01}} & 0 & \frac{R_{02}\,R_{03}\,R_{04}\,R_{06}}{C_{01}} & 0 & \frac{R_{02}\,R_{03}\,R_{04}\,R_{05}}{C_{01}} & 0 \\
K_{12} & 0 & \frac{R_{03}\,R_{04}\,R_{05}\,R_{06}}{3600Q} & 0 & \frac{R_{02}\,R_{04}\,R_{05}\,R_{06}}{3600Q} & 0 & \frac{R_{02}\,R_{03}\,R_{05}\,R_{06}}{3600Q} & 0 & \frac{R_{02}\,R_{03}\,R_{04}\,R_{06}}{3600Q} & 0 & \frac{R_{02}\,R_{03}\,R_{04}\,R_{05}}{3600Q} & 0 \\
\frac{R_{03}\,R_{04}\,R_{05}\,R_{06}}{C_{02}} & 0 & K_{21} & 0 & \frac{R_{01}\,R_{04}\,R_{05}\,R_{06}}{C_{02}} & 0 & \frac{R_{01}\,R_{03}\,R_{05}\,R_{06}}{C_{02}} & 0 & \frac{R_{01}\,R_{03}\,R_{04}\,R_{06}}{C_{02}} & 0 & \frac{R_{01}\,R_{03}\,R_{04}\,R_{05}}{C_{02}} & 0 \\
\frac{R_{03}\,R_{04}\,R_{05}\,R_{06}}{3600Q} & 0 & K_{22} & 0 & \frac{R_{01}\,R_{04}\,R_{05}\,R_{06}}{3600Q} & 0 & \frac{R_{01}\,R_{03}\,R_{05}\,R_{06}}{3600Q} & 0 & \frac{R_{01}\,R_{03}\,R_{04}\,R_{06}}{3600Q} & 0 & \frac{R_{01}\,R_{03}\,R_{04}\,R_{05}}{3600Q} & 0 \\
\frac{R_{02}\,R_{04}\,R_{05}\,R_{06}}{C_{03}} & 0 & \frac{R_{01}\,R_{04}\,R_{05}\,R_{06}}{C_{03}} & 0 & K_{31} & 0 & \frac{R_{01}\,R_{02}\,R_{05}\,R_{06}}{C_{03}} & 0 & \frac{R_{01}\,R_{02}\,R_{04}\,R_{06}}{C_{03}} & 0 & \frac{R_{01}\,R_{02}\,R_{04}\,R_{05}}{C_{03}} & 0 \\
\frac{R_{02}\,R_{04}\,R_{05}\,R_{06}}{3600Q} & 0 & \frac{R_{01}\,R_{04}\,R_{05}\,R_{06}}{3600Q} & 0 & K_{32} & 0 & \frac{R_{01}\,R_{02}\,R_{05}\,R_{06}}{3600Q} & 0 & \frac{R_{01}\,R_{02}\,R_{04}\,R_{06}}{3600Q} & 0 & \frac{R_{01}\,R_{02}\,R_{04}\,R_{05}}{3600Q} & 0 \\
\frac{R_{02}\,R_{03}\,R_{05}\,R_{06}}{C_{04}} & 0 & \frac{R_{01}\,R_{03}\,R_{05}\,R_{06}}{C_{04}} & 0 & \frac{R_{01}\,R_{02}\,R_{05}\,R_{06}}{C_{04}} & 0 & K_{41} & 0 & \frac{R_{01}\,R_{02}\,R_{03}\,R_{06}}{C_{04}} & 0 & \frac{R_{01}\,R_{02}\,R_{03}\,R_{05}}{C_{04}} & 0 \\
\frac{R_{02}\,R_{03}\,R_{05}\,R_{06}}{3600Q} & 0 & \frac{R_{01}\,R_{03}\,R_{05}\,R_{06}}{3600Q} & 0 & \frac{R_{01}\,R_{02}\,R_{05}\,R_{06}}{3600Q} & 0 & K_{42} & 0 & \frac{R_{01}\,R_{02}\,R_{03}\,R_{06}}{3600Q} & 0 & \frac{R_{01}\,R_{02}\,R_{03}\,R_{05}}{3600Q} & 0 \\
\frac{R_{02}\,R_{03}\,R_{04}\,R_{06}}{C_{05}} & 0 & \frac{R_{01}\,R_{03}\,R_{04}\,R_{06}}{C_{05}} & 0 & \frac{R_{01}\,R_{02}\,R_{04}\,R_{06}}{C_{05}} & 0 & \frac{R_{01}\,R_{02}\,R_{03}\,R_{06}}{C_{05}} & 0 & K_{51} & 0 & \frac{R_{01}\,R_{02}\,R_{03}\,R_{04}}{C_{05}} & 0 \\
\frac{R_{02}\,R_{03}\,R_{04}\,R_{06}}{3600Q} & 0 & \frac{R_{01}\,R_{03}\,R_{04}\,R_{06}}{3600Q} & 0 & \frac{R_{01}\,R_{02}\,R_{04}\,R_{06}}{3600Q} & 0 & \frac{R_{01}\,R_{02}\,R_{03}\,R_{06}}{3600Q} & 0 & K_{52} & 0 & \frac{R_{01}\,R_{02}\,R_{03}\,R_{04}}{3600Q} & 0 \\
\frac{R_{02}\,R_{03}\,R_{04}\,R_{05}}{C_{06}} & 0 & \frac{R_{01}\,R_{03}\,R_{04}\,R_{05}}{C_{06}} & 0 & \frac{R_{01}\,R_{02}\,R_{04}\,R_{05}}{C_{06}} & 0 & \frac{R_{01}\,R_{02}\,R_{03}\,R_{05}}{C_{06}} & 0 & \frac{R_{01}\,R_{02}\,R_{03}\,R_{04}}{C_{06}} & 0 & K_{61} & 0 \\
\frac{R_{02}\,R_{03}\,R_{04}\,R_{05}}{3600Q} & 0 & \frac{R_{01}\,R_{03}\,R_{04}\,R_{05}}{3600Q} & 0 & \frac{R_{01}\,R_{02}\,R_{04}\,R_{05}}{3600Q} & 0 & \frac{R_{01}\,R_{02}\,R_{03}\,R_{05}}{3600Q} & 0 & \frac{R_{01}\,R_{02}\,R_{03}\,R_{04}}{3600Q} & 0 & K_{62} & 0
\end{bmatrix}$$

where

$$K_{11} = -\frac{R_{02}\,R_{03}\,R_{04}\,R_{05} + R_{02}\,R_{03}\,R_{04}\,R_{06} + R_{02}\,R_{03}\,R_{05}\,R_{06} + R_{02}\,R_{04}\,R_{05}\,R_{06} + R_{03}\,R_{04}\,R_{05}\,R_{06}}{C_{01}}$$

$$K_{12} = -\frac{R_{02}\,R_{03}\,R_{04}\,R_{05} + R_{02}\,R_{03}\,R_{04}\,R_{06} + R_{02}\,R_{03}\,R_{05}\,R_{06} + R_{02}\,R_{04}\,R_{05}\,R_{06} + R_{03}\,R_{04}\,R_{05}\,R_{06}}{3600Q}$$

$$K_{21} = -\frac{R_{01}\,R_{03}\,R_{04}\,R_{05} + R_{01}\,R_{03}\,R_{04}\,R_{06} + R_{01}\,R_{03}\,R_{05}\,R_{06} + R_{01}\,R_{04}\,R_{05}\,R_{06} + R_{03}\,R_{04}\,R_{05}\,R_{06}}{C_{02}}$$

$$K_{22} = -\frac{R_{01}\,R_{03}\,R_{04}\,R_{05} + R_{01}\,R_{03}\,R_{04}\,R_{06} + R_{01}\,R_{03}\,R_{05}\,R_{06} + R_{01}\,R_{04}\,R_{05}\,R_{06} + R_{03}\,R_{04}\,R_{05}\,R_{06}}{3600Q}$$

$$K_{31} = -\frac{R_{01}\,R_{02}\,R_{04}\,R_{05} + R_{01}\,R_{02}\,R_{04}\,R_{06} + R_{01}\,R_{02}\,R_{05}\,R_{06} + R_{01}\,R_{04}\,R_{05}\,R_{06} + R_{02}\,R_{04}\,R_{05}\,R_{06}}{C_{03}}$$

$$K_{32} = -\frac{R_{01}\,R_{02}\,R_{04}\,R_{05} + R_{01}\,R_{02}\,R_{04}\,R_{06} + R_{01}\,R_{02}\,R_{05}\,R_{06} + R_{01}\,R_{04}\,R_{05}\,R_{06} + R_{02}\,R_{04}\,R_{05}\,R_{06}}{3600Q}$$

$$K_{41} = -\frac{R_{01}\,R_{02}\,R_{03}\,R_{05} + R_{01}\,R_{02}\,R_{03}\,R_{06} + R_{01}\,R_{02}\,R_{05}\,R_{06} + R_{01}\,R_{03}\,R_{05}\,R_{06} + R_{02}\,R_{03}\,R_{05}\,R_{06}}{C_{04}}$$

$$K_{42} = -\frac{R_{01}\,R_{02}\,R_{03}\,R_{05} + R_{01}\,R_{02}\,R_{03}\,R_{06} + R_{01}\,R_{02}\,R_{05}\,R_{06} + R_{01}\,R_{03}\,R_{05}\,R_{06} + R_{02}\,R_{03}\,R_{05}\,R_{06}}{3600Q}$$

$$K_{51} = -\frac{R_{01}\,R_{02}\,R_{03}\,R_{04} + R_{01}\,R_{02}\,R_{03}\,R_{06} + R_{01}\,R_{02}\,R_{04}\,R_{06} + R_{01}\,R_{03}\,R_{04}\,R_{06} + R_{02}\,R_{03}\,R_{04}\,R_{06}}{C_{05}}$$

$$K_{52} = -\frac{R_{01}\,R_{02}\,R_{03}\,R_{04} + R_{01}\,R_{02}\,R_{03}\,R_{06} + R_{01}\,R_{02}\,R_{04}\,R_{06} + R_{01}\,R_{03}\,R_{04}\,R_{06} + R_{02}\,R_{03}\,R_{04}\,R_{06}}{3600Q}$$

$$K_{61} = -\frac{R_{01}\,R_{02}\,R_{03}\,R_{04} + R_{01}\,R_{02}\,R_{03}\,R_{05} + R_{01}\,R_{02}\,R_{04}\,R_{05} + R_{01}\,R_{03}\,R_{04}\,R_{05} + R_{02}\,R_{03}\,R_{04}\,R_{05}}{C_{06}}$$

$$K_{62} = -\frac{R_{01}\,R_{02}\,R_{03}\,R_{04} + R_{01}\,R_{02}\,R_{03}\,R_{05} + R_{01}\,R_{02}\,R_{04}\,R_{05} + R_{01}\,R_{03}\,R_{04}\,R_{05} + R_{02}\,R_{03}\,R_{04}\,R_{05}}{3600Q}$$

$$B = \frac{1}{\phi}\begin{bmatrix} \frac{R_{02}\,R_{03}\,R_{04}\,R_{05}\,R_{06}}{C_{01}} \\ \frac{R_{02}\,R_{03}\,R_{04}\,R_{05}\,R_{06}}{3600Q} \\ \frac{R_{01}\,R_{03}\,R_{04}\,R_{05}\,R_{06}}{C_{02}} \\ \frac{R_{01}\,R_{03}\,R_{04}\,R_{05}\,R_{06}}{3600Q} \\ \frac{R_{01}\,R_{02}\,R_{04}\,R_{05}\,R_{06}}{C_{03}} \\ \frac{R_{01}\,R_{02}\,R_{04}\,R_{05}\,R_{06}}{3600Q} \\ \frac{R_{01}\,R_{02}\,R_{03}\,R_{05}\,R_{06}}{C_{04}} \\ \frac{R_{01}\,R_{02}\,R_{03}\,R_{05}\,R_{06}}{3600Q} \\ \frac{R_{01}\,R_{02}\,R_{03}\,R_{04}\,R_{06}}{C_{05}} \\ \frac{R_{01}\,R_{02}\,R_{03}\,R_{04}\,R_{06}}{3600Q} \\ \frac{R_{01}\,R_{02}\,R_{03}\,R_{04}\,R_{05}}{C_{06}} \\ \frac{R_{01}\,R_{02}\,R_{03}\,R_{04}\,R_{05}}{3600Q} \end{bmatrix}$$

$$C = \frac{1}{\phi}\begin{bmatrix} P_1 & 0 & R_{03}\,R_{04}\,R_{05}\,R_{06} & 0 & R_{02}\,R_{04}\,R_{05}\,R_{06} & 0 & R_{02}\,R_{03}\,R_{05}\,R_{06} & 0 & R_{02}\,R_{03}\,R_{04}\,R_{06} & 0 & R_{02}\,R_{03}\,R_{04}\,R_{05} & 0 \\ R_{03}\,R_{04}\,R_{05}\,R_{06} & 0 & P_2 & 0 & R_{01}\,R_{04}\,R_{05}\,R_{06} & 0 & R_{01}\,R_{03}\,R_{05}\,R_{06} & 0 & R_{01}\,R_{03}\,R_{04}\,R_{06} & 0 & R_{01}\,R_{03}\,R_{04}\,R_{05} & 0 \\ R_{02}\,R_{04}\,R_{05}\,R_{06} & 0 & R_{01}\,R_{04}\,R_{05}\,R_{06} & 0 & P_3 & 0 & R_{01}\,R_{02}\,R_{05}\,R_{06} & 0 & R_{01}\,R_{02}\,R_{04}\,R_{06} & 0 & R_{01}\,R_{02}\,R_{04}\,R_{05} & 0 \\ R_{02}\,R_{03}\,R_{05}\,R_{06} & 0 & R_{01}\,R_{03}\,R_{05}\,R_{06} & 0 & R_{01}\,R_{02}\,R_{05}\,R_{06} & 0 & P_4 & 0 & R_{01}\,R_{02}\,R_{03}\,R_{06} & 0 & R_{01}\,R_{02}\,R_{03}\,R_{05} & 0 \\ R_{02}\,R_{03}\,R_{04}\,R_{06} & 0 & R_{01}\,R_{03}\,R_{04}\,R_{06} & 0 & R_{01}\,R_{02}\,R_{04}\,R_{06} & 0 & R_{01}\,R_{02}\,R_{03}\,R_{06} & 0 & P_5 & 0 & R_{01}\,R_{02}\,R_{03}\,R_{04} & 0 \\ R_{02}\,R_{03}\,R_{04}\,R_{05} & 0 & R_{01}\,R_{03}\,R_{04}\,R_{05} & 0 & R_{01}\,R_{02}\,R_{04}\,R_{05} & 0 & R_{01}\,R_{02}\,R_{03}\,R_{05} & 0 & R_{01}\,R_{02}\,R_{03}\,R_{04} & 0 & P_6 & 0 \end{bmatrix}$$

where

$$P_1 = -\left(R_{02}\,R_{03}\,R_{04}\,R_{05} + R_{02}\,R_{03}\,R_{04}\,R_{06} + R_{02}\,R_{03}\,R_{05}\,R_{06} + R_{02}\,R_{04}\,R_{05}\,R_{06} + R_{03}\,R_{04}\,R_{05}\,R_{06}\right)$$
$$P_2 = -\left(R_{01}\,R_{03}\,R_{04}\,R_{05} + R_{01}\,R_{03}\,R_{04}\,R_{06} + R_{01}\,R_{03}\,R_{05}\,R_{06} + R_{01}\,R_{04}\,R_{05}\,R_{06} + R_{03}\,R_{04}\,R_{05}\,R_{06}\right)$$
$$P_3 = -\left(R_{01}\,R_{02}\,R_{04}\,R_{05} + R_{01}\,R_{02}\,R_{04}\,R_{06} + R_{01}\,R_{02}\,R_{05}\,R_{06} + R_{01}\,R_{04}\,R_{05}\,R_{06} + R_{02}\,R_{04}\,R_{05}\,R_{06}\right)$$
$$P_4 = -\left(R_{01}\,R_{02}\,R_{03}\,R_{05} + R_{01}\,R_{02}\,R_{03}\,R_{06} + R_{01}\,R_{02}\,R_{05}\,R_{06} + R_{01}\,R_{03}\,R_{05}\,R_{06} + R_{02}\,R_{03}\,R_{05}\,R_{06}\right)$$
$$P_5 = -\left(R_{01}\,R_{02}\,R_{03}\,R_{04} + R_{01}\,R_{02}\,R_{03}\,R_{06} + R_{01}\,R_{02}\,R_{04}\,R_{06} + R_{01}\,R_{03}\,R_{04}\,R_{06} + R_{02}\,R_{03}\,R_{04}\,R_{06}\right)$$
$$P_6 = -\left(R_{01}\,R_{02}\,R_{03}\,R_{04} + R_{01}\,R_{02}\,R_{03}\,R_{05} + R_{01}\,R_{02}\,R_{04}\,R_{05} + R_{01}\,R_{03}\,R_{04}\,R_{05} + R_{02}\,R_{03}\,R_{04}\,R_{05}\right)$$

$$D = \frac{1}{\phi}\begin{bmatrix} R_{02}\,R_{03}\,R_{04}\,R_{05}\,R_{06} \\ R_{01}\,R_{03}\,R_{04}\,R_{05}\,R_{06} \\ R_{01}\,R_{02}\,R_{04}\,R_{05}\,R_{06} \\ R_{01}\,R_{02}\,R_{03}\,R_{05}\,R_{06} \\ R_{01}\,R_{02}\,R_{03}\,R_{04}\,R_{06} \\ R_{01}\,R_{02}\,R_{03}\,R_{04}\,R_{05} \end{bmatrix}$$

CHALMERS

UNIVERSITY OF TECHNOLOGY